Doctoral Thesis

Design of Touch Screen Controller IC for Transparent Fingerprint Sensor

Sanghyun Heo

Department of Electrical Engineering

Graduate School of UNIST

2018

Design of Touch Screen Controller IC for Transparent Fingerprint Sensor

Sanghyun Heo

Department of Electrical Engineering

Graduate School of UNIST

Design of Touch Screen Controller IC for Transparent Fingerprint Sensor

A thesis/dissertation
submitted to the Graduate School of UNIST
in partial fulfillment of the
requirements for the degree of
Doctor of Philosophy

Sanghyun Heo

12/12/2017 of submission

Approved by

Advisor
Franklin Bien

Design of Touch Screen Controller IC for Transparent Fingerprint Sensor

Sanghyun Heo

This certifies that the thesis/dissertation of Sanghyun Heo is approved.

12/12/2017 of submission

signature

Advisor: Franklin Bien

signature

Jaehyouk Choi: Thesis Committee Member #1

signature

Seong-Jin Kim: Thesis Committee Member #2

signature

Myunghee Lee: Thesis Committee Member #3

signature

Sung-Tae Hong: Thesis Committee Member #4;

Acknowledgement

I would like to acknowledge the Prof. Franklin Bien. Without his sober-headed guidance, this work would not have been possible. He always encouraged me to explore logical thinking.

I would like to express my appreciation to committee members: Prof. Jaehyouk Choi, Prof. Seong-jin Kim, Prof. Myunghee Lee, and Prof. Sung-Tae Hong for giving me insightful instructions on my dissertation.

During my doctoral course, I learned a lot through Samsung Display and industry-university collaborative research. In addition, after graduation, I was able to work on Samsung Display and continue my research. Thank you to Franklin Bien for all your support.

I am very thankful to the members of my research group who have made my stay memorable.

Finally, I would like to express the deepest gratitude to my dear parents. Without their love, patience and generous support all the time, I would not be able to reach this far.

Finally, thank you for my girlfriend.

Abstract

A design of system architecture and analog-front-end (AFE) with high SNR and high frame rate for mutual capacitive touch screen with multiple electrodes is presented.

Firstly, a differential continuous-mode parallel operation architecture (DCPA) is proposed for large-sized TSP. The proposed architecture achieves a high product of signal-to-noise ratio (SNR) and frame rate, which is a requirement of ROIC for large-sized TSP. DCPA is accomplished by using the proposed differential sensing method with a parallel architecture in a continuous-mode. A continuous-type differential charge amplifier removes the common-mode noise component, and reduces the self-noise by the band-pass filtering effect of the continuous-mode charge amplifier. In addition, the differential parallel architecture cancels the timing skew problem caused by the continuous-mode parallel operation and effectively enhances the power spectrum density of the signal. The proposed ROIC was fabricated using a 0.18-um CMOS process and occupied an active area of 1.25 mm^2. The proposed system achieved a 72 dB SNR and 240 Hz frame rate with a 32 channel TX by 10 channel RX mutual capacitive TSP. Moreover, the proposed differential-parallel architecture demonstrated higher immunity to lamp noise and display noise. The proposed system consumed 42.5 mW with a 3.3-V supply.

Secondly, readout IC (ROIC) with a differential coded multiple signaling method (DCMS) is proposed to detect an atto-farad capacitance difference for fingerprint recognition in fingerprint TSP. A readout IC with high SNR and fast frame rate are required in the fingerprint recognition. However, the capacitance difference by the ridge and valley of the fingerprint is very small, so that the signal-to-noise ratio is very low. In addition, it takes long time to scan whole fingerprint TSP with multiple electrodes. A fully differential architecture with differential signaling is proposed to detect the low capacitance difference in fingerprint TSP. The internal noise generated is minimized by 2nd fully differential operational amplifier and external noise is eliminated by a lock-in sensing structure. In addition, DCMS reduces an AC offset and enhances a higher product of SNR and frame rate in multiple channels. The proposed architectures can distinguish a 50-atto-farad which is a capacitance difference resulted from the ridges and valley of the finger under the 0.3T glass. The total scan time for 42 × 42 fingerprint TSP is less than 21 ms and the power consumption is below 20 mW at 3.3 V supply voltage. IC has been fabricated using a 0.18 μm standard CMOS process.

Kew Words—Differential sensing, Parallel Operation, Touch Screen Panel, Common-mode feedback, Capacitor Sensor, Fingerprint recognition, capacitive touch screen panel, fully differential receiver, fully differential multi-driving.

Contents

List of figures

List of tables

Nomenclature

TSP	Touch Screen Panel
TSC	Touch Screen Controller IC
IC	Integrated Circuit
ROIC	Readout Integrated Circuit
ITO	Indium Tin Oxide
SC	Switched Capacitor
TDMA	Time-interleaved Method
CDMS	Code Division Multiple Sensing Method
WHC	Walsh Hadmard Code
SNR	Signal-to-Noise Ratio
CDMA	Code Division Multiple Access
ADC	Analog-to-Digital Converter
MCU	Micro Controller Unit
FPGA	Field-programmable gate array
MAE	Moving Average Effect
RMS	Root mean square
CA	Charge Amplifier
TX	Transmitter
RX	Receiver
SCA	Single-Ended Charge Amplifier
SCPA	Single-ended Continuous-mode Parallel Operation Architecture
SDPA	Single-ended Discrete-mode Parallel Operation Architecture
DCTA	Differential Continuous-mode Parallel Operation Architecture
DCPA	Differential Continuous-mode Parallel Architecture
DCA	Differential Charge Amplifier
DGA	Differential Gain Amplifier
ICMFB	Input-Common-Mode Feedback
OCMFB	Output-Common-Mode Feedback
DDA	Differential Difference Amplifier
CMFB	Common-mode Feedback Circuit
STX	Single-ended Driving
DTX	Differential Driving
LPF	Low-Pass-Filter
MCU	Micro Controller Unit

FPGA	Field-programmable gate array
OCMFB	Output Common-Mode Feedback
CMFB	Common-mode Feedback
CMRR	Common-mode rejection ratio

Chapter 1

I. Introduction

1.1 Motivation

Fig.1. 1 Finger Print Touch Screen of the Mobile Phone

There are numerous input devices available for electronic devices, including a mouse, trackball, touch screen panel (TSP), keyboards, and buttons. Among these, TSPs have been given increased attention because they provide users with intuitive and convenient functions like an advanced graphical user interface. Mutual capacitive touch screen sensors are widely used because they are intuitive and convenient, and offer multi-touch functions with superior touch sensitivity [1.1]. The use of mutual capacitive touch screen has become diversified and now covers form factors that range from mobile devices to larger touch screens. A smart device, such as a mobile phone, a smart watch, has been widely used in these days. Since a smart device has user's private information such as a payment-related information, a personal information, it is necessary to have a device that can keep the user's information. A fingerprint recognition is a convenient and reliable solution for the security of smart devices because it allows individual recognition by touching the fingerprint without inputting the code. A capacitive fingerprint sensor was firstly used on the home button in the mobile devices. However, the display size of mobile devices is gradually increasing and a wearable device such as a smart watch does not include a home button. As a result, a fingerprint recognition touchscreen with high sensitivity that can be mounted on a display is required as shown in Fig.1.

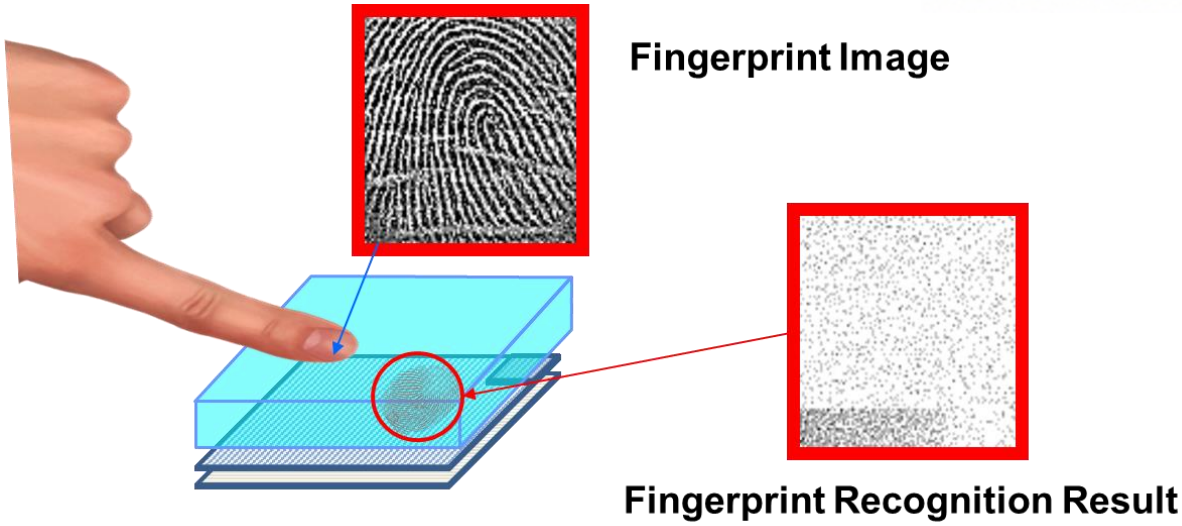

Fig.1. 2 Low sensitivity of the fingerprint TSP due to the cover glass

Among the various candidates, a transparent capacitive-type fingerprint touchscreen has attention because of its various advantages such that it can be mounted on both LCD and OLED display at a low price and it can be used as touch screen with fingerprint recognition However, there is also a disadvantage in a transparent mutual capacitive TSP for fingerprint. The biggest drawback is low sensitivity due to cover glass. In the case of a general touch screen, the change in capacitance is measured by the presence or absence of a touch by the finger. Whereas in the case of a fingerprint recognition TSP, the change in capacitance is occurred due to the difference in depth of valley and ridge of the finger. The depth difference of the valley and the ridge is lower than 100um [1.2]. In addition, a cover glass is placed on the display panel to protect the display. The cover glass increases the distance between the touch screen and the fingerprint. As a result, the change in capacitance due to the valley and the ridge of finger is reduced. Due to these problems, a touch screen controller IC for fingerprint recognition requires a technique which have a higher sensitivity that is different from existing touch screen controller IC.

1.2 Thesis Organization

This thesis focuses on the design of fingerprint capacitive touchscreen controller IC. This thesis is described as follows.

Chapter II introduces the basic research of touch screen controller IC. After describing the system structure of the touch screen controller IC, it describes the principle of the capacitance change by finger and fingerprint in capacitive touch screen. Additionally, it presents how to evaluate the noise and performance of the touch screen.

Chapter III discusses the preliminary research into touchscreen controller ICs for large touchscreens prior to the fingerprint recognition touchscreen. After discussing design issues in large touch screen, chapter III describes system structure and circuit with high speed and high SNR on large touch screen. After then, the measurement results of system and circuit are presented

Based on basic research, Chapter IV proposes a system architecture and circuits suitable for fingerprint capacitive touch screen. First, it deals with design issues for TSC for fingerprint recognition. Then, the fingerprint recognition system structure and circuit are presented for the fingerprint mutual capacitive TSP. Also, the measurement results are presented.

Finally, Chapter V presents conclusion and summary on the results of the thesis.

Chapter II

II. Basic Research on Touch Screen Controller IC

2.1 System Architecture Overview

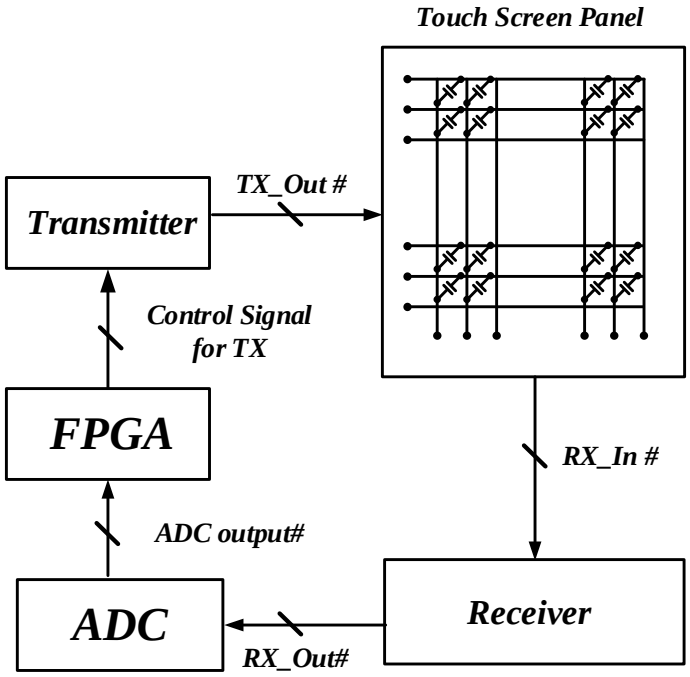

Fig.2. 1 Block Diagram of the Touch Screen Controller IC

In this section, how the TSC is configured and how it senses the mutual capacitive TSP are presented [2.1]. Fig. 2.1 shows the overall block diagram of touch screen readout IC. The system is composed of a transmitter, analog-front-end, analog-to-digital converter and field programmable gate array (FPGA). A transmitter sends a driving signal to the electrode of the lower layer in the TSP. This driving signal is converted to the current signal which is proportional to the mutual capacitor value. These current signals go through the analog-front-end circuit. Analog-front-end converts these current to the voltage signal depending on the driving signal and mutual capacitor values. The outputs of the analog-front-end are connected to the analog-to-digital converter (ADC). ADC converts the analog signal to the digital signal. In the FPGA, the processor distinguishes the touch and un-touch conditions depending on the output of ADC. Digital processing is very important because the touch screen is composed of arrays of capacitors. The FPGA has to decide how to send the signal divided by time in the transmitter, store the data in real time in the receiver, and decide whether to touch or not.

2.1.1 A Mutual Capacitive Touch Screen Panel

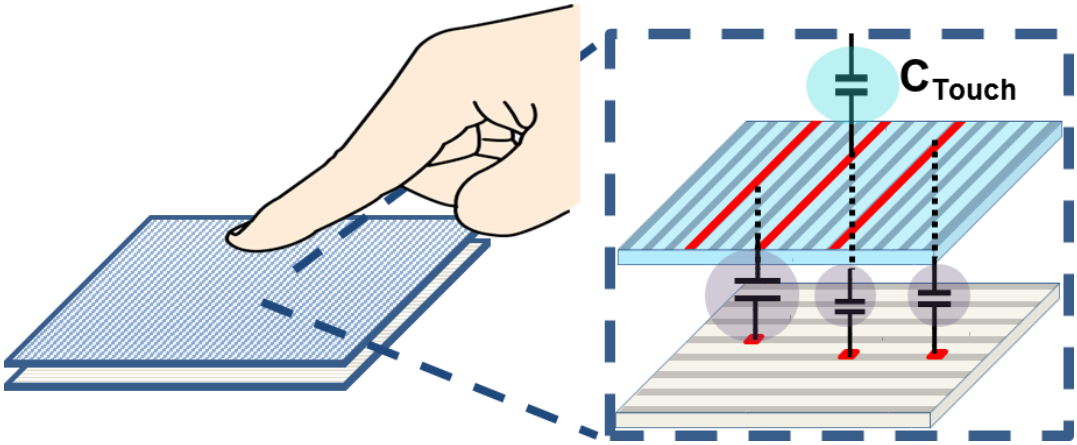

Fig.2. 2 A Mutual Capacitive Touch Screen Panel

Fig. 2.2 show a mutual capacitive touch screen architecture. Mutual TSP is composed of two layers. Each layer has numerous parallel electrodes. These electrodes from upper layer and lower layer are positioned perpendicularly to each other. At the crossing point of this upper and lower layer's electrodes, mutual capacitor is constructed. When a finger is touched on to this TSP, additional capacitance is formed between the finger and top layer electrode. With this additional capacitance between the finger and the top layer, the effective mutual capacitance is reduced at the touch point on the TSP.

The mutual capacitance type TSP is an array type capacitive sensor, and thus it exists as a plurality of capacitor arrays. In the case of a capacitor in the form of an array, the advantage is that it can scan the transmitter electrode line by line for detecting multiple capacitors. Therefore, the number of transmitter part and receiving parts is small compared with the case where there is a sensor for each node. In the mutual capacitive TSP, the number of the transmitter channels is equal to the number of the electrodes of the transmitter, and the number of the receiver channels is equal to the number of the receiver electrodes.

The transparent capacitive TSP consists of a transparent transmitter and receiver electrodes. The most typical transparent electrode is indium tin oxide (ITO) [2.1]. The advantages of ITO are high transmittance and high conductivity. However, the disadvantage of ITO is that the sheet resistance component is very large. Therefore, the resistance component of the electrode of the TSP is increased, so that the high frequency signal cannot be transmitted well. To overcome this, a metal mesh electrode is developed. The advantage of metal mesh is that sheet resistance component is lower than ITO. However, transparency is low, and research is needed.

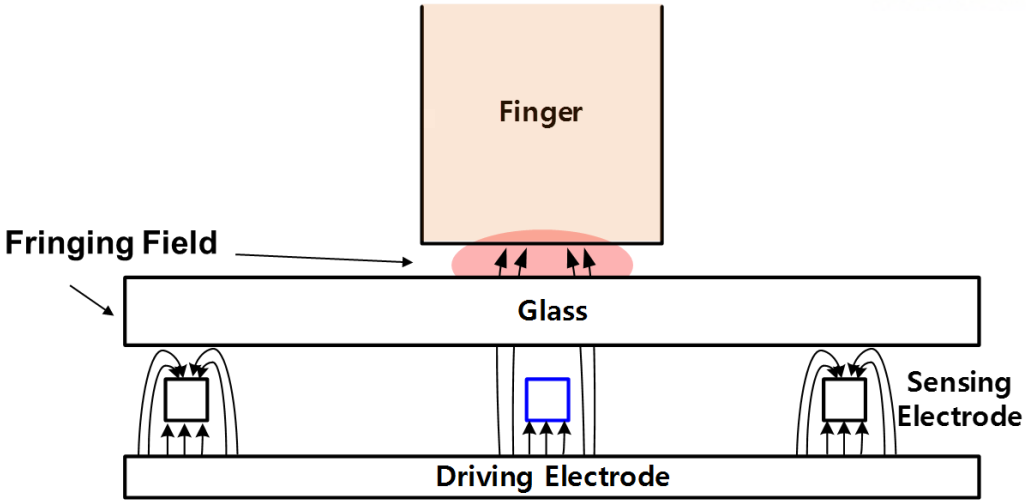

Fig.2. 3 Electric field of mutual capacitive TSP

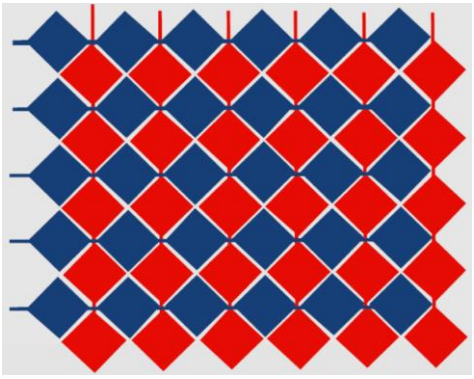

Fig.2. 4 ITO-Diamond pattern

Fig. 2.3 shows an electric filed of a mutual capacitive TSP. When a voltage is applied to driving electrodes, an electric field is generated between driving electrodes and sensing electrodes. In addition, there are additional electric field at the edge of the electrodes, which is called fringing field. When a finger touches TSP, the finger absorbs the fringing field. As a result, an effective mutual capacitor is reduced.

In other words, the change of the mutual capacitance in the mutual capacitance type TSP is proportional to the fringing filed component generated in the edge of the sensing electrode and the driving electrode. To maximize the fringing field, various electrode patterns have been researched. As shown in Fig. 2.4, the most representative of these is the Diamond Pattern of ITO. In the case of Diamond Pattern, it is an example of a pattern that increases the capacitance change by touch by maximizing the Fringing Filed.

2.1.2 Readout IC

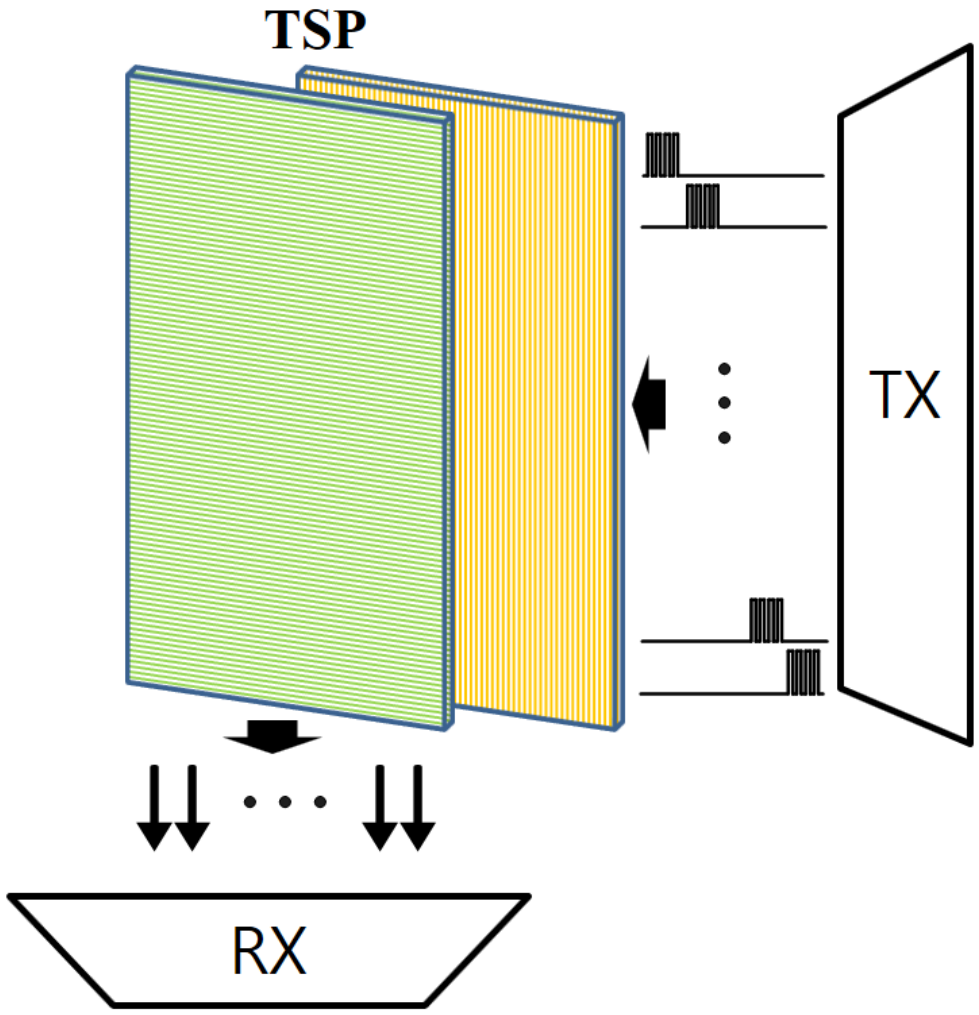

Fig.2. 5 A readout IC for mutual capacitive touch screen

Fig.2.5 shows a readout IC for mutual capacitive TSP. It is composed of transmitter and receiver. To sense the mutual capacitance on TSP, Transmitter sends AC signal through the lower layer electrodes. Pulse signal or sinusoidal signal is used for AC signal. The AC signal is retrieved through the Receiver located at the end of electrodes in the upper layer. The receiver circuit is connected to the receiver electrode respectively.

Since the finger's touch on TSP affects the effective mutual capacitance at that point, it is possible to detect the touch point based on the current received at the Receiver side.

The receiver circuit is connected to the receiver electrode respectively. The advantage of the capacitive touch screen is that the channel of the transmitter and the receiver are not proportional to the number of capacitor nodes, but are proportional to the number of transmitters and receiver electrodes due to the capacitor of the array type.

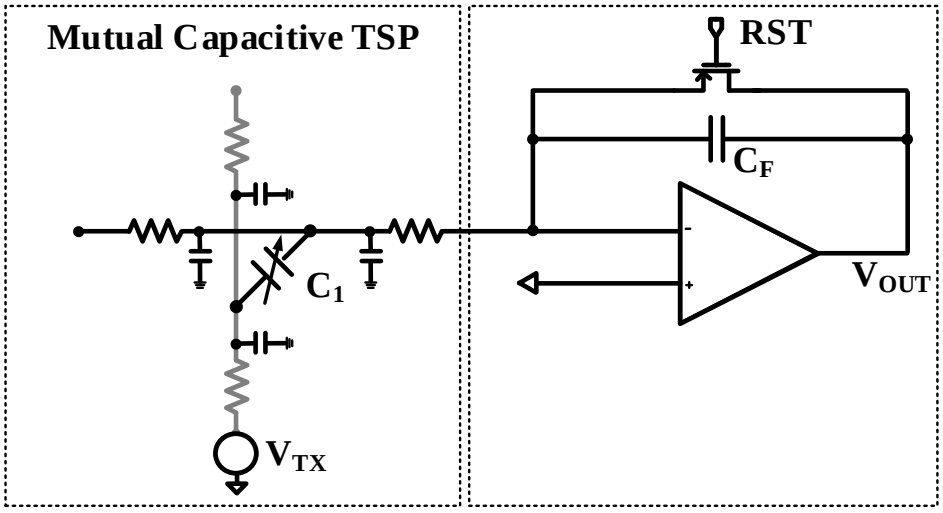

Fig.2. 6 A single-ended switched capacitor amplifier

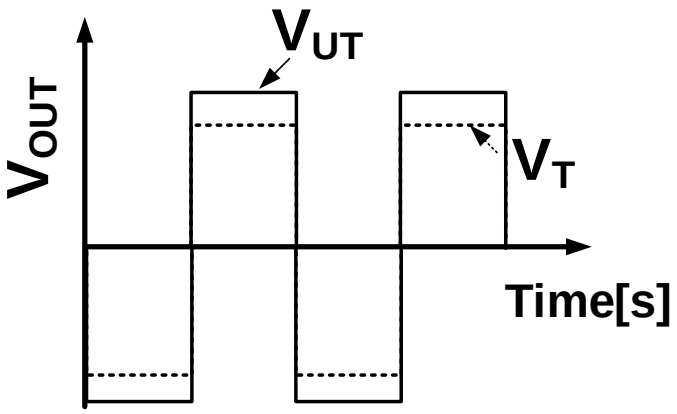

Fig.2. 7 An output of the single-ended switched capacitor amplifier

$$V_{SCA} = -\frac{C_1 - \Delta C_1}{C_F} V_{TX} \qquad (2.1.2.1)$$

In this section, the analog-front-end circuits for the mutual-capacitive touch screen system are presented. Fig.2.6. shows the switched capacitor (SC) amplifier and Fig. 2.6 shows an output of the single-ended switched capacitor amplifier [2.1], [2.2]. The output voltage is proportional to the input voltage and the ratio of sense capacitor and feedback capacitor regardless of the frequency of the input signal. The capacitance variation due to the touch is only about 5~10% of the entire mutual capacitor value. As a result, the output of the single-ended amplifier has an offset-capacitor value which is shown in fig. 2.7

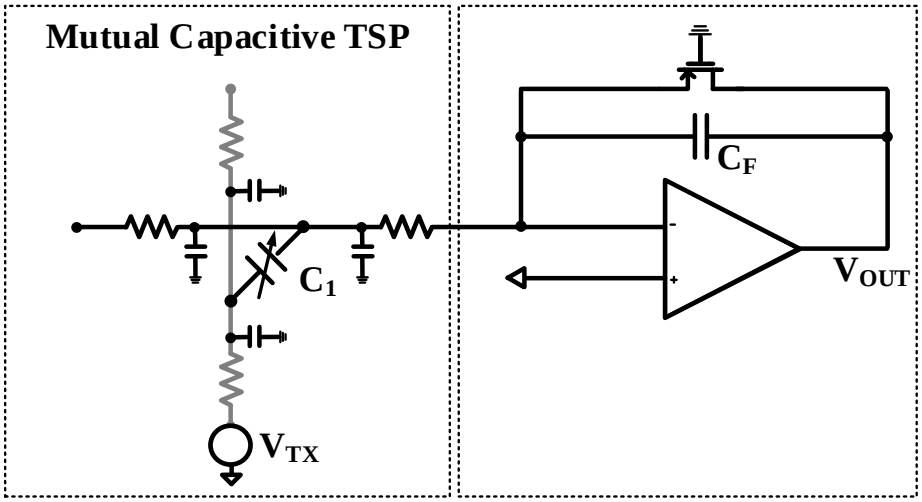

Fig.2. 8 A single-ended charge amplifier

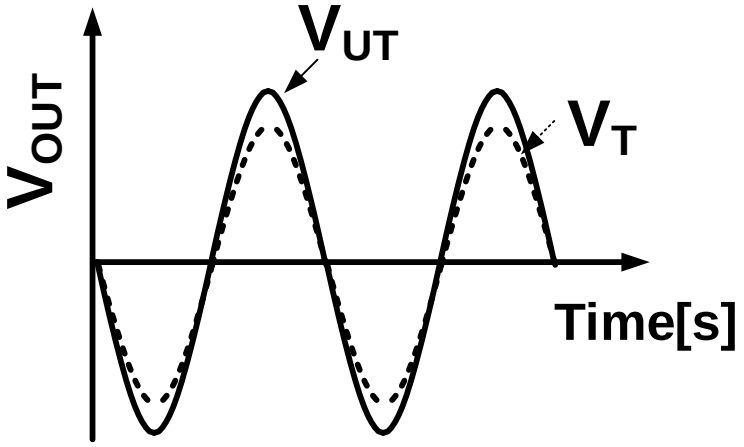

Fig.2. 9 An output of the single-ended charge amplifier

$$V_{SCA} = -\frac{C_1 - \Delta C_1}{C_F} V_{TX} \qquad (2.1.2.2)$$

In contrast with the SC amplifier, the charge amplifier is a continuous amplifier and plays role of the band pass filter [2.3]. The output voltage is proportional to the input voltage and the Ratio of sense capacitor and feedback capacitor. When touch is made, this sense capacitance is lowered by 10% that is caused by the mutual capacitance change. Fig. 2.8 shows a single-ended charge amplifier and Fig. 2.9 shows an output of the single-ended charge amplifier. Though the display noise of which frequency is 10~50kHz and the lamp noise of which frequency is 100~200kHz are filtered by the band pass filter, the dynamic range of the single-ended amplifier is too low and common-noise like a display noise is not completely removed.

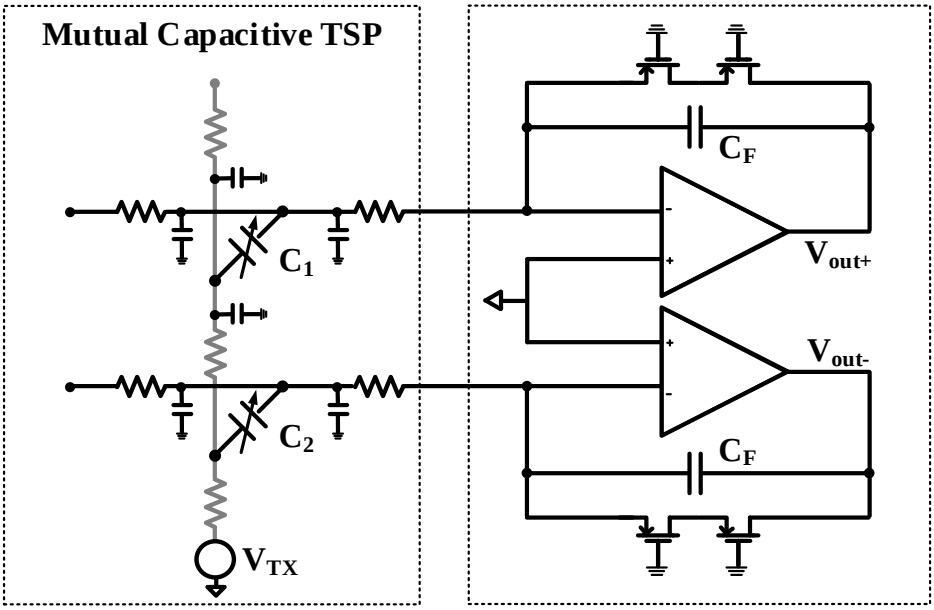

Fig.2. 10 A pseudo differential charge amplifier with two single-ended charge amplifiers

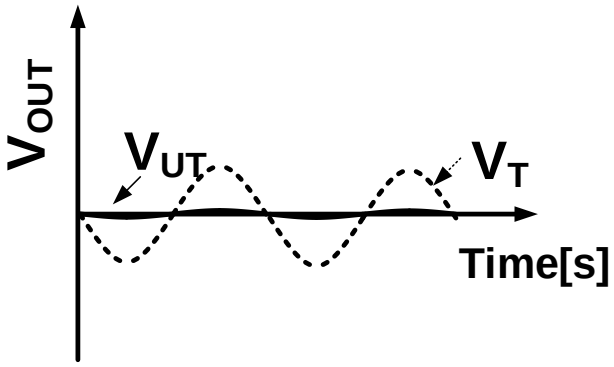

Fig.2. 11 An output of a pseudo differential charge amplifier with two single-ended charge amplifiers

$$V_{out} = V_{out+} - V_{out-} = -V_{TX}\frac{C_1 - C_2}{C_F} - V_{TX}\frac{\Delta C_1 - \Delta C_2}{C_F} \qquad (2.1.2.3)$$

Fig. 2.10 shows a pseudo differential charge amplifier with two single-ended charge amplifiers. An output of the pseudo differential amplifies is only proportional to the capacitor difference only compared to the single-ended amplifier. As a result, the differential amplifier effectively distinguishes the capacitance variance only without the static component of the capacitor. Fig. 2.11 shows an output of a pseudo differential charge amplifier with two single-ended charge amplifiers. A differential charge amplifier amplifies only delta signal and attenuates the noise signals by the band-pass filter.

2.1.3 Signal Processing

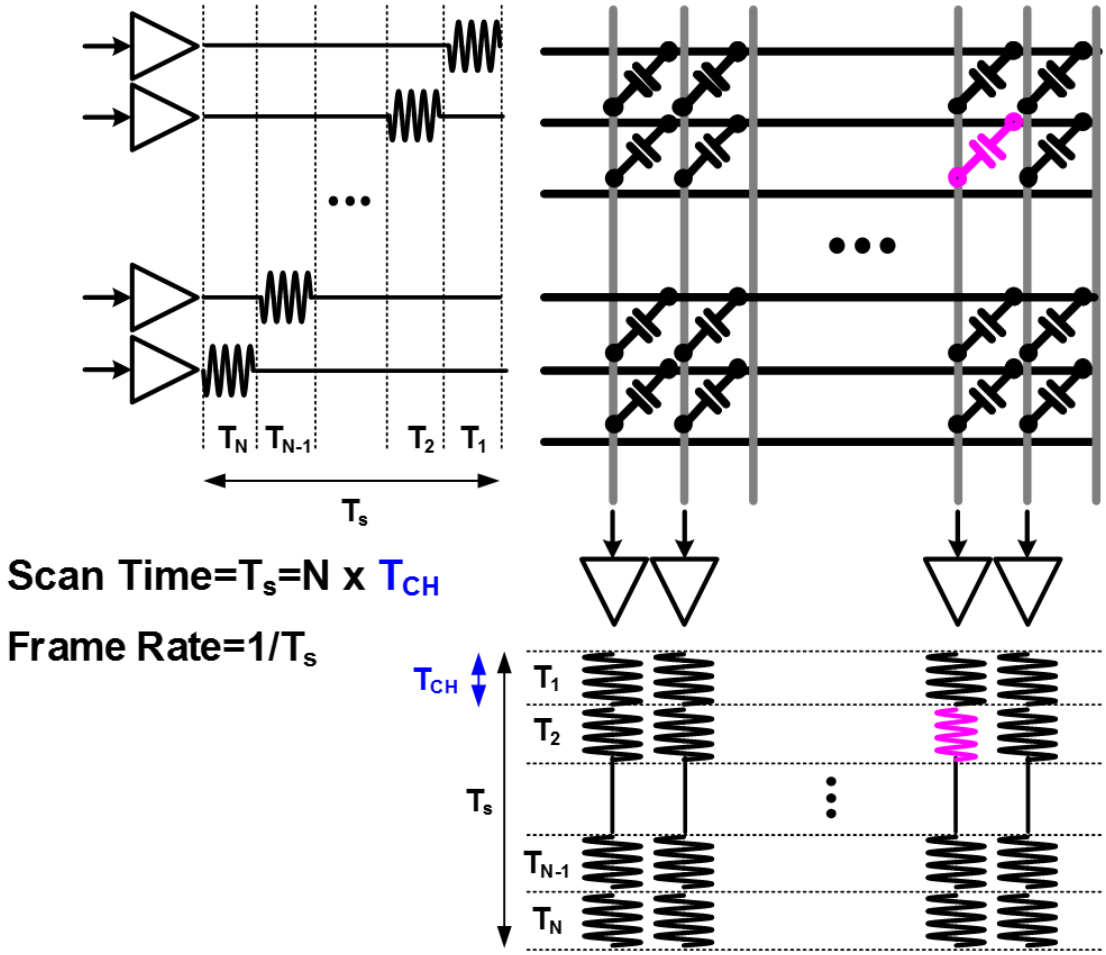

Fig.2. 12 Time-interleaved method for readout IC for mutual capacitive touch screen panel

A mutual capacitive TSP have a capacitor in a lattice structure. The simplest method for sensing the capacitors of such a lattice structure is the time-interleaved method (TDMA) [2.3]. The time division scheme divides the time and transmits the signal to the transmitter electrode line by line. Fig. 2.12 shows a TDMA scheme that divides the time to transmit signals to the transmitter electrode. The receiver can store a time-divisional output as shown in Fig. 2.12 to draw a capacitor maps in a lattice structure in mutual capacitive TSP. Let T_{CH} be the time required for each channel when transmitting a signal. The time that the transmitter sends a signal to N^{th} electrode is expressed as a product of N and T_{CH}, which can be defined as Scan Time, T_s. The inverse of Scan Time is defined as the Frame Rate. During the transmission time, T_{CH}, the AC signal with a specific frequency is transmitted. The transmission signal period is less than T_{CH}, and the signal of several cycles is sent to the transmitter electrode. The reason is that the capacitor size is confirmed by multiple sampling.

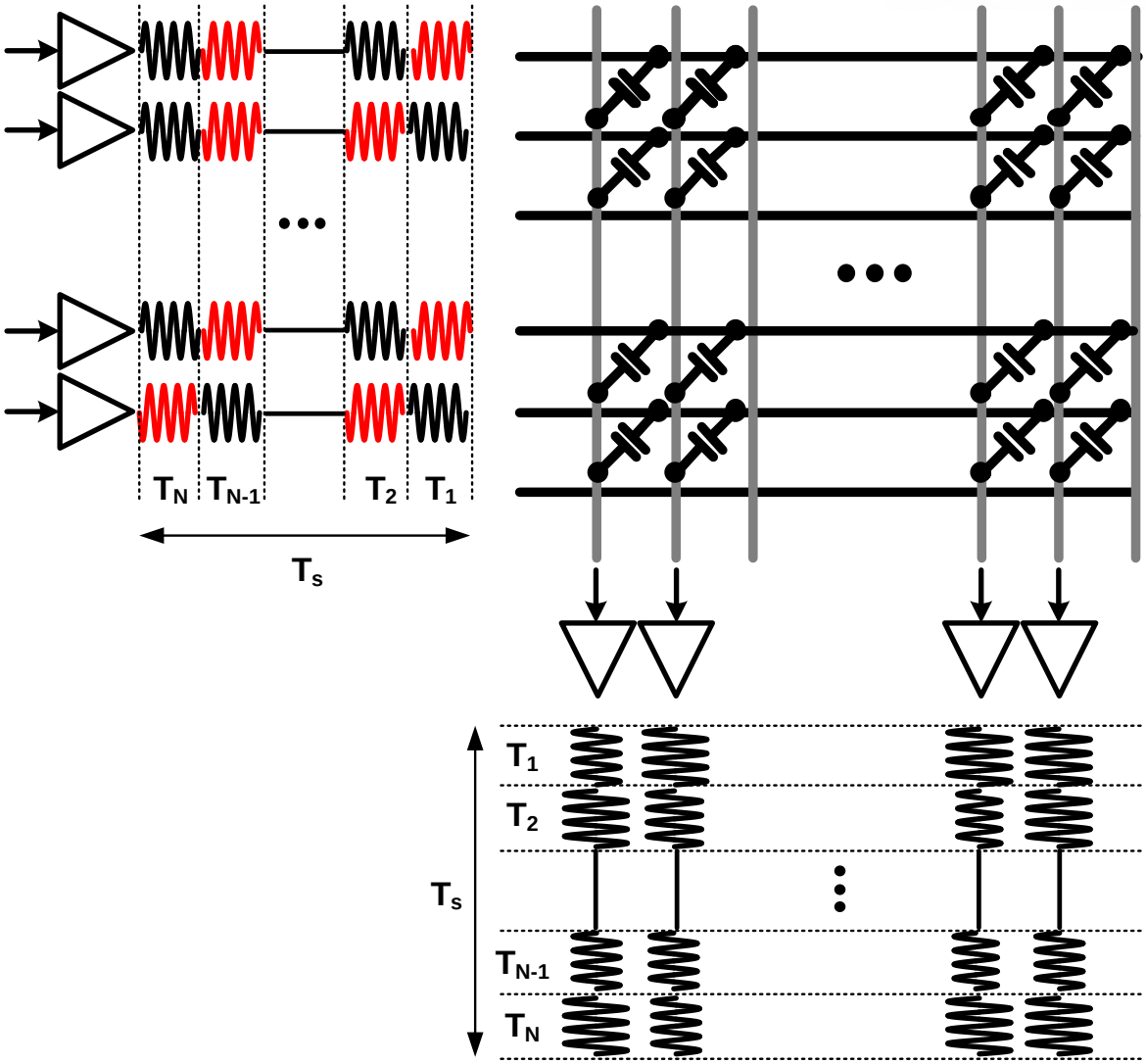

Fig.2. 13 Code Division Multiple Sensing Method for TSP with large number of channel

Also, if the multiple sampling is done at a high sampling rate, the random noise is reduced, and signal intensity is increased. This is called the moving average effect. Therefore, it is important to increase the T_{CH} to enhance the SNR. However, an increase in T_{CH} causes an increase in the scan time, that is, a decrease in the frame rate. As a result, it takes a long time to sense the entire touch screen, and the response time to the touch decreases. The same problem arises when the number of electrodes in the transmitter increases, like a large-sized TSP.

To overcome these issues, Code Division Multiple Sensing Method (CDMS) is presented, as shown in Fig 2.13 [2.3]. The SNR along with the frame rate and the total number of TX channel is the important parameter of the large touch screen application.

When transmitter sends the orthogonal code signals through each channel at the same time, it is called the CDMS or the parallel operation. The orthogonal signals are perpendicular each other. Though the orthogonal signals are mixed, the mixed signals are separated by multiplying the orthogonal signal of

each channel.

CDMS is made possible by utilizing an orthogonal code signal like CDMA theory [2.4]. This orthogonal code signal is a series of code signals composed of low-state or high-state signals. The product of the same orthogonal code signals is one, but the product of two other orthogonal code signals is always zero. The orthogonal signaling principles are given by

$$\begin{aligned} < X_i, X_i >= X_i \times X_i = 1 \\ < X_i, X_j >= X_i \times X_j = 0 \end{aligned} \tag{2.1.3.1}$$

Although the orthogonal signals are mixed, these mixed signals can be demodulated using the orthogonal signaling principle as in equation (2.1.3.1). The operation of a parallel architecture of a TSP is shown in Fig. 1. The transmitter sends orthogonal code signals to the electrodes of the transmitter on the TSP simultaneously. After orthogonal code signals are coupled to the mutual capacitor of the TSP, current from coupling capacitors is mixed in the electrode of the receiver on the TSP and flows from the TSP to the receiver. The receiver senses this current signal and by demodulation of this signal, it is possible to obtain the mutual capacitor value. The modulation and demodulation process is given by

$$\begin{aligned} H \times X + V_{noise} &= K + V_{noise} \\ X_{recover} &= H^{-1} \times K + H^{-1} \times V_{noise} \\ &= X + H^{-1} \times V_{noise} \end{aligned} \tag{2.1.3.2}$$

Where the H matrix represents the orthogonal signal, X means the capacitor matrix of the TSP, the K matrix means the output that the receiver receives without noise and the V_{noise} matrix is the external noise that is sampled at the receiver.

In the modulation process, H matrix is firstly multiplied by the X matrix, which means the capacitor of TSP is modulated by the orthogonal code signal. In this process, the V_{noise} matrix, which represents the sampled noise when the receiver receives the code signal, is added to K matrix, the modulated signals. In the demodulation process, the capacitor matrix, X is recovered by multiplying the inverse matrix of H. Although noise is inserted into the matrix of K, the noise matrix N is also multiplied by matrix H^{-1}. The inverse matrix of H is given by

$$\begin{aligned} H^{-1} &= \frac{1}{n} \times H \\ \left| H_{ij} \right| &= 1 \; ; i=1,2,...,n \; , \; j=1,2,...,n \end{aligned} \tag{2.1.3.3}$$

In case H is an $n \times n$ matrix of a Walsh-Hadmard Code (WHC), the inverse matrix of H is equal to a H matrix multiplied by 1 over n resulted from a Walsh-Hadmard transform. The external noise matrix multiplied by the inverse matrix of H is given by

$$(H^{-1}V_{noise})_{(i,j)} \approx \frac{1}{n}\sum_{k=1}^{n} h_{(i,k)} v_{noise,(k,j)} \;;i=1,2,...,n\ ,\ j=1,2,...,m \qquad (2.1.3.4)$$

Where $(H^{-1}V_{noise})_{(i,j)}$ is the noise component which is added to the capacitor component between ith driving line and jth sensing line and v_{noise} is the sampled noise at the time the receiver receives the mixed current. The external noise matrix demodulated by an inverse matrix of H is the average of the sampled external noise signal multiplied by WHC. Due to a moving average effect and orthogonality between the external noise and WHC, external noise is considerably distributed. Furthermore, by using a N size of WHC, it is possible to use the N-channels for multi-driving resulting in a N-stimes channel usage larger than that of a time-interleaved method. Consequently, to increase the size of WHC, N enhances the SNR and frame rate product per the channel thanks to both the noise distribution and the extended channel usage.

$$SNR_{CDMA} \propto \sqrt{N} \times SNR_{TDMA} \qquad (2.1.3.5)$$

$$E = \int_{-\infty}^{\infty} |x(t)|^2 \, dt = \int_{-\infty}^{\infty} |X(f)|^2 \, df \qquad (2.1.3.6)$$

As a result, the SNR by the CDMS scheme is root N times increased compared with the scheme by the TDMA. Where N is equal to the number of codes that are sent simultaneously from the CDMA to the transmitter. The reason is by Parseval's theorem. Parseval's theorem is the sum (or integral) of the square of a function. The time of the signal transmitted by the CDMS method is increased by N times as compared with the time of the signal transmitted by the TDMA method. This increases the Signal Intensity by a factor of N times, so that the SNR increases by the same amount as the TDMA. However, in CDMS, this effect should be considered because the SNR is reduced to some extent by the inter-channel interference.

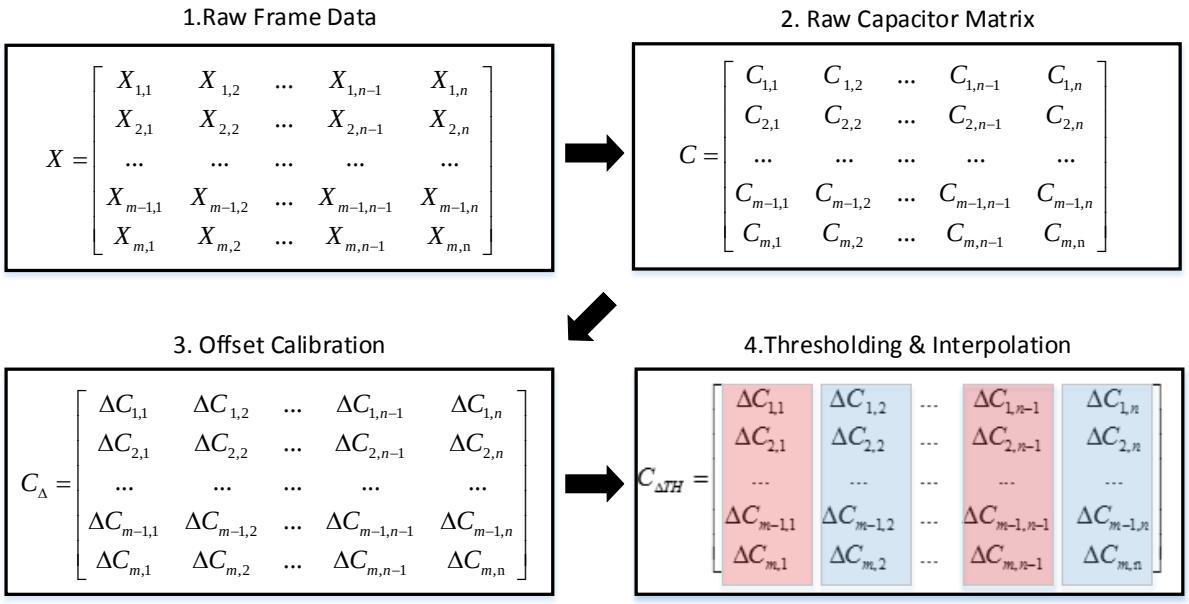

Fig.2. 14 Digital Processing of Fingerprint Recognition

The transmitter transmits the AC signal to the transmitter electrode through TDMA or CDMS method, and the receiver receives the current signal from the touch screen and converts it into the voltage signal. This voltage signal is converted to a digital signal through an analog-to-digital converter (ADC). A digital processor, such as microcontroller unit (MCU), or field-programmable gate array (FPGA) converts digital raw data into a fingerprint image. Digital Process generates frame data matrix as shown in Figure 2.14 using received digital signal [2.5]. The form of the raw frame data is determined by the signaling of the transmitter and the circuit of the receiver.

In the case of a single-ended output circuit, a capacitor of each point of the mutual capacitive TSP is immediately corresponded to the single-ended output. In the case of a differential output circuit, however, it represents a value corresponding to the difference between two adjacent capacitors. In the case of the output of the TDMA, the time is divided to divide the Transmitter Electrode, but in the case of the CDMA output, an output corresponding to the sum of the products of the orthogonal signals and the corresponding mutual capacitors is generated. In this case, an additional demodulation process is required. A several of outputs are converted into a capacitor array matrix form through the demodulation process such as an Equation 2.1.3.2. After the demodulation process, raw capacitor matrix, C (i, j), is obtained, which is equal to the mutual capacitor value in the intersection of the i^{th} driving electrode and the j^{th} sensing electrode.

The Raw Capacitor Matrix output is subjected to an offset calibration process to generate the output CΔ matrix. CΔ matrix is processed through thresholding and interpolation to finally generate the fingerprint image.

2.2 Fingerprint Mutual Capacitive Touch Screen Panel

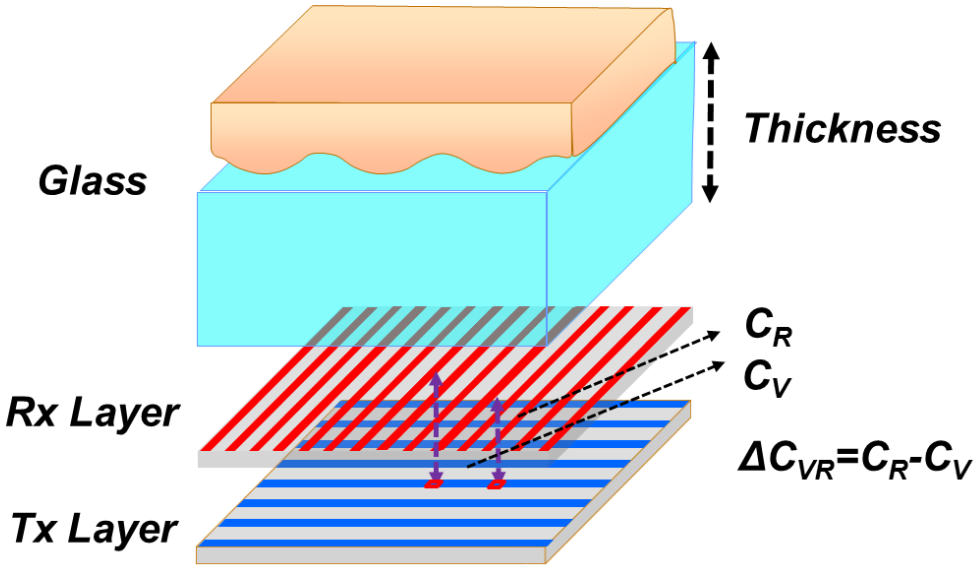

Fig.2. 15 The fingerprint mutual capacitive TSP

The structure of the capacitive fingerprint recognition touch screen, cover glass and fingerprint are shown in Figure 2.15. The biggest difference between the TSP for fingerprint and the existing mutual capacitive TSP is the pitch between the electrodes of transmitter layer and receiver layer. In the case of conventional touch screens, the gap between the electrodes is 0.3 to 0.5 mm. However, the pitch between the electrodes in the fingerprint recognition touch screen is about 50μm ~ 80μm. A resolution of mutual capacitive fingerprint TSP is 500 dpi when a pitch is about 50 μm. A 500 dpi resolution is required by FBI-compliant systems. The minimum resolution for confirming fingerprints is at least about 300 dpi. In Figure 2.15, the lowest layer is the Transmitter layer, and the receiver layer is placed on it. The size of the mutual capacitance under the ridge of the fingerprint is defined as C_R, and the size of the mutual capacitance under the fingerprint valley is defined as C_V. The capacitance difference due to the fusion and the bone of the fingerprint is defined as ΔC_{VR}. As the ΔC_{VR} value become larger, the fingerprint mutual capacitive TSP has the higher the sensitivity. The sensitivity of the conventional mutual capacitive TSP is about several tens to several hundred fF, which is the difference in capacitance between the touch and the un-touch. However, the capacitance difference between ridges and valley of the fingerprints in the fingerprint recognition TSP falls below 1fF. The thicker the thickness of the glass, the smaller sensitivity becomes [2.6].

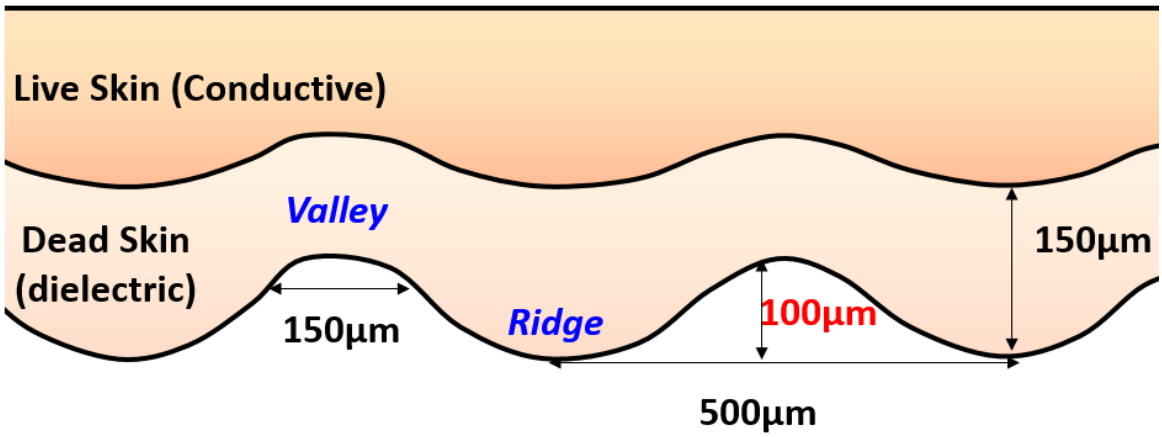

Fig.2. 16 The cross-section of fingerprint

Fig. 2.16 shows a simplified structural model of the human skin. The human skin is composed of the dermis layer and epidermis layer. The epidermis layer is a dry dead skin cells which have low electrical conductivity. This region behaves as a dielectric. The dermis layer are live cells which is moist and electrically conductive.

A fingerprint is made of many ridges and valleys on the surface of the finger. Ridges are the outside skin layer segments of the finger and valleys are the inside skin layer segments. The width of the ridges varies between 0.5 ~ 0.7 µm and the width of the valleys are ~ 0.15 µm. The depth of the valley varies between ~150 µm. Since the depth of the valley is lower than 150 µm, the capacitor difference due to the valley and ridge is also very small. In contrast with the touch screen, a fingerprint touch screen should distinguish the pattern of the valley of which depth is lower than ~150 µm [2.6].

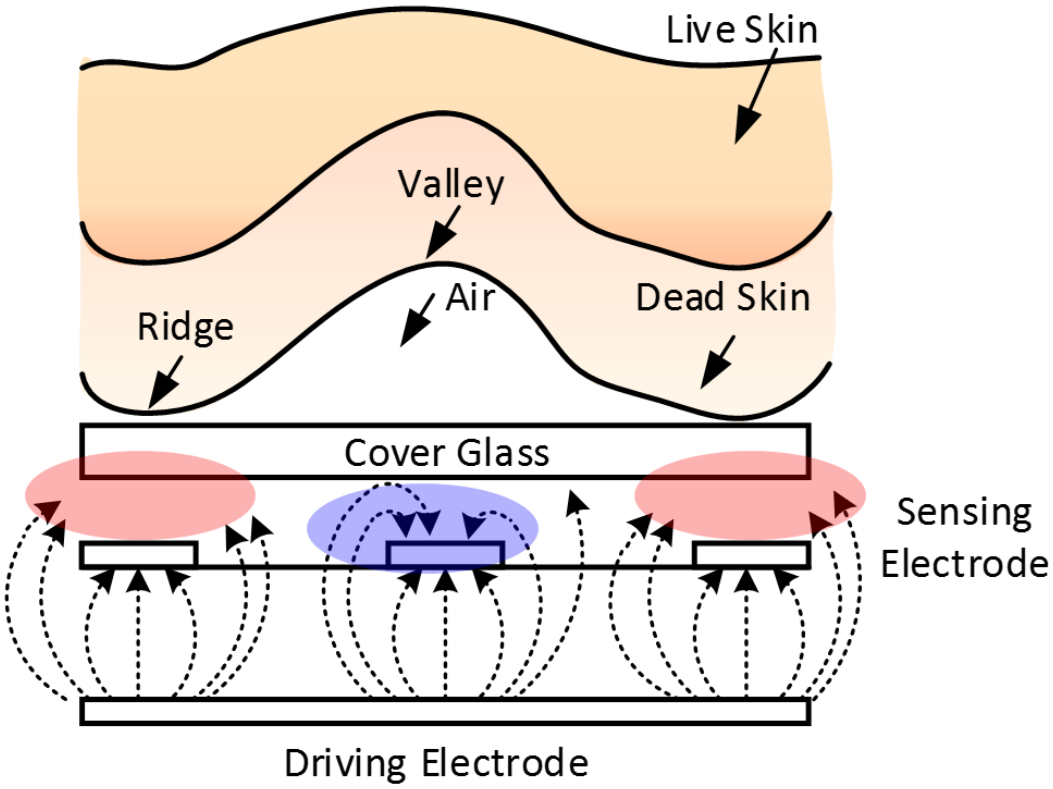

Fig.2. 17 The cross-section of fingerprint and fingerprint TSP

Fig. 2.17 shows the pixel structure and electric field geometry for a fingerprint mutual-capacitive sensor. When transmitter sends AC signal to driving electrode fig. 2.17, a fixed charge is placed on the electrode of the driving. There are electric fields between the driving electrodes and the sensing electrode of mutual capacitive fingerprint TSP. In addition, there are additional electric fields at the edge of the electrodes. This is a capacitive fringing field, so the field geometry is hemispherical.

When a ridge patterns of the finger touches the fingerprint TSP, the electric fields are shunt to the ground through the ridges patterns. The electric field appearing at a ridge pattern is different from those appearing at the valley patterns. There is an air gap between the valley and the cover glass, which make a different electric field.

As a result, since there are permittivity difference between dead skin and air, the absorbed fringing field from the electrode to the valley is lower than that absorbed from the electrode to the ridge. Therefore, the valley will show a lower capacitance variation than the ridge. By sensing the depth difference from the capacitance difference affected by the fringing field difference, it is possible to distinguish between ridges and valleys.

2.3 Touch Screen Environment Noise

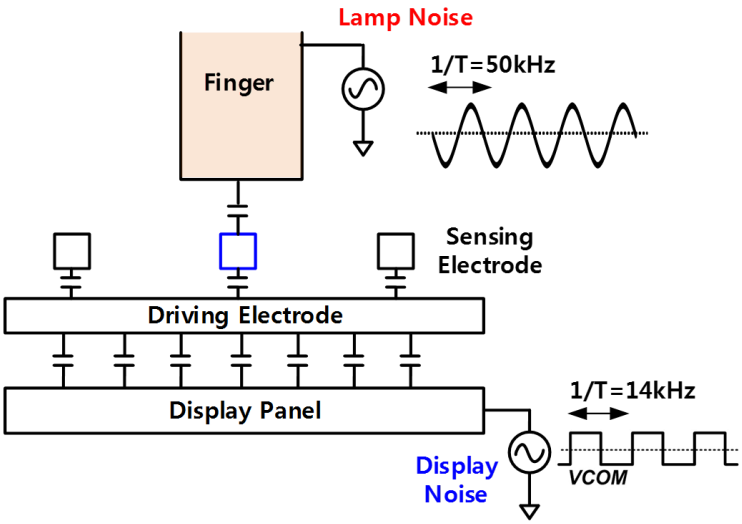

Fig.2. 18 Touch Screen Environment Noise: Lamp Noise and Display Noise

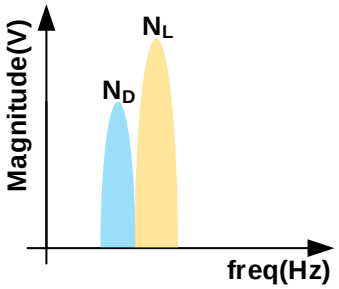

Fig.2. 19 Frequency Spectrum of Touch Screen Noise: N_L: Lamp Noise, N_D: Display Noise, N_W: White Noise, N_F: Flicker Noise

However, in realistic TSP environment, we need to consider some common noise sources in TSP. Fig. 2.18 shows the display backlight noise and lamp noise. Display backlight noise is a coupling noise caused by the back-light of each TSP. There are coupling capacitor between TSP and the given Display Panel. When display backlight is lit, a display backlight noise is coupled into the TSP thorough this coupling capacitor to suppress this noise, it is necessary to use differential architecture since this display backlight noise is a common noise. In the meantime, a Lamp Noise is different. Lamp noise is originated from lamps in vicinity. Ordinary Lamps produces AC noise signal that can be coupled through the finger that is touching the TSP. This noise originated from a neighboring lamp is coupled into the electrodes inside a TSP. Hence, this is not a common noise that can be easily suppressed with differential architecture. Fig.2.19 shows a frequency spectrum of touch screen noise. Additional, internal noise source like white noise and flicker noise effect SNR of readout IC

2.4 Performance evaluation

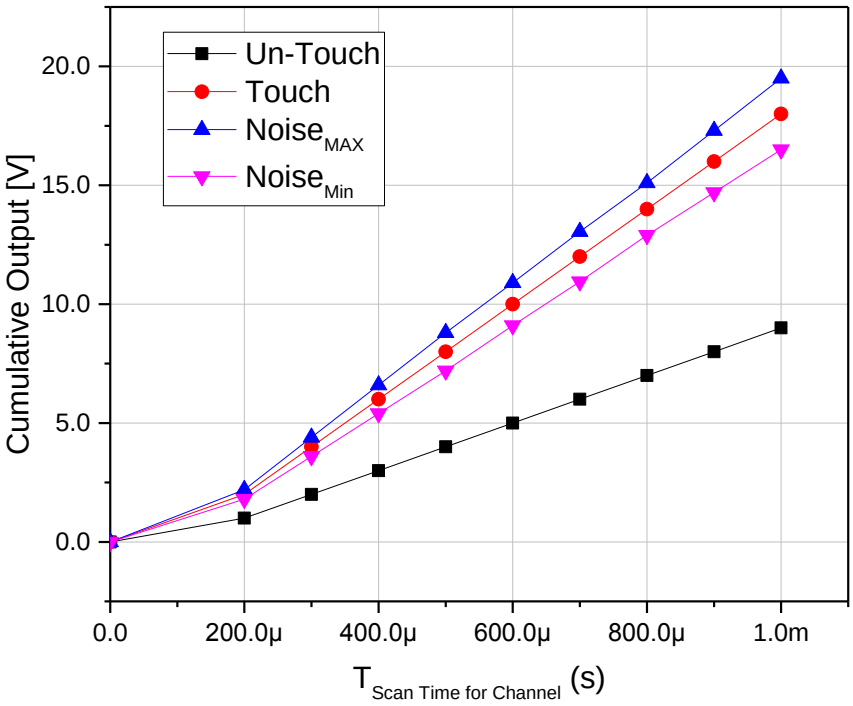

Fig.2. 20 Cumulative Output according to the scan time for channel

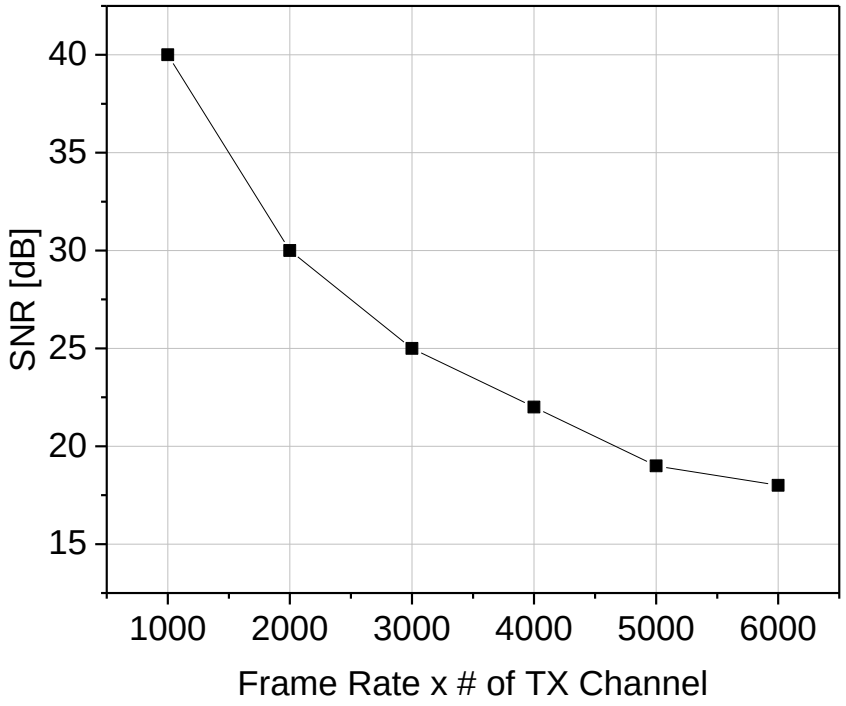

Fig.2. 21 Signal to Noise Ratio according to the frame rate and the number of TX channel

SNR and Frame rate are important parameter to evaluate performance of readout IC for touch screen

panel. SNR means how readout IC can detects touch screen accurately and Frame rate means how fast readout IC detects touch screen.

$$SNR(dB) = 20Log(TouchStrengh / NoiseTouched_{RMS}) \quad (2.1.3.7)$$

$$TouchStrength = SignalTouched_{AVG,N} - SignalUntouched_{AVG,N} \quad (2.1.3.8)$$

$$NoiseTouched_{RMS} = \sqrt{\frac{\sum_{k=1}^{N}(Singal[k] - \mathrm{SignalTouched}_{AVG,N})^2}{N}} \quad (2.1.3.9)$$

To enhance the environmental noise of a touch screen, multiple sampling and averaging of the output signal is required for the readout IC (ROIC) of a device with a touch screen. Fig. 2.20 shows the accumulated signal and the RMS noise according to the scan time allocated to the channel, when the TCH is increased. No matter how small the signal is, if the signal is accumulated after sampling several times, the accumulated signal will increase in size. In case of noise, it is dispersed by Moving Average Effect (MAE). Thus, Root-Mean-Square (RMS) noise is decreased.

Through the cumulative output, the SNR can be obtained from Equation 2.1.3.7 to Equation 2.1.3.9. In equation, 2.1.3.8, TouchStrength is the difference between the average of N samples when touching and the average of N sample when not touching. Equation 2.1.3.9, RMS Noise is equal to the variance of the value obtained by subtracting the average of N samples when touching the accumulated SNR steadily increases within a certain scan time. As shown in Fig. 2.21, SNR is decreased when product of frame rate and the number of TX channels is increased, since the TCH is decreased. Thus, it is necessary to consider both Frame rate and SNR simultaneously.

Chapter III

III. Preliminary Research for TSC in Large-sized TSP

3.1 Design Issues of Multiple Channel Touch Screen Panel

Fig.3. 1 Large-size Touch Screen Panel with Multiple Channel

Fig. 3.1. Shows a large-size Touch Screen Panel with multiple channel. A mutual capacitive TSP is susceptible to environmental noise such as from the display backlight, charger and lamp. To reduce the environmental noise of a touch screen, multiple sampling and averaging of the output signal is required for the readout IC (ROIC) of a device with a touch screen.

However, as TSP size increases, both parasitic resistance and capacitance values increase. This increased RC time constant limits the sampling rate, resulting in fewer samples for a given time. Moreover, in a larger-sized TSP, the total number of sensing channels increases, resulting in a reduced scan time allotted to each channel. Consequently, the reduced scan time per channel limits the ability to perform multiple sampling, resulting in a deteriorated signal-to-noise ratio (SNR).

Therefore, for an accurate evaluation of TSP ROIC performance in a large-sized TSP, it is important to recognize, not just the SNR alone, but the SNR along with frame-rate and total number of TX channels.

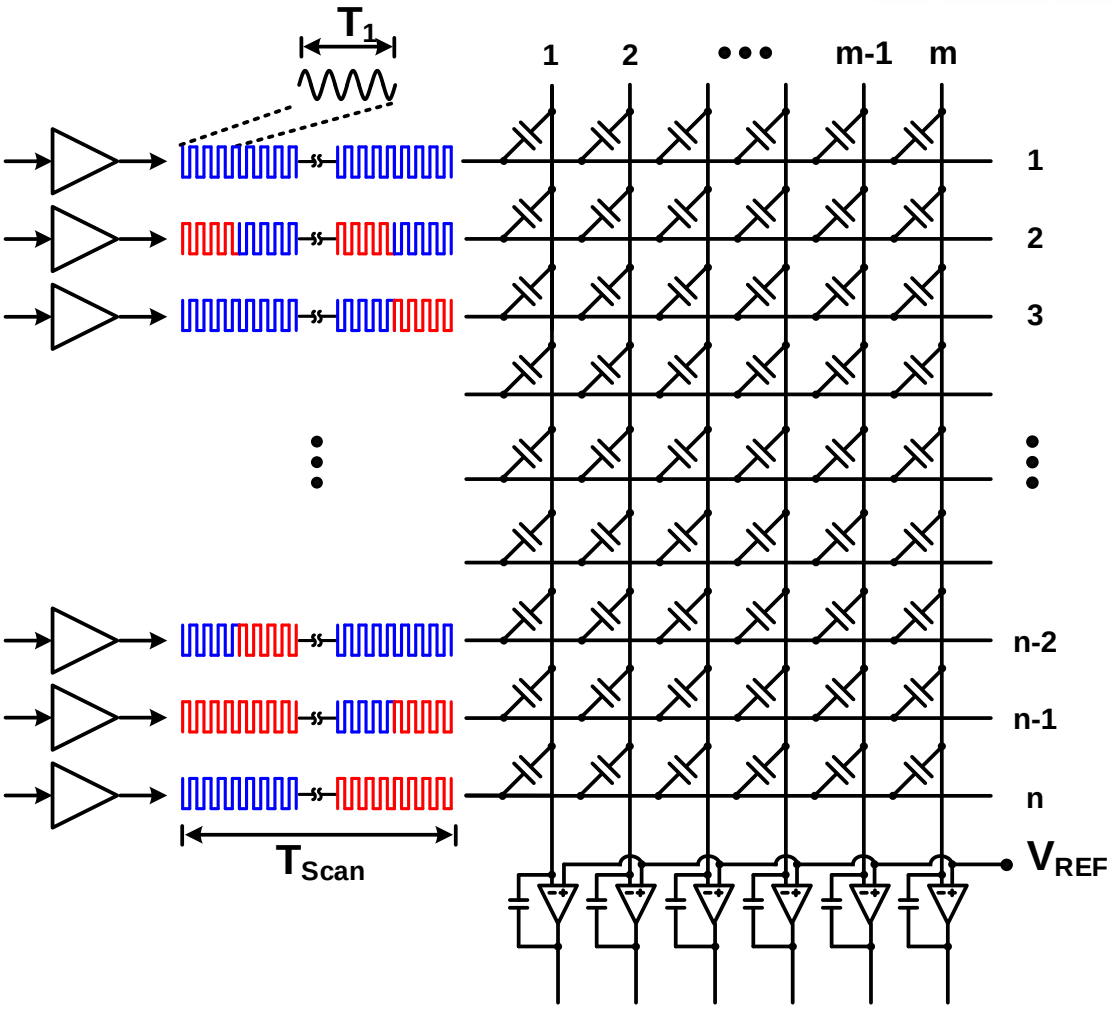

Fig.3. 2 Single-ended Amplifier with Discrete-mode parallel operation architecture (SDPA)

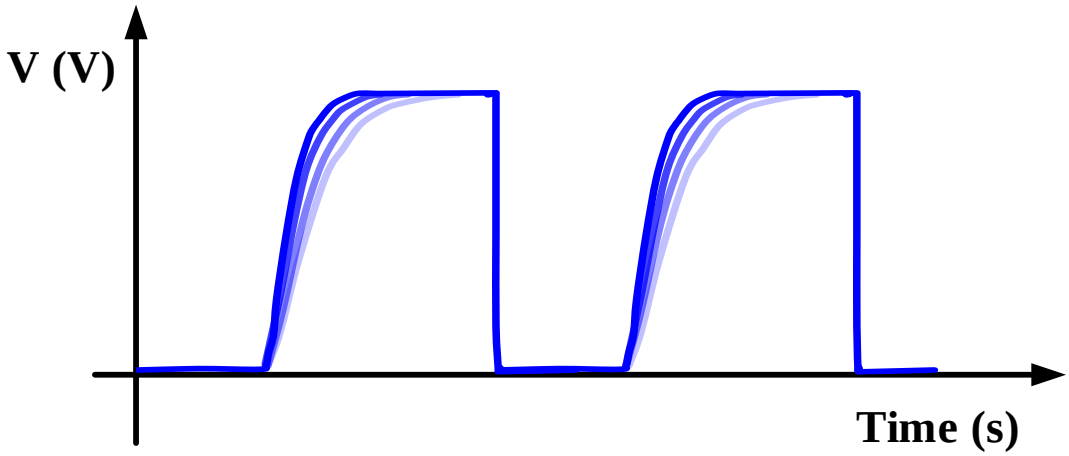

Fig.3. 3 Single-Ended Parallel Discrete-mode Output of Switched Capacitor Amplifier

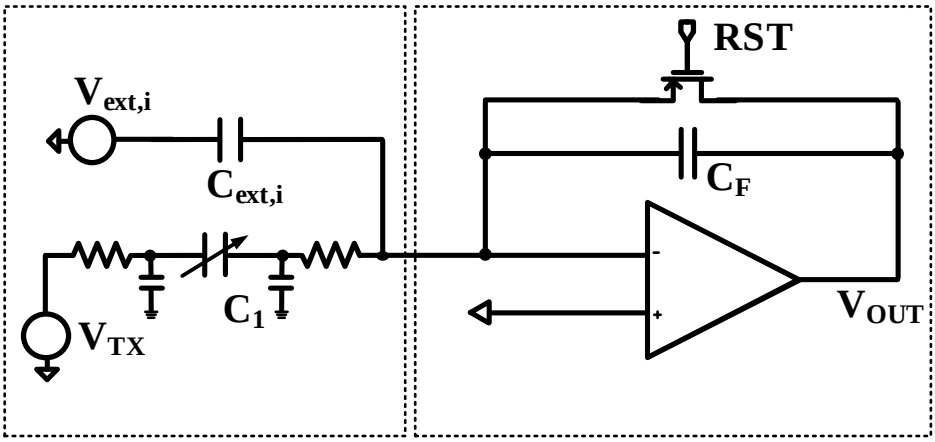

Fig.3. 4 A Single-ended Switched Capacitor (SC) Amplifier

One way to enhance the SNR in a limited time in a large-sized TSP is a code-division multiple sensing (CDMS) method. In this method, multiple orthogonal signals go through TX electrodes simultaneously. Compared to a time-interleaved method, it is possible to emit a higher excitation signal power in the same period through multiple signalling with the CDMS method [3.1], [3.2], [3.3]. Previously, a switched capacitor amplifier with a parallel operation method (SDPA) has been used in a mutual capacitive TSP sensor interface circuit as shown in Fig.3.2. This switched-capacitor amplifier (SC) with a parallel operation architecture obtained a higher SNR in a limited time than that of a time-interleaved method. In addition, SC with parallel operation does not have a low channel interference since the operation of SC is based on sampling and hold

However, the main disadvantage of the SC amplifier with a parallel operation based on a sample-data system is that it cannot alleviate the self-noise, which is a non-common noise, where the frequency is close to the input frequency [3.2].

$$V_{out} = -V_{TX}\frac{C_1}{C_F} + \sum_{i=1}^{N} V_{Noise,i}\frac{C_{ext,i}}{C_F} + \sum_{k=1}^{N} V_{Noise,\mathrm{k}}\frac{C_{ext,\mathrm{k}}}{C_F} \qquad (3.1.1)$$

Fig.3.4 shows a single-ended SC amplifier with external noise source, $V_{ext,i,}$, and coupling capacitor, $C_{ext,i}$. Equation 3.1.1 shows a output of SC amplifier. SC amplifier cannot remove an external noise sources due to the sampling method.

As a result, even though the CDMS method can increase signal power density, the sampled noise without a self-noise immunity circuit significantly decreases the signal-to-noise ratio (SNR).

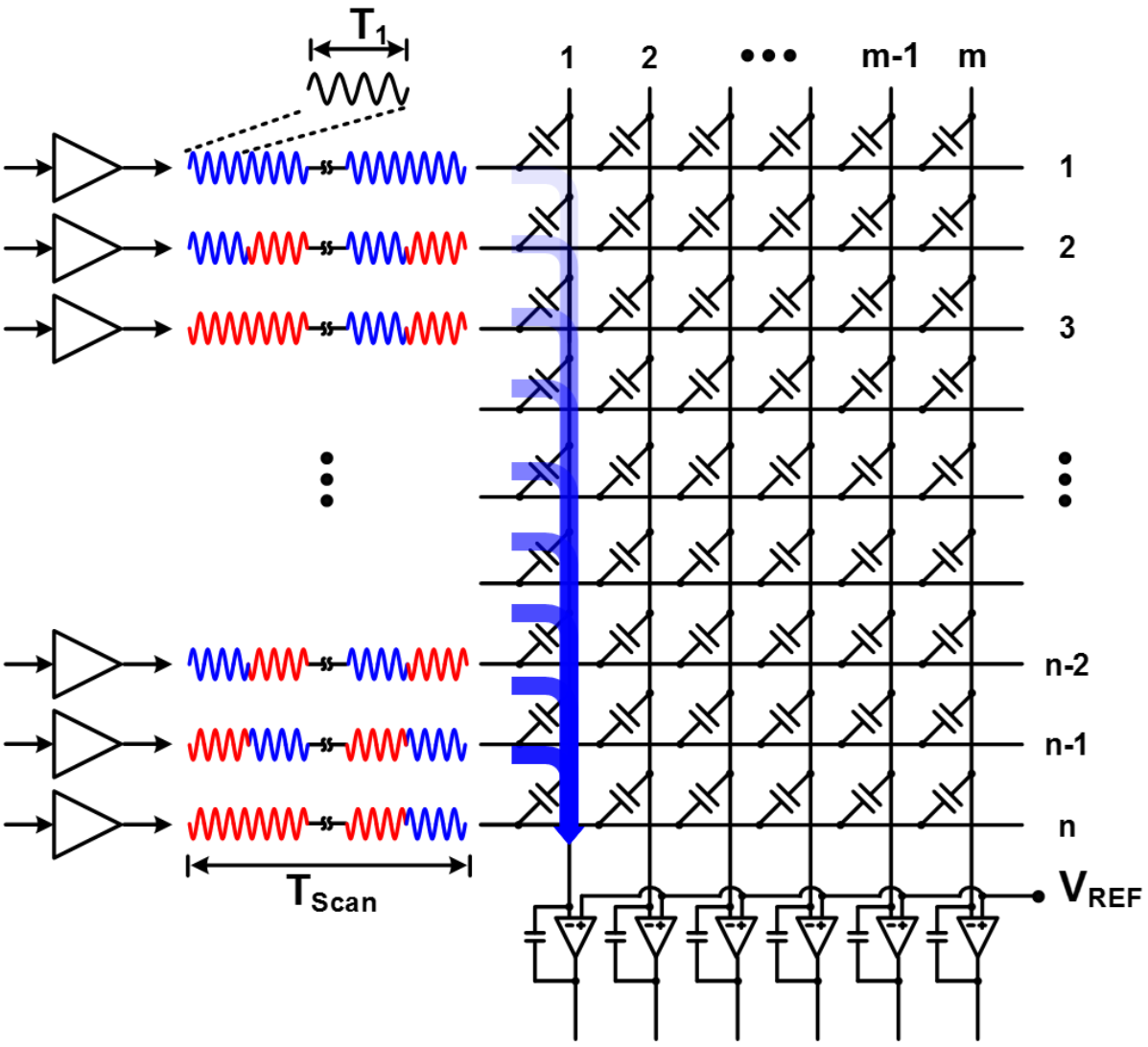

Fig.3. 5 Single-Ended Amplifier and Parallel Driving Operation with Channel Interference

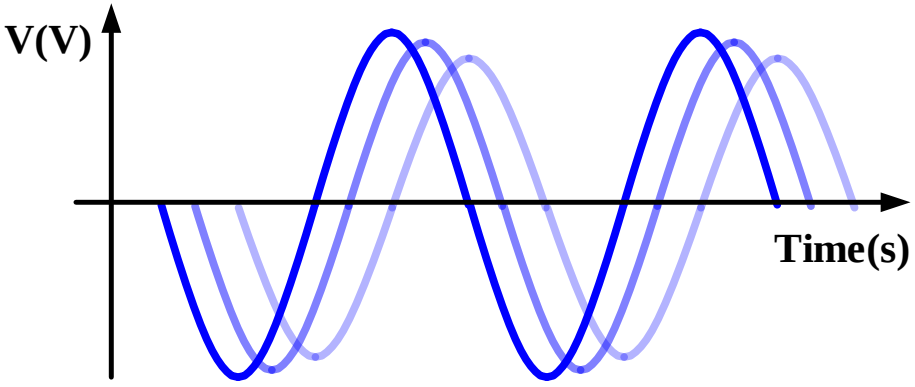

Fig.3. 6 Channel Interference in Single-Ended Parallel Continuous Amplifier with Channel Interference

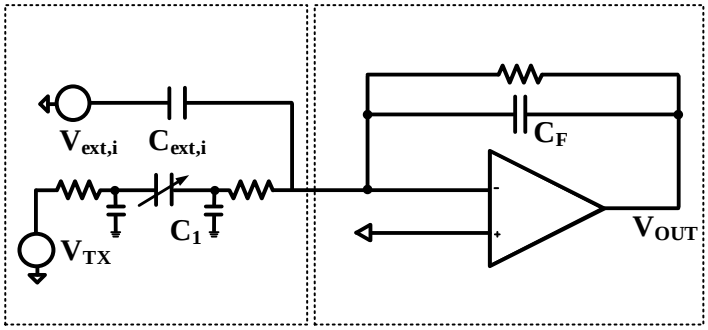

Fig.3. 7 A Single-ended Charge Amplifier

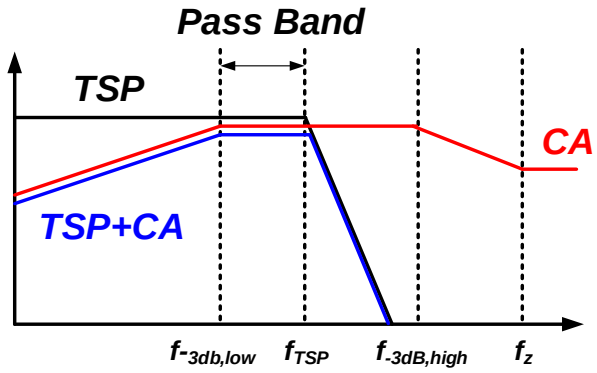

Fig.3. 8 Frequency Characteristic of Charge Amplifier

$$V_{out} = -V_{TX}\frac{sR_FC_1}{1+sR_FC_F} + \sum_{i=1}^{N} V_{ext,i}\frac{sR_FC_{ext,i}}{1+sR_FC_F} \qquad (3.1.)$$

Fig.3.5 shows a Single-Ended Charge Amplifier (SCA) as the receiver circuits with parallel architecture. Fig.3.6 shows a channel interference by the resistive and capacitive load of the mutual capacitive TSP [3.4], [3.5]. Fig.3.7 shows a single-ended charge amplifier (SCA) circuit. It has a band-pass filter characteristic as shown in Fig.3.8. Thus, it is possible to attenuate touch-injection noise signal like lamp noise. SCA with a parallel operation can alleviate the self-noise and increase the signal power spectrum density simultaneously. As a result, it can accomplish the higher SNR compared to that of SDPA.

However, there are channel interference due to the resistive and capacitive load of the mutual capacitive TSP as shown in fig3.5 and fig.3.6 [3.6]. As a result, the number of orthogonal code to send transmitter electrodes is limited. There is limitation of the SNR improvement of the SCA with parallel operation. In addition, SCPA does not have a common-mode noise immunity due to the single-ended architecture.

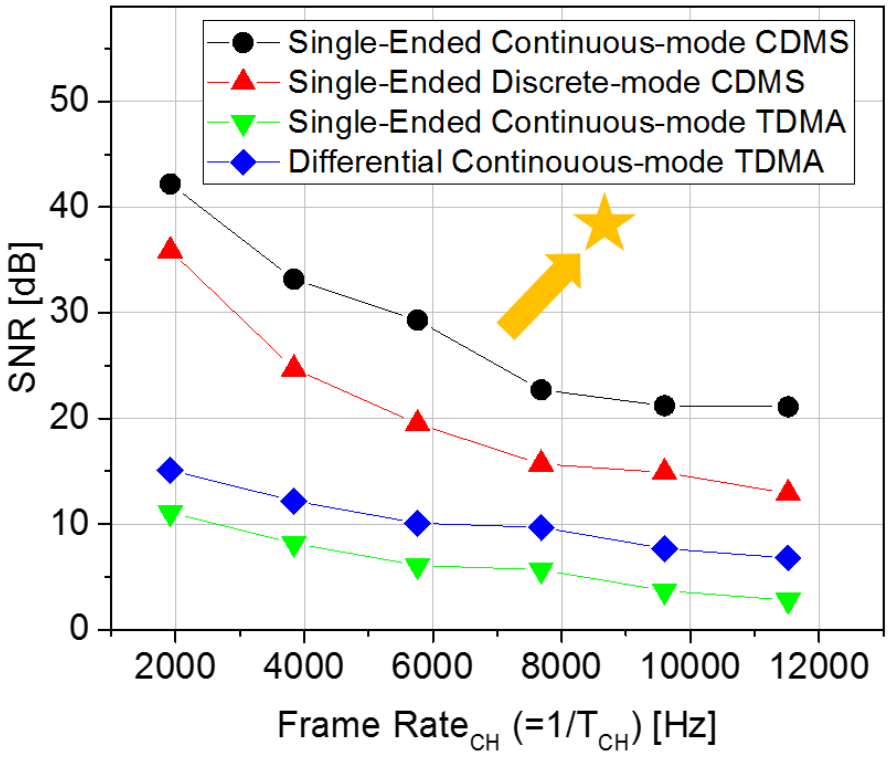

Fig.3. 9 A mutual capacitive touch screen architecture

Previously, the parallel operation architecture is applied to the single-ended circuits due to the absence of the demodulation of the differential parallel operation. However, it is necessary to enhance a higher SNR with high frame rate, a differential parallel architecture is requited. Fig.3.9 shows a SNR along with the frame rate and the number of TX channel of previous architecture. SCPA (Single-Continuous-Mode Parallel Architecture) does not have a common-mode noise immunity and suffers from channel interference in the load of the mutual capacitive TSP. SDPA avoid the channel interference due to the discrete mode. However, SDPA does have a touch-injection noise and common-mode noise immunity. DCTA (Differential-Continuous-Mode-Time-interleaved Method) has a higher noise immunity, however, it is not suitable for the architecture in large-sized TSP due to the time-interleaved method.

In this section, a differential continuous-mode parallel operation architecture (DCPA) is proposed to achieve a high SNR and frame rate product in a large-sized TSP. DCPA is composed of a differential parallel architecture that is operated in a continuous-mode.

DCPA has a higher noise immunity due to the DCA. Also, it has high signal intensity in large sized TSP due to the parallel operation. In this section, to realize DCPA, a differential parallel modulation and demodulation is presented in this section. In addition, receiver circuits to appropriate the DCPA is presented.

3.2 The Differential-Continuous-mode Parallel Architecture

3.2.1 SNR of Differential Continuous Parallel Architecture

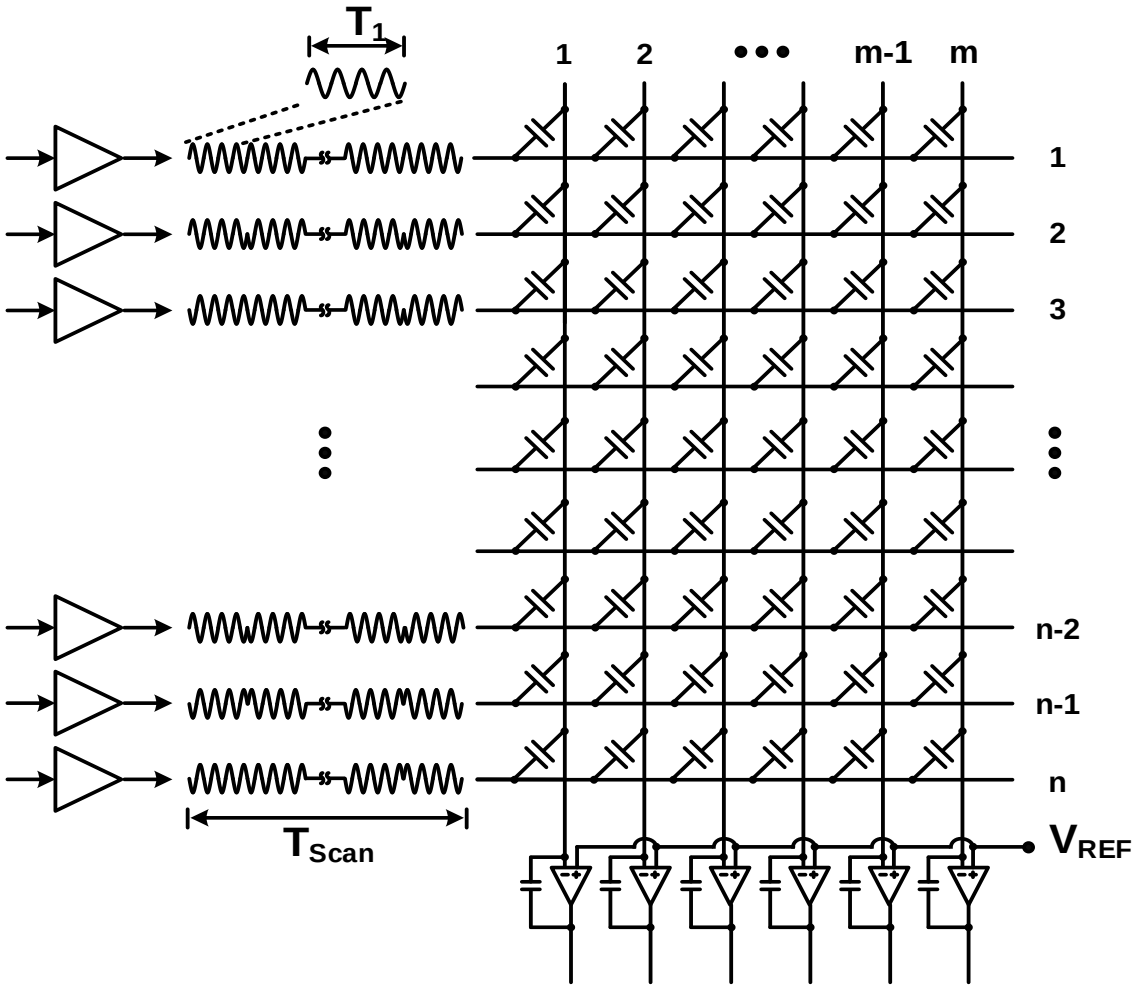

Fig.3. 10 Mutual capacitance and parasitic component in the single-ended-continuous-mode parallel operation architecture (SCPA)

A Charge Amplifier (CA) has been widely used as capacitor sensing circuit for high SNR systems since this circuit continuously attenuates touch screen environment noise like a band-pass filter when the frequency is close to the frequency of the input signal [3.6], [3.7]. To enhance SNR for a limited time in a large-sized TSP, the parallel operation architecture ROIC is implemented in a CA circuit. Since a CA circuit with a parallel operation architecture can increase power spectral density at the same time to attenuate noise, it is suitable for a large-sized TSP where the allotted time slot is limited for each channel.

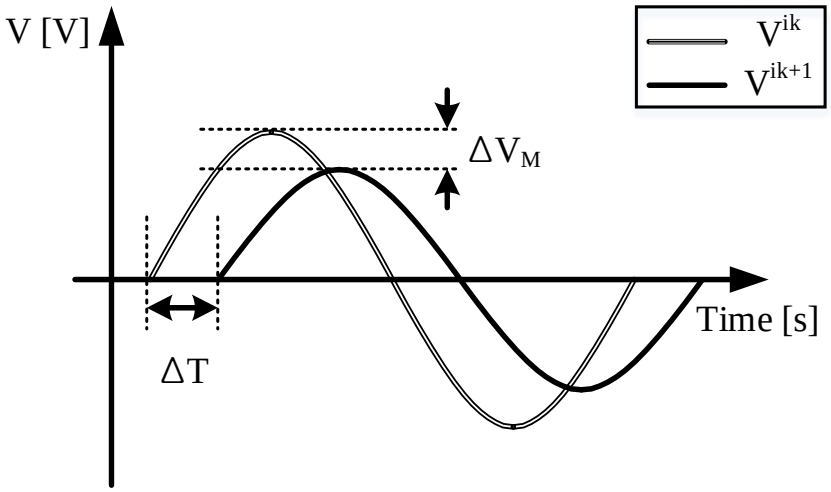

Fig.3. 11 The output of CA circuit in a large-sized touch screen

Fig. 3.10 shows SCPA as an analog-front-end circuit in a mutual capacitive TSP. The output of SCPA in a j^{th} sensing electrode is given by the following equation:

$$V_{SCPA,j}(t) = \sum_{i=1}^{n}\left[A_m H_i(t) \frac{C^{(i,j)}}{C_F} \sin wt \right] \qquad (3.2.1)$$
$$: j=1,2,\cdots,m \text{ and } H_i(t)=-1 \text{ or } 1$$

Where T_1 is the time for the multiple sampling of low-state or high-state signal, T_{Scan} is the scan time the read-out IC scans the whole TSP, and the column conductors of TSP, 1, 2, …, n are connected to a driving signal and the row conductors of the TSP. 1, 2, …, m are connected to the input of the CA circuit, Am is amplitude of the modulation signal, Hi is a orthogonal code signal's coefficient of i^{th} driving line, CF is the feedback capacitance, C(i,j) is mutual capacitance between i^{th} driving line and j^{th} sensing line and sin(wt) means continuous signal with no additional delay.

However, the output of CA in a large-sized TSP is affected by parasitic components resulting in timing skew and gain error. The CA output in a large-sized TSP is now given by

$$V_{SCPA,j}(t) = \sum_{i=1}^{n}\left[A_m H_i(t) \frac{C^{(i,j)}}{C_F} \sin(wt+\phi_{(i,j)})\left(1-\frac{C^{(i,j)}}{C^{(i,j)}+C_F+C_p^{(i,j)}}\right) \right] \qquad (3.2.2)$$
$$: j=1,2,..,m \text{ and } H_i(t) = -1 \text{ or } 1$$

Where $C^p(i,j)$ is the parasitic capacitance projected by C(i,j), φ(i,j) is an additional phase caused by

the parasitic resistor and capacitance and sin(wt+ φ(i,j)) is a time delayed component of the CA output.

In Fig 3.11, V_{ik} is the CA output signal in response to a k^{th} driving signal and mutual capacitance between an ith driving line and kth sensing line. ΔT means timing skew between V_{ik} and V_{ik+1}, ΔV_M means the output difference resulted from the gain error. The overlapped output signal of a CA circuit in SCPA is digitally demodulated by multiplying the orthogonal code sequences of each driving line.

In SCPA, the gain error and timing skew problems severely decrease SNR in a large-sized TSP. The CA output of SCPA is the sum of the products of the orthogonal signal, mutual capacitor and gain of each channel. The gain error and timing skew distort the CA output of SCAP since the outputs of SCPA are not synchronized. The CA output of SCPA in large-sized TSP are given by

$$\begin{aligned} V_{SCPA,j}(t) &\approx \sum_{i=1}^{n} A_m H_i(t) \frac{C^{ij}}{C_F} \sin(wt + \phi_{(i,j)}) \varepsilon_{gain} \\ &\approx \sum_{i=1}^{n} A_m H_i(t) \frac{C^{ij}}{C_F} (\sin wt \cos \phi_{(i,j)} + \cos wt \sin \phi_{(i,j)}) \varepsilon_{gain} \\ &: j=1,2,\cdots,m \text{ and } H_i(t) = -1 \text{ or } 1 \end{aligned} \tag{3.2.3}$$

Where ε_{gain} is the gain error component, cos φ(i,j) is the coefficient of the synchronous component and a sin φ(i,j) is the coefficient of the asynchronous component. As the parasitic resistor and capacitance become larger in a larger-sized TSP, an additional phase φ is also increased. As a result, in a large-sized TSP, the amplitude of a synchronous component, sin wt is decreased and the amplitude of an asynchronous component, cos wt is increased. Furthermore, due to the gain error of each channel, the reference-output value to determine a touch or un-touch state becomes ambiguous. The time delay and the gain error seriously worsen the performance of SCPA as both the parasitic component becomes larger and the number of driving signals simultaneously injected to the TSP are increased. As a result, even though the number of driving channels is increased, the SNR of SCPA is decreased because of the distorted output of SCPA.

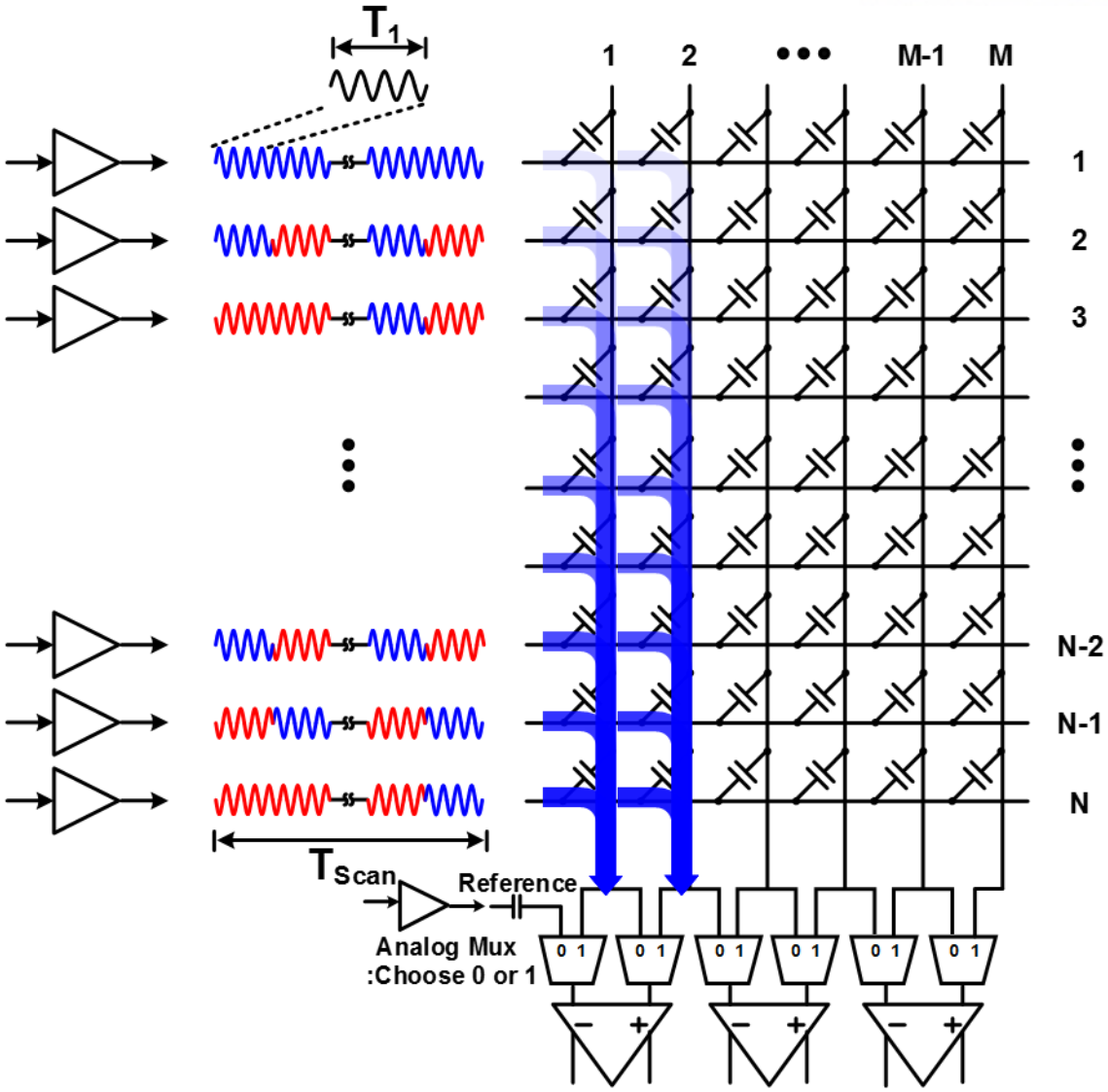

Fig.3. 12 Differential continuous-mode parallel operation architecture (DCPA) as analog-front-end circuit at a mutual capacitive TSP.

A differential continuous-mode parallel operation architecture (DCPA) to enhance the SNR for the limited time in a large-sized TSP regardless of the parasitic effect is presented. DCPA employs a differential CA circuit with a parallel operation. DCPA has several important advantages, including common-noise rejection such as display noise in a TSP by the differential-architecture. DCPA has a band-pass filter characteristic to attenuate self-noise such as a lamp noise [3.8], [3.9], [3.10], [3.11].

Further, this approach enhances signal power spectral density by using a parallel operation architecture regardless of the timing skew and gain error caused by the parasitic component. To enhance SNR along with frame-rate and total number of TX channels in a large-sized TSP, the number of driving channels should be increased based on the principle of parallel operation described earlier in this section.

In SCPA, timing-skew and gain error limit the number of driving channels caused by the parasitic

components. In contrast with SCPA, DCPA can effectively increases SNR along with the frame-rate and total number of TX channels in a large-sized TSP by canceling the timing skew and gain error in continuous-mode parallel architecture.

The output of DCPA in a large-sized TSP, which is the same as the difference between the SCPA's output of the j[th] sensing electrode and that of the (j+1)th sensing electrode, is given by the following equation:

$$V_{DCPA,j}(t) = \sum_{i=1}^{N}\left[A_m H_i(t)\left\{ \frac{C^{(i,j)}}{C_F}\sin(wt+\phi_{(i,j)}) - \frac{C^{(i,j+1)}}{C_F}\sin(wt+\phi_{(i,j+1)}) \right\}\varepsilon_{gain} \right]$$
$$= \sum_{i=1}^{N}\left[A_m H_i(t)\frac{\Delta C^{(i,j)}}{C_F}\sin(wt+\phi_{(i,j)})\varepsilon_{gain} \right] \quad (3.2.4)$$
$$: j=1,2,\cdots,m \text{ and } H_i(t) = -1 \text{ or } 1$$

Where ΔC(i,j) is the difference in capacitance between adjacent sensing electrodes in DCPA [3.12].

The output of DCPA is only proportional to the capacitor-difference between the adjacent capacitors in a TSP. The additional phase caused by the parasitic component, φ(i,j), is almost same as the adjacent phase, φ(i,j+1), since the effect of phase delay between adjacent sensing electrodes is almost the same.

The output of DCPA for a single-channel depends on the capacitor difference given by

$$V_{DCA\_different\_cap,j}(t) = A_m H_i(t)\frac{\Delta C^{(i,j)}}{C_F}\sin(wt+\phi_{(i,j)})\varepsilon_g \quad (3.2.5)$$

$$V_{DCA\_different\_cap,j}(t) = A_m H_i(t)\frac{\Delta C^{(i,j)}}{C_F}\sin(wt+\phi_{(i,j)})\varepsilon_g \quad (3.2.6)$$

$$V_{DCA\_same\_cap,j}(t) \approx 0 \quad (3.2.7)$$

According to above equation, firstly, there are no common-mode components, since the output of DCPA is only proportional to the capacitor difference. Secondly, the same capacitances in both an un-touched area and touched area of the TSP are nothing in the output of DCPA. As a result, DCPA is not influenced by timing-skew and gain error from the common-mode component when capacitances are

the same. In addition, timing skew and the gain error problem caused by different capacitances is alleviated in the demodulation process due to the orthogonality between the driving channels. As a result, timing-skew and the gain error problem is effectively canceled in DCPA.

The output of DCPA with external noise sources is given by

$$V_{DCPA\_ext,j}(t) \approx V_{DCPA,j}(t) + \sum_i \alpha_i \frac{C_{ext,i}}{C_F} V_{n,self,i}(t) \quad : j=1,2,\cdots,m \tag{3.2.8}$$

Where $V_{n,self,i}$ is the external self-noise source and $C_{ext,i}$ is the coupling capacitor connected to the external self-noise source. The proposed architecture, DCPA, can reject the common-mode noise and attenuate the self-noise with the frequency that is close to input frequency by the band-pass filter characteristic of the CA circuit. Furthermore, after demodulation, the self-noise source is distributed by the parallel operation method.

3.2.2 System block of differential continuous-mode parallel architecture

A. System Block Diagram

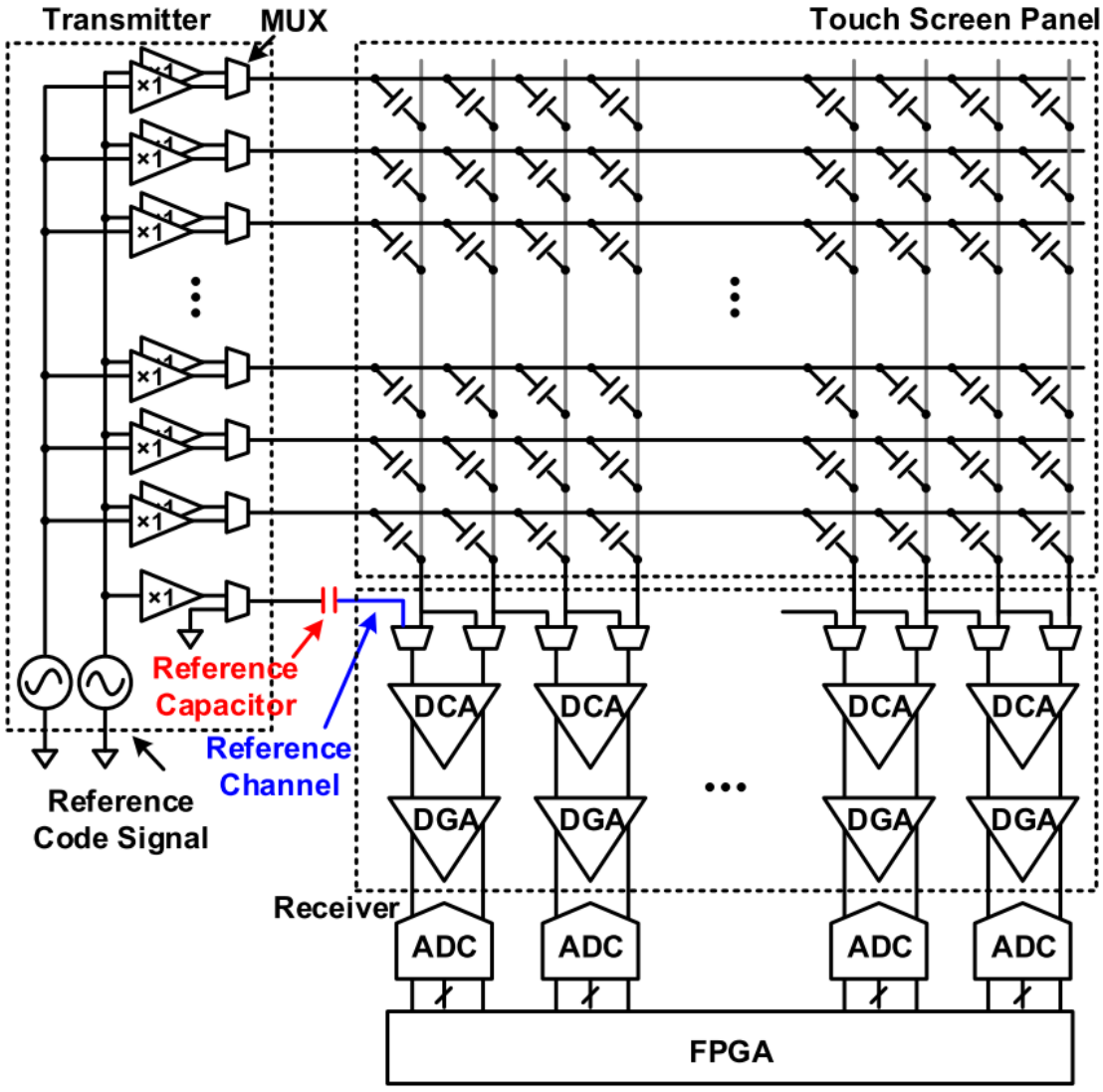

Fig.3. 13 Block diagram of the proposed differential continuous-mode parallel architecture (DCPA)

Fig. 3.13 shows the block diagram of a DCPA readout IC. It is composed of a transmitter with continuous-mode signaling and a fully differential receiver with a parallel driving architecture.

On the transmitter side, a coded signal is transmitted with two continuous-mode sinusoidal signals that are out-of-phase with each other. The in-phase signal represents a logic high, while the out-phase signal represents a logic low. One of these two signals is selected based on the incoming transmitted code via an analog multiplexer (MUX) and drives the electrodes on the lower layer of the TSP. This signal is coupled via the mutual capacitance formed between the upper and lower layers of the TSP.

Meanwhile, the receive path is composed of an analog MUX, differential charge amplifier (DCA),

differential gain amplifier (DGA), analog-to-digital converter (ADC), and field programmable gate array (FPGA). The analog MUX selects one of the receive paths between two adjacent electrode lines. The analog MUX output is connected to the input of the DCA.

By combining the analog MUX and DCA, it is possible to compare the capacitive values of the two adjacent RX channels. For differential–parallel sensing, reference data illustrated in Fig. 3.14 is used to compare the other lines. In the proposed system, the reference capacitor with transmitter signal in Fig. 3.14 connected to the DCA creates a reference value for comparison.

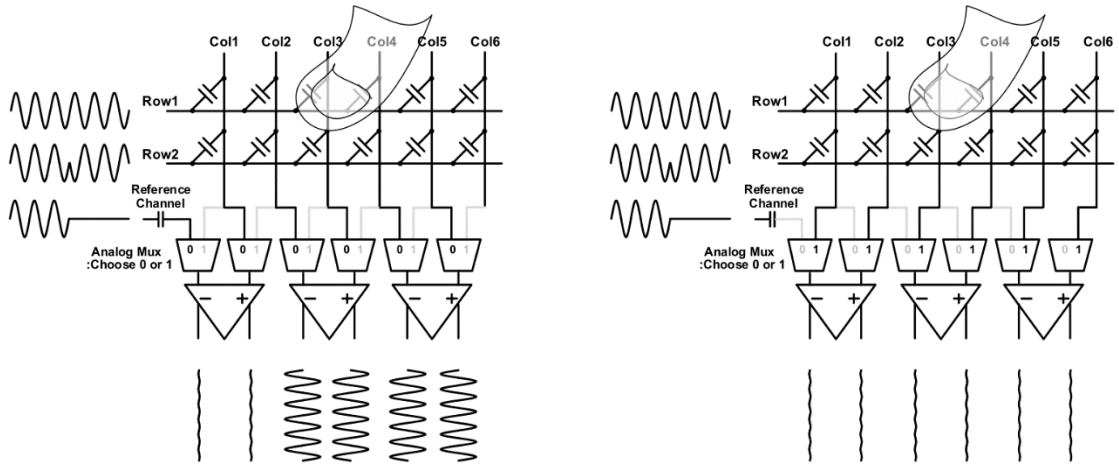

(a) The control signal of multiplexer is low (b) The control signal of multiplexer is high

Fig.3. 14 The proposed differential parallel signaling method with 2-bit Walsh Hadamard Code

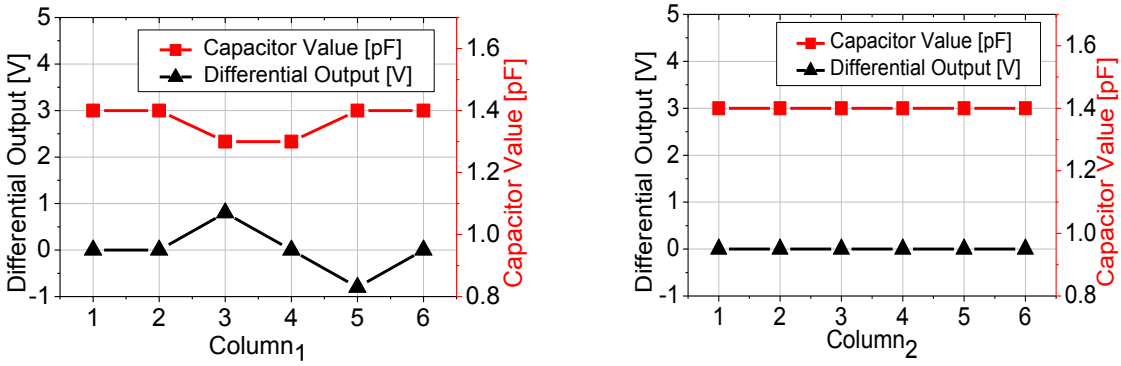

(a) Output result of row 1 (b) Output result of row 2

Fig.3. 15 The differential output signal and the capacitor value after the demodulation of the differential output

When the transmitter signals are coupled to the mutual capacitors of each node, the DCA output is

obtained. The output of the DCA is proportional to the difference in the capacitor values of the adjacent RX lines. The DCA, with a feedback capacitor and resistor, has moderate gain while acting as a band-pass filter. The output of DCA is based on a comparison between the adjacent capacitors of RX lines. The differential output of the DCA is amplified by the DGA. This output signal is converted to a digital signal by the ADC. The digital output signal is demodulated by the FPGA. In this paper, the transmitter and receiver which is highlighted are on-chip and ADC, FPGA are out-chip.

B. Differential-Parallel Sensing Method

The differential-parallel operation method is composed of the differential sensing method and parallel operation method. Both methods are applied to the TSP simultaneously. Since each method is operated independently, it is possible to achieve the advantages of both methods. More importantly, it is possible to demodulate the output signal generated by the differential-parallel operation method.

The differential sensing method is based on a comparison between the adjacent capacitors of RX lines using a multiplexer and differential amplifier. Through the control signal of the multiplexer, all of the adjacent capacitors are compared, including the reference line. The reference capacitor is used to create a reference value to compare with the other capacitors of the TSP. This reference value is defined as a_{REF}. After this comparison is completed using the differential amplifier, a differential output, b_k, is obtained. This differential amplifier output is proportional to the difference in the single-ended output of a_k, which can be formulated as in equation 3.2.9

$$b_k = a_k - a_{k-1} \tag{3.2.9}$$

$$a_k = (a_{REF} + \sum_{k=1}^{n-1} b_k) \tag{3.2.10}$$

Equation 3.2.15 shows how the single-ended output is expressed using the reference signal a_{REF} and differential output of b_k, which means the single-ended output is recovered using the differential output and reference value. Through the singled-ended output value, it is possible to determine the capacitor value of each node. When both adjacent capacitors are touched or un-touched, the output of DCA is same due to the same capacitor-difference without the proposed differential sensing. By converting the differential output value to the single-ended output value, the proposed differential sensing method can

acquire the touch information regardless that both capacitors are touched or un-touched.

Thus, the proposed differential sensing method realizes a parallel driving operation with differential sensing. In Fig. 3.14, the two orthogonal code signals go through the TSP simultaneously. This voltage is converted to a current, which is proportional to the capacitor value of each node. The differential amplifier of the receiver converts the RX current difference into a voltage. By utilizing the differential sensing method with the multiplexer and differential amplifier, every adjacent RX line is compared. In the differential-parallel operation, the output voltage of the differential amplifier contains information about each capacitor that receives the transmitter signal, and demodulation is necessary to recover the capacitor information of each node.

For example, a finger touches the electrodes of column 3 and 4 of the row 1 of a TSP in Fig. 3.14. Fig. 3.15 (a) and (b) shows the results of the differential amplifiers, which depend on the multiplexer code signal. The differential output is proportional to the difference between adjacent capacitors. A reference channel with the reference capacitor is used to compare the 1st sensing channel. If a capacitor value is the same as the adjacent RX line, the output of the differential amplifier is near zero except for the mismatch of the load. In contrast, if the capacitor values are different due to the touch action, the output of the differential amplifier is a non-zero value. The magnitude of the differential amplifier output is proportional to the capacitance difference and magnitude of the input signal. The output signal is the same as the code signal that goes through the touched capacitor. In a multi-touch situation, the output signal is proportional to the sum of the code signals received by the touched capacitors and the capacitor difference.

$$B = H^{-1} \times K \tag{3.2.11}$$

$$a_k = (a_{REF} + \sum_{k=1}^{n-1} b_k) \tag{3.2.12}$$

To demodulate the output signal in the differential-parallel operation, two steps are necessary. First, the orthogonal signal of each TX line is multiplied to demodulate the mixed parallel signal. Fig. 3.13 (a) and (b) shows the results for a differential output signal that is multiplied by each orthogonal code signal. Since a finger touches the row 1 line of the TSP, there are only output differences in the row 1 line. There are no output differences in the row 2 line. Second, the differential sensing method is applied to the results of the parallel signaling. The differential output is changed to a single-ended format by applying the differential sensing method. Equations 3.2.11, 3.2.12 show the demodulation process of

the differential-parallel operation. In equation 3.2.11, the H matrix is the orthogonal code signal. The K matrix is the output of the differential-parallel signaling, and the B matrix is the demodulated output of the parallel signaling. After the demodulation of the parallel signaling, the B matrix is obtained. Since matrix B is the differential output of the differential amplifier, it is demodulated using the differential sensing method, as shown in equation 3.2.12.

3.3 Circuit Implementation

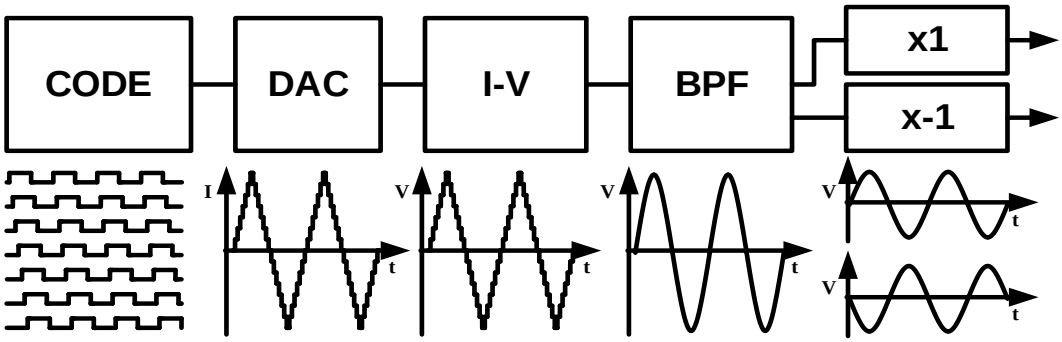

Fig.3. 16 Parallel-code signal generator

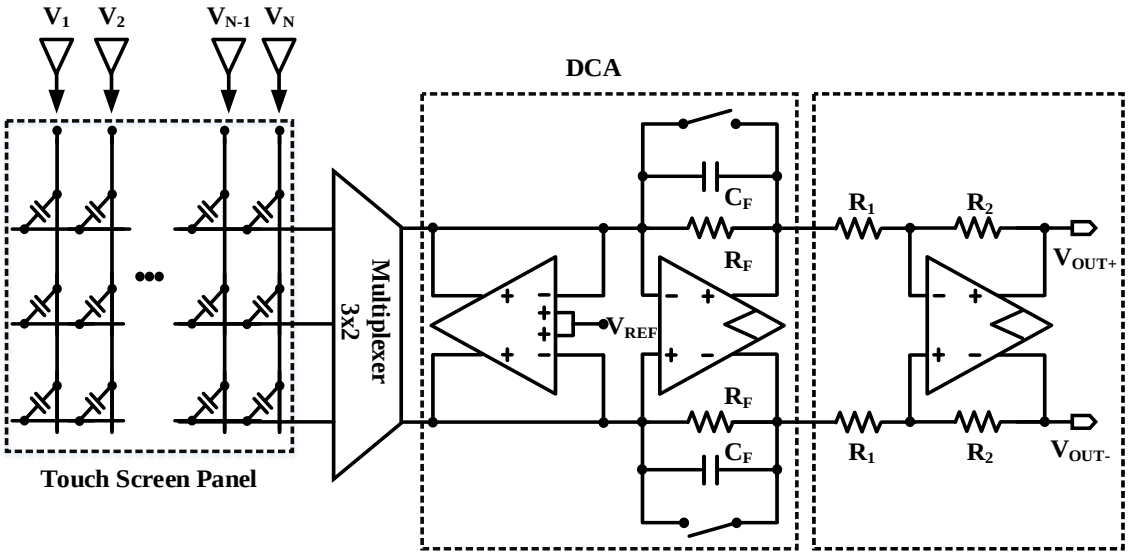

Fig.3. 17 Continuous-mode fully differential receiver–1 channel

The parallel signal code is generated using in-phase and out-phase signals because the orthogonal code signal is composed of a series of in-phase and out-phase signals. The code generator consists of a reference signal generator part and a code selection part. The reference signal generator part and code selection part are described in Fig. 3.14. A reference signal generator with a step current signal is employed in this work. A step current is generated by a digital code generator block and DAC. This step current is converted into a step voltage using an I-V converter. This voltage is converted to a sinusoidal signal through the band-pass filter. After the sinusoidal signal passes through the positive and negative unity gain buffer, in-phase and out-phase reference signals are generated. The code selection part chooses either the in-phase or out-phase reference signal. A code signal output is selected based on the control signal of the multiplexer.

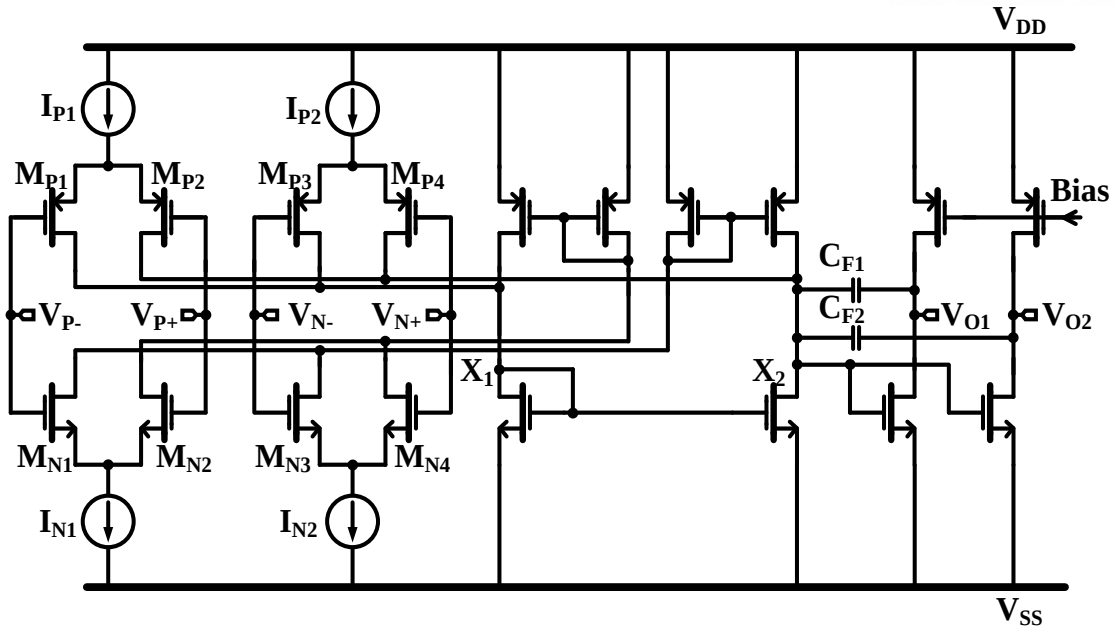

Fig.3. 18 Differential-difference amplifier for input common-mode feedback

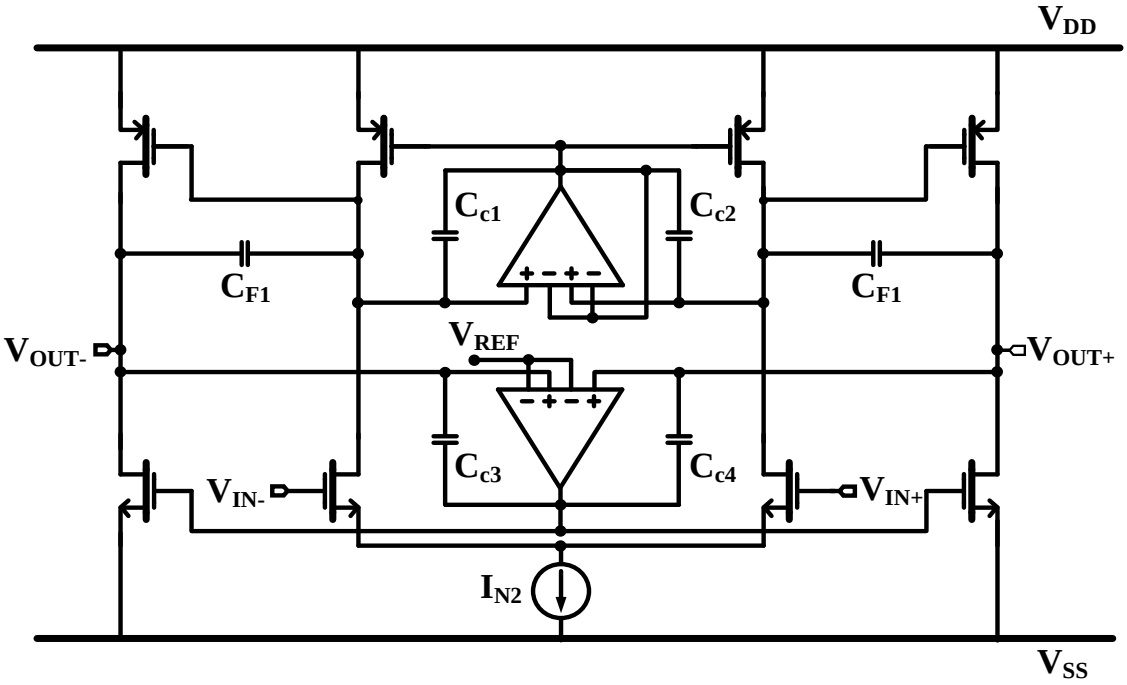

Fig.3. 19 Differential amplifier with output-common mode feedback circuit

Fig. 3.17 shows the fully differential receiver for the differential-parallel operation. The receiver is composed of an analog multiplexer, differential amplifier with input common-mode feedback (ICMFB) as the DCA, and DGA [3.13]-[3.20]. The outputs of DCPA are given by

$$\Delta V_{out} = V_{out+} - V_{out-} = -\sum_{k=1}^{N} \frac{R_2}{R_1} \frac{\Delta C_{s.k}}{C_F} V_{TX.k} \tag{3.3.1}$$

Previously, the differential-continuous sensing method was implemented using two single-ended amplifiers at the first stage and a differential gain amplifier at the second stage [3.8].

However, this topology has limited headroom when parallel-operation is applied, and common-noise is inserted. Since only a certain portion of the overall sensing capacitors are changed, a single-ended amplifier's output always has a large common-mode component. Moreover, in parallel operation, multiple driving signals go through the TSP simultaneously. If either high-state signals or low-state signals go through the TSP simultaneously, the output signals are overlapped at the single-ended amplifier, and excessive current is integrated in the feedback capacitor. This means the common-mode component in a single-ended amplifier's output is increased, which saturates a single-ended amplifier's output.

One solution is to use a large feedback capacitor for the low gain of the first-stage amplifier to prevent the single-ended amplifier's output from being saturated. However, the dynamic range of the single-ended amplifier output is reduced by the low gain of the first-stage.

the proposed receiver employs a DCA with ICMFB to remove the large common-mode component in the continuous-mode. The output of this DCA in Fig. 9 is only proportional to the difference between the adjacent capacitor value and magnitude of the input signal without the common-mode component. This means the large common-mode noise signal and the common-mode component caused by parallel signaling is removed in the DCA. The DCA is required to have a high common-mode rejection. By DCA with a high common-mode rejection, it is possible to increase the gain of the first stage by removing the common-component. As a result, the dynamic range of the first-stage is enhanced.

The operation of the DCA with ICMFB is based on amplifying the capacitor difference by absorbing the common current and sourcing the differential current. When the common current passes through the input of the differential amplifier, it flows to the ICMFB. A differential current is integrated in the feedback capacitor of the DCA. In the proposed system, a differential-difference amplifier (DDA) is

used as an ICMFB to accurately integrate only the differential current in a continuous-mode.

The proposed continuous-time ICMFB with a DDA is shown in Fig 3.18. The ICMFB is used to maintain the common-mode voltage, and supply or sink common currents by comparing to the reference voltage and input voltage in a continuous-mode. Negative feedback for the ICMFB makes the op-amp input equal to the reference voltage.

If the output voltage connected to the negative input of the DDA is higher than the reference voltage, then the output voltage is reduced to the reference voltage. In addition, the DDA sinks the current from the output load to ground. On the other hand, if the output voltage connected to the negative input of the DDA is lower than the reference voltage, then an output voltage is increased to the reference voltage. In addition, the DDA sources the current to the load from a positive power supply. In this process, the DDA supplies or sinks the common current, and only the differential current flow into the output feedback capacitor.

Fig. 3.19 shows a differential amplifier based on a two-stage amplifier with an output common-mode feedback circuit (OCMFB). This amplifier is used in the DCA and DGA as the main amplifier. The output range of the two-stage amplifier is rail to rail. A one-stage DDA is used as common-mode feedback circuit (CMFB) in OTA. The negative inputs of the upper DDA are connected to the output of the upper DDA in DCA for the diode connection. The negative inputs of the lower DDA are connected to the reference voltage which is used for the common-mode DC bias.

For stability in the CMFB, the two CMFBs are designed as a one-stage DDA circuit. Since the common-mode feedback loops of CMFB are high gain loops, compensation is necessary. In this paper, a compensation capacitor ($C_{c1\text{-}4}$) was used for compensation of the two common-mode feedback loops. The PM of the upper common-mode feedback loops was 61 degrees and that of the lower common-mode feedback loops was 58 degrees. CMFB keeps the common-mode voltage stable for differential-amplifier circuits. There are several kinds of common-mode feedback circuits such as a switched-capacitor CMFB, resistor-averaged CMFB and DDA CMFB. Since the proposed circuits are operated in continuous-mode, it requires larger feedback resistance than output impedances, and as such, DDA CMFB is suitable for a differential system [3.21]-[3.23].

The outputs of the DCA are connected to the inputs of the DGA. The gain of the DGA is adjustable from 1 to 20 V/V. The RX circuit is designed to operate with a 100-kHz continuous signal.

3.4 Offset, Slew rate and Noise Analysis

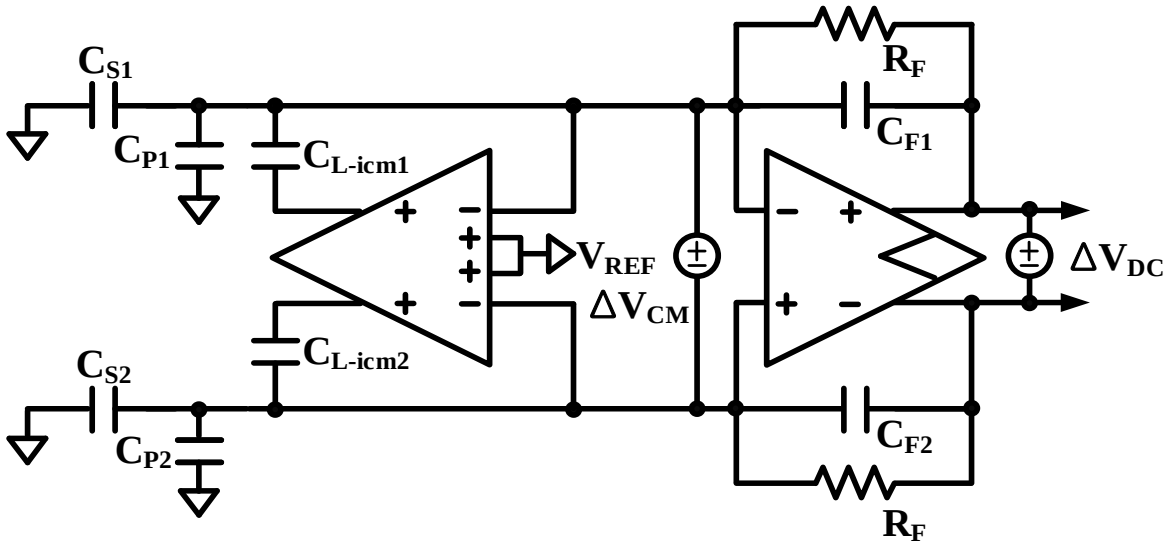

Fig.3. 20 Offset source in the proposed differential charge amplifier (DCA) with the input common-mode feedback circuit (ICMFB)

Fig.3.20 shows an offset source in the proposed DCA with ICMFB. Where $C_{s1\text{-}2}$ is the sensing capacitors, $C_{p1\text{-}2}$ is the parasitic capacitors, $C_{L\text{-}icm1\text{-}2}$ is the load capacitor of ICMFB, ΔV_{CM} is the offset in the inputs of DCA and ΔV_{DC} is an offset in the output node. An offset in the input node of DCA causes the output offset, ΔV_{DC}, which includes AC and DC offset in the output node. AC offset is proportional to the driving signal, resulting in the additional offset in the output of DCA.

Without ICMFB, the dominant reason for AC offset is a mismatch of the parasitic and feedback capacitor. In the operation of DCA with ICMFB, the mismatch component is amplified by the gain of DCA. The mismatch-dependent AC offset is given by

$$\begin{aligned}\Delta V_{out} &= V_{out+} - V_{out-} = -(V_{drv} - \Delta V_{CM})\frac{\Delta C_S}{C_F} \\ &= -V_{drv}\left(\frac{\Delta C_S}{C_F} - \frac{\Delta C_F + \Delta C_P}{C_F}\right) \text{:without ICMFB}\end{aligned} \tag{3.4.1}$$

Where ΔC_S is the capacitor difference of the sensing capacitor C_{S1} and C_{S2}, ΔC_F is the capacitor difference of the feedback capacitor C_{F1} and C_{F2}, ΔC_P is the capacitor difference of the feedback capacitor C_{P1} and C_{P2}. The parasitic mismatch component, ΔC_P, in TSP is several picofarads, which make AC offset in the output of DCA. As a result, the common-mode AC component take possession

of the output of DCA, which reduces the dynamic range of DCA output. By using the ICMFB in DCA, ICMFB keeps the input common-mode of OTA constant. As a result, the mismatch-dependent AC offset from the parasitic and the feedback capacitor is removed.

However, the differential offset from ICMFB causes additional AC and DC offset in the output of DCA. The offset from ICMFB is given by

$$\begin{aligned}\Delta V_{out} &= -(V_{drv} - \Delta V_{ICMFB})\frac{\Delta C_s}{C_f} + \Delta V_{DC} \\ &= -V_{drv}\left(\frac{\Delta C_s}{C_F} - \frac{\Delta C_{L-icm}}{C_F}\right) + \Delta V_{DC} \ :\text{with ICMFB}\end{aligned} \tag{3.4.2}$$

Where ΔV_{ICMFB} is a differential offset in the inputs of DCA due to ICMFB and $\Delta C_{L\text{-}icm}$ is the capacitor difference of the $C_{L\text{-}icm1}$ and $C_{L\text{-}icm2}$. The load capacitor mismatch of ICMFB produces the AC offset component. However, the load capacitor mismatch, $\Delta C_{L\text{-}icm}$, is lower than the parasitic capacitor mismatch, ΔC_P, the AC offset is greatly reduced in the output of DCA.

However, there is DC offset resulting from the OTA, which cannot be removed as it is out of the loop. In addition, the differential offset from ICMFB is amplified by the open loop gain of OTA and highly increases DC offset in the output node.

To minimize the DC offset in the output node, it is necessary to reduce the differential offset from ICMFB. The transconductance of ICMFB, which is the key parameter, is given by

$$g_{m,CMFB} = \frac{I_{O_{CM}}}{V_{CM.ERR}} = \frac{I_{O_{CM}}}{V_{CM} - V_{REF}} = \frac{I_{O_{CM}}}{\Delta V_{icm}} \tag{3.4.3}$$

The transconductance of ICMFB is the output current divided by the common-mode error, $V_{CM,ERR}$, which is the common-mode error, that is the difference between the reference and common mode voltage. The large transconductance reduces the common-mode error by the negative feedback loop of ICMFB. Thus, the ICMFB circuit in Fig. 9 is designed with a two-stage DDA structure. This two-stage DDA has large transconductance, which minimizes the offset of the differential input stage.

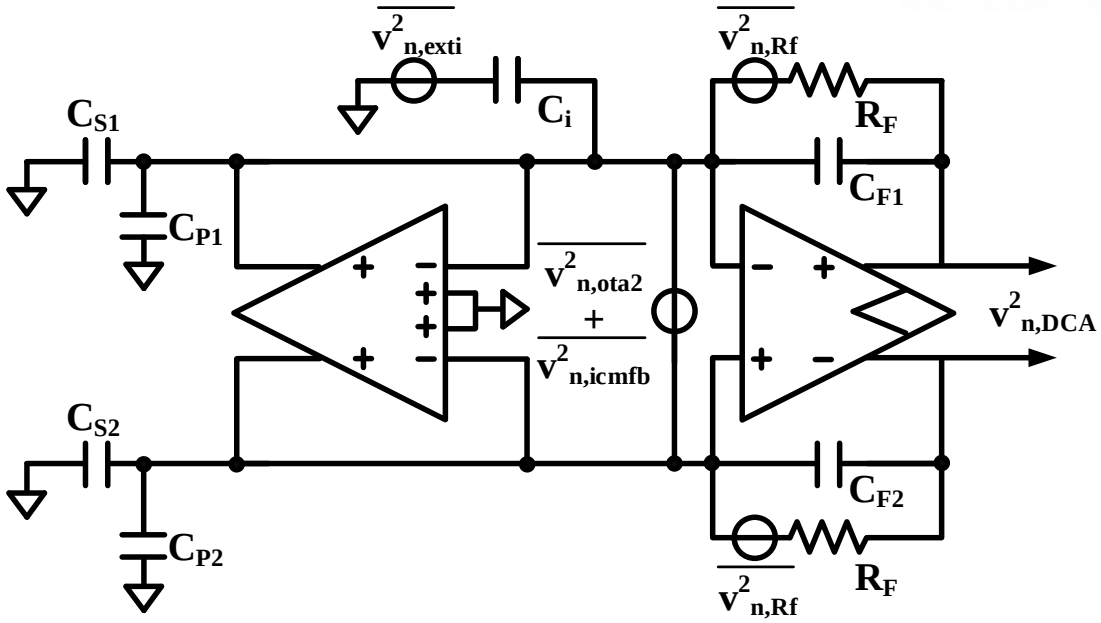

Fig.3. 21 Noise sources in the proposed DCA with ICMFB

The common-mode and differential offset from DDA (ICMFB) itself is greatly reduced in the feedback loop due to the two-stage structure of ICMFB. The Phase Margin (PM) of the loops of ICMFB circuits is 51 degree and open loop gain of ICMFB is 70 dB.

In addition, it is required to keep the layout tight and symmetrical for the differential pair of OTA and ICMFB for low DC offset in the output of DCA. Fortunately, since the DCA is operated in a continuous mode, DC offset can be easily removed by the chopper or digital band pass filter. In the proposed differential sensing, ICMFB source or absorb the common-mode current continuously and only differential current is integrated in DCA. If the response time of ICMFB is slower than the maximum rate of the output voltage change per time, the output of DCA is distorted.

This means the response time should be sufficiently fast to keep up with the continuous signal of the DCA. The response time of the ICMFB is associated with the slew rate.

Fig.3.21 show a noise sources and parasitic component in the proposed DCA with ICMFB. The output-referred noise power of the DCA is given by

The gate slew rate is determined by the current of M_{N1}-M_{N4} and M_{P1-4} in Fig. 3.16. When the gate voltage of M_{N1} is instantaneously larger than the gate voltage of M_{N2}, the bias current of I_{N1} flows in M_{N1}. This current is charged in the capacitor of node X_1. In other words, the slew rate of the ICMFB is I_{N1} divided by the capacitor of node X_1 or X_2. To support a fast response, the slew rate of ICMFB is sufficiently larger than the input voltage divided by the time. In addition, the output current of ICMFB

is designed to sufficiently source or sink the common-mode current such as the common current by the 32 WHC and common-mode noise like display noise.

$$\overline{v_{n,DCA}^2} = \frac{1}{k_{CMRR}} \left(\left(1+\frac{C_S+C_P}{C_F}\right)^2 \left(\overline{v_{n,ota1}^2}+\overline{v_{n,icmfb}^2}\right) + 2\left(\frac{1}{2\pi f R_F C_F}\right)^2 \overline{v_{n,R_F}^2} + \sum_i \frac{C_{ext,i}}{C_F}\overline{v_{n,ext,i}^2} \right) \quad (3.4.3)$$

Where Cs is the sensing capacitance, Cp is the parasitic capacitance of the sensing electrode, $\overline{v_{n,DCA}^2}$ is the output referred noise of DCA, $\overline{v_{n,OTA}^2}$ is the input referred noise of OTA, $\overline{v_{n,\imath cmfb}^2}$ is the output referred noise of ICMFB, $\overline{v_{n,R_F}^2}$ is the thermal noise of a feedback resistance and $\overline{v_{n,ext,\imath}^2}$ is the external noise source coupling from external capacitance, $C_{ext,i}$.

k_{CMRR} is the coefficient of common-mode rejection ratio in the differential structure. The differential structure cancels the common-noise component of DCA with ICMFB and the external noise source.

The sum of the input referred noise of OTA and the output referred noise of ICMFB is amplified by the $1+(C_S+C_P)/C_F$. Since C_P is higher than C_F, the output noise increases greatly. Thus, it is necessary to avoid using the low C_F to reduce the noise from the output referred noise of ICMFB and input-referred noise of OTA. The noise from feedback resistor, v_{n,R_F}^2 is low pass filtered by the feedback capacitor and resistor.

Since the input of DCA is a floating node that is not connected to dc bias, a large flicker noise from ICMFB or OTA and environment noise causes input of common mode voltage railing in the common mode feedback operation. Also, if the multi-driving signal comes to the differential amplifier input of the RX, the common mode voltage of the differential amplifier input of the RX will be changed in an instant, causing the input common-mode voltage to move beyond the operating range of OTA. To prevent the above problems, a large feedback resistor between the input node and the output node of DCA is used to keep the common mode voltage constant. A large feedback resistance prevents a small amount of charge leakage onto or off this node. Regardless of large flicker noise or external noise, the input common mode voltage is constantly maintained.

3.5 Measurement Result

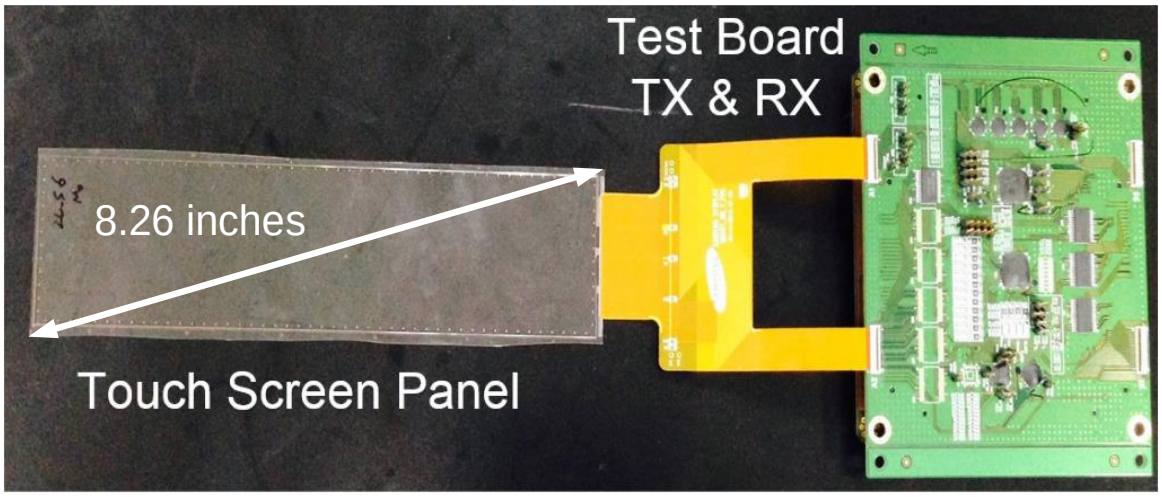

Fig.3. 22 Test-platform of proposed system

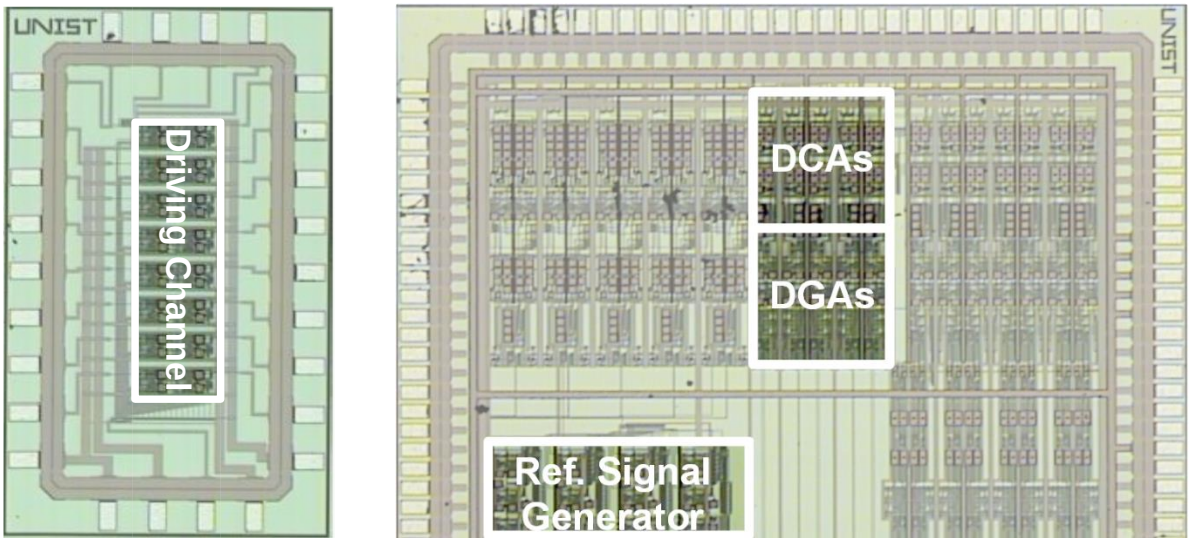

(a) 8-channel Transmitter (b) 10-channel Receiver

Fig.3. 23 Photomicrograph of the fabricated ROIC

Fig. 3.22 shows the test board designed for IC verification, which is composed of a 8.26-inch TSP, a RX, a TX, external ADC and FPGA. Fig. 3.23 shows chip photographs of the 8-channel TX and 10-channel RX. Fig. 15 show the measurement results of the proposed structure. In this measurement, the test environment of the differential parallel drive system was set as follows. Four TX chips and one RX chip were used for the measurement of the 32 × 8 channel capacitive TSP. The transmitter and receiver for the differential-parallel architecture were used to determine the touch screen sensing. In addition, a FPGA was used to create a parallel code signal and perform demodulation.

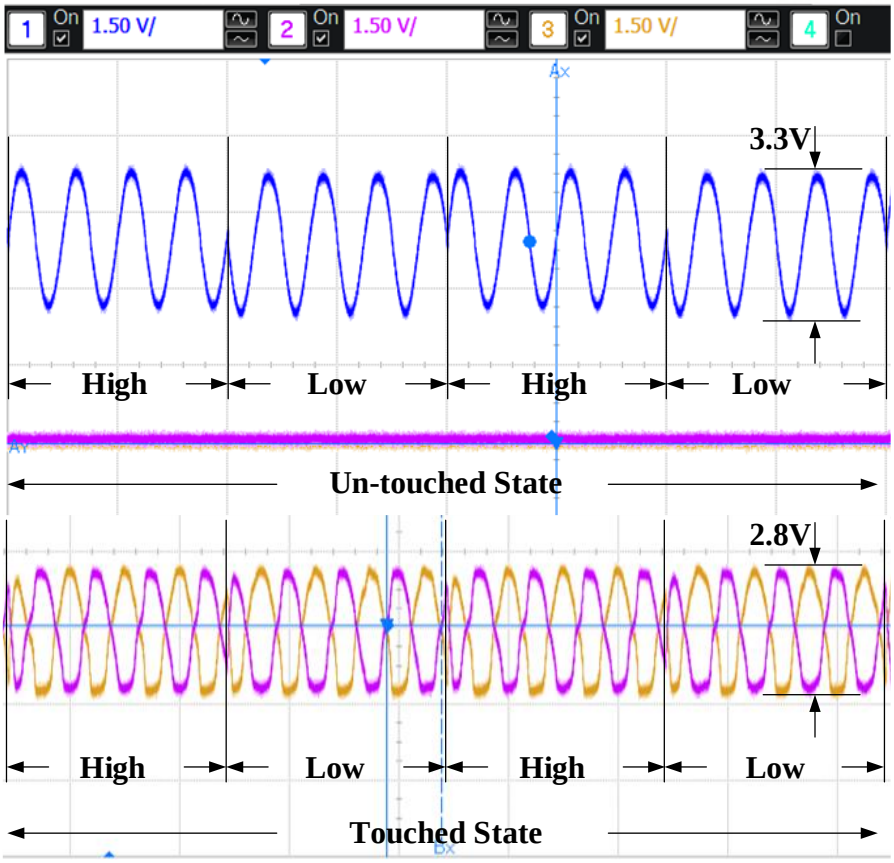

Fig.3. 24 Measurement of receiver in un-touched and touched state

The transmitter sends 100-kHz parallel code signals to the TSP. The peak-to-peak voltage of the output is 3.3 V. A parallel code signal is generated in consideration of 32 WHC, the number of repetition, and TSP channel, while the frame rate is 240 Hz. The transmitter generates a parallel code signal based on the control signal of the FPGA and sends this signal to the TSP. The fully differential receiver is connected to the TSP electrode on the receiver side. In this measurement, a 32-channel driving code signal is used simultaneously for TX signaling.

In the un-touched state, the output signal of the receiver is zero. In the touched state, the output signal of the receiver is proportional to the signal received by the touched capacitor. Fig. 3.24 show the receiver outputs when a finger does or does not touch the TSP. The upper signal is the code signal received by the touched capacitor. The lower signals are the receiver outputs. The output of the receiver is converted to a digital signal in the external ADC, which is connected to the FPGA. Since the frequency of the output signal is 100 kHz, the sampling frequency should be higher than 200 kHz by Nyquist rate. In this system, the sampling frequency of ADC was chosen as 1 MHz to acquire the multiple samplings. In this measurement, a 12bit, 1MSPS, dual-mode 10-channel external ADC was used. After that, the output signals are demodulated in the FPGA.

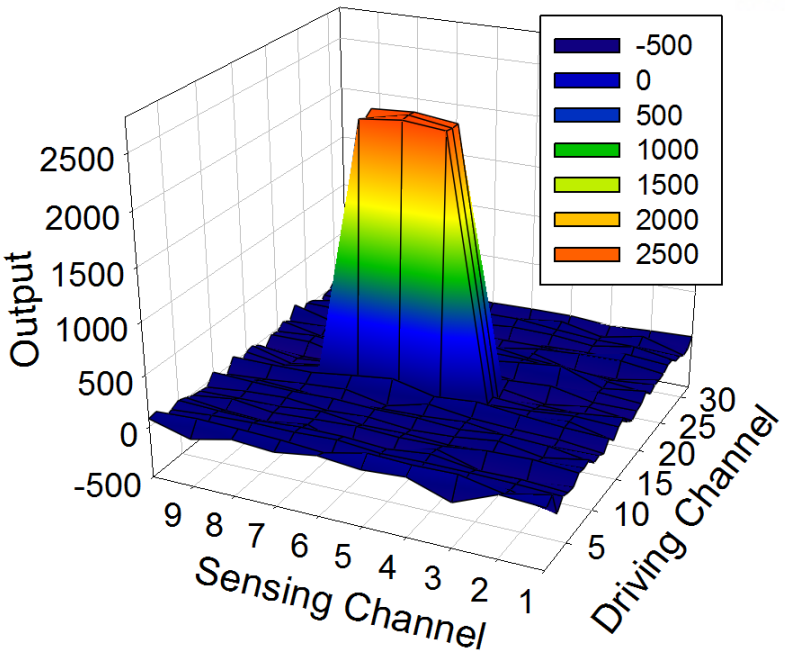

Fig.3. 25 Three-dimensional graph based on measured results for differential parallel continuous operation method without noise; configuration: input voltage: 3.3 V pp, SNR = 72 dB, frame rate=240 Hz

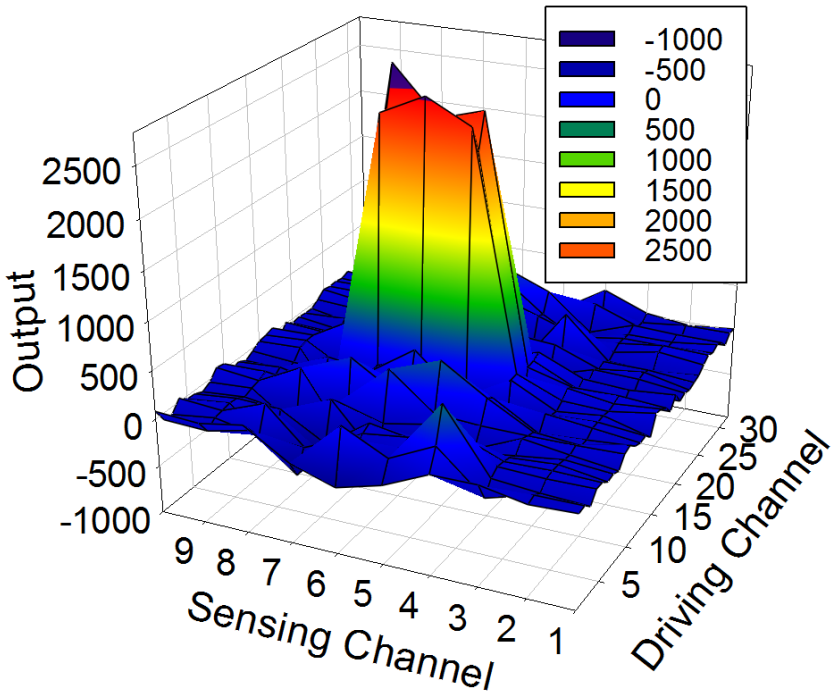

Fig.3. 26 Three-dimensional graph based on measured results for differential parallel continuous operation method with external noise; configuration: input voltage: 3.3 Vpp , display noise: 6 Vpp , 14 kHz, lamp noise: 20 Vpp, 51 kHz, SNR=36.1 dB, frame rate=240 Hz

Fig. 3.25 shows a three-dimensional graph based on the measured results for the differential-parallel operation method. The demodulation for the differential-parallel signaling is conducted based on the output results for the measured data in Fig. 3.22. In this Matlab reconstruction of the measured data, the frame rate is 240 Hz. The TSP has 32 driving channels and 10 sensing channels. The SNR of the proposed system is 72 dB after the demodulation of the differential parallel signaling method is conducted.

OTA consumes 0.29mW, OCMFB consumes 0.132mW and ICMFB consumes 0.8382mW. ICMFB is designed to sufficiently source or sink the common-mode current. The output current of ICMFB is used to remove the offset current of 32 WHC and common-mode noise component [12-13]. An external ADC power consumption is 11.6mW.

Fig. 3.27 compares the SNR along with the frame rate and total number of TX channels in recently published TSP ROIC.

By applying the proposed continuous differential-parallel method, this work achieves the sum of product of TX channels and frame rate parameters, 7680 and 72 dB SNR simultaneously. Furthermore, the proposed work can effectively reduce display noise and lamp noise. Compared to other single-ended methods in Fig. 3.27, this work has the advantage of common-mode noise component rejection. Also, compared to other differential methods in Fig. 3.27, the proposed work achieves the highest SNR and sum of product of TX channel and frame rate that is essential for lager-sized TSP [6]-[7].

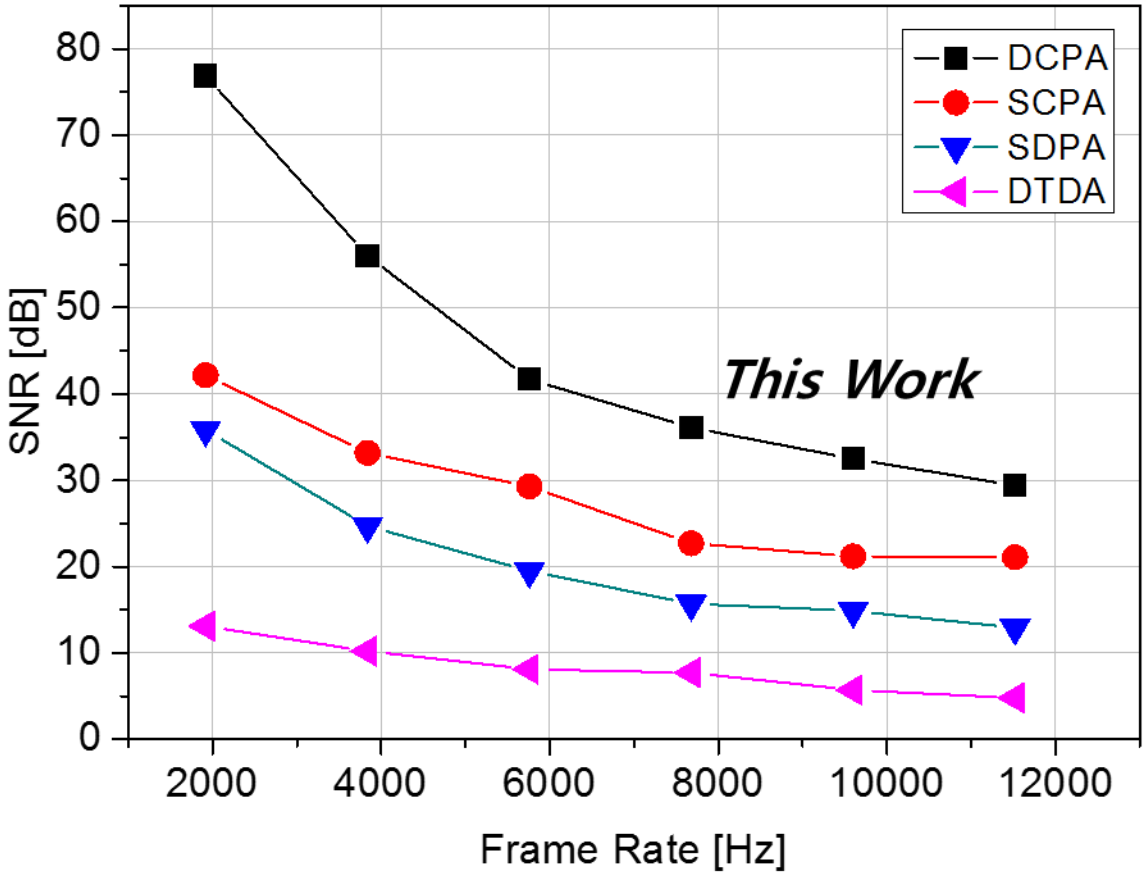

Fig.3. 27 Comparison of relative SNR verse Frame Rate with the proposed architecture and other architecture

To fully appreciate the true performance of ROIC for a TSP application, it is important to analyze the SNR under a practical TSP noise environment that has added display noise and/or added lamp noise. This display noise and lamp noise interferes with capacitive touch sensing. Hence, it is important to verify the noise immunity of the ROIC under a realistic TSP noise environment.

A noise analysis was conducted using a Matlab reconstruction based on the measured data to show the noise immunity of the proposed architecture. A noise signal was logically added to output measured data. Proposed a continuous-mode differential-parallel architecture shows further enhance SNR performance under a stressed TSP noise environment in a large-sized TSP.

Fig.3.26 shows a three-dimensional graph based on measured results for the differential parallel continuous operation method with added practical TSP environmental noise. The configuration included an input voltage of 3.3 V_{pp}. Additionally, noise signals were logically added to the results of the measured data for a noise analysis. First, a display noise signal at 14 kHz was added to the overall TX line, which is common noise. Second, a 51-kHz lamp noise signal, which is self-noise, was added to the TX line where the finger touches.

Table 1 Comparison Table for TSC in large-sized TSP

	T-CE 10 [1]	T-CE 11 [2]	ISSCC 13 [4]	JSSC 14 [6]	ISSCC 13 [9]	ISSCC 14 [10]	This work
Process	0.35 µm	0.35 µm	0.35 µm	0.18 µm	0.18 µm	0.18 µm	0.18 µm
Supply Voltage	3.3	3.3	3.3V	2.1 – 3.3 V	2.5–3.3 V	1.8/3.3 V	3.3 V
Channel	TX: 9 RX: 7	TX: 29 RX: 53	Tx: 27 Rx: 43	TX: 12 RX:8	TX: 30 RX: 24	TX: 24 RX: 16	TX: 32 RX: 10
Mode	Discrete Singled-ended TDMA	Discrete Differential TDMA	Continuous Differential TDMA	Continuous Differential TDMA	Discrete Single-ended CDMA	Discrete Differential CDMA	Continuous Differential CDMA
SNR	21.3	12.6	39dB	60 dB	55 dB	53 dB	72 dB (w/o external noise) [2]36.1 dB (with external noise)
Frame rate	-	140	120	200 Hz	240 Hz	160 Hz	240 Hz
# of TX and frame rate	-	4060	3240	2400	7200	3840	7680
Power	4.3mW	19mW	18.7mW	6.26mW	52.8 mW	2.6 mW	TX: 34.2 mW / RX: 8.43 mW
Area	-	20mm^2	10.4mm^2	[1]2.2mm^2	10.4 mm^2	[1]0.46 mm^2	[1]1.25 mm^2
TSP-type	Mutual	Mutual	Mutual	Mutual	Mutual	Mutual	Mutual

The amplitudes of display noise, and lamp noise were 6 V_{pp}, and 20 V_{pp}, respectively. The SNR in the touch screen noise environment was 36.1 dB after demodulation with the differential signaling method. In contrast to the previous parallel operation, the proposed architecture has superior noise immunity under a noisy TSP environment. A common noise signal such as display noise was suppressed by the differential architecture. A 51-kHz lamp noise signal was attenuated by the band-pass filter. Moreover, the parallel signaling enhances the overall the SNR and frame-rate product in a large-sized TSP.

To compare the proposed architecture and other architectures fairly, a comparison of SNR vs. Frame Rate graph presents each architecture in a touch screen noisy environment in Fig 3.25. This simulation is conducted by adding logical noise to each modeled architecture in Matlab. In this comparison, the TX channel is 32, the amplitude and the frequency of the input signal is 3.3V, 100 kHz and ΔC, the capacitance difference when touched or untouched, is 0.1 pF. As an environment noise which is logically added to the output, the display noise with a frequency of 14 kHz and amplitude 6 V_{pp} was added to all electrodes as common noise and lamp noise with a frequency of 51 kHz and amplitude 20 V_{pp}, which was added to the touched electrodes as self-noise. The external coupling capacitor of the display noise and lamp noise was selected as 0.1 pF. For the multiple sampling, 1MSPS, 12bit ADC is used. Multiple sampling was equally applied to all the architectures.

Table I provides a performance comparison among recently published TSP ROIC. The SNR of the proposed architecture was 72 dB with a 240-Hz frame rate for the TSP with 32 TX channels and 10 RX channels. The total power consumption was 42.5 mW. The power consumption of a reference generator part in TX is 7.7mW and that of a code selection part with rail-to-rail class AB output stage is 26.4mW. In total, TX consume 34.2mW which is 80% of total power consumption due to the analog transmitter. The power consumption of RX 10 CH is 8.43mW.

Chapter IV

IV. TSC for Fingerprint TSP

4.1 Design Issues for TSC in Fingerprint Touch Screen Panel

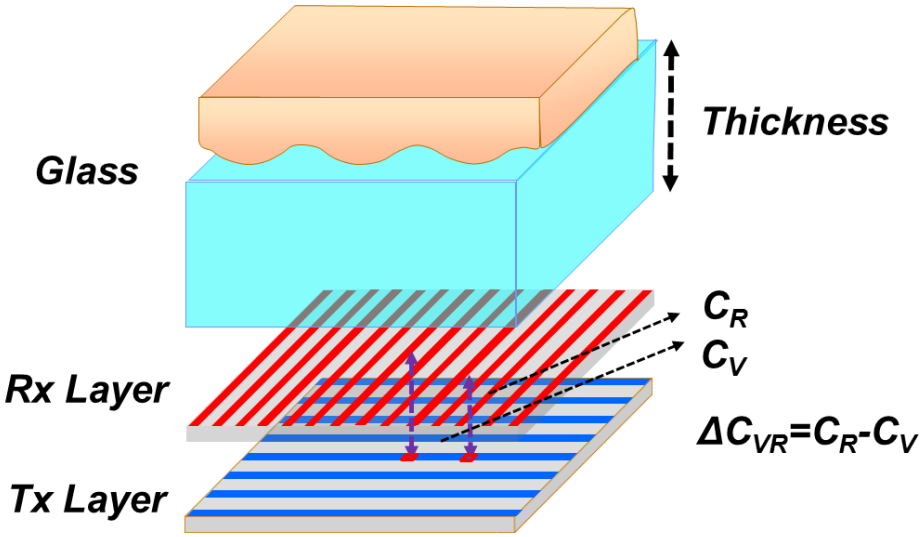

Fig.4. 1 Side view of fingerprint recognition touch screen

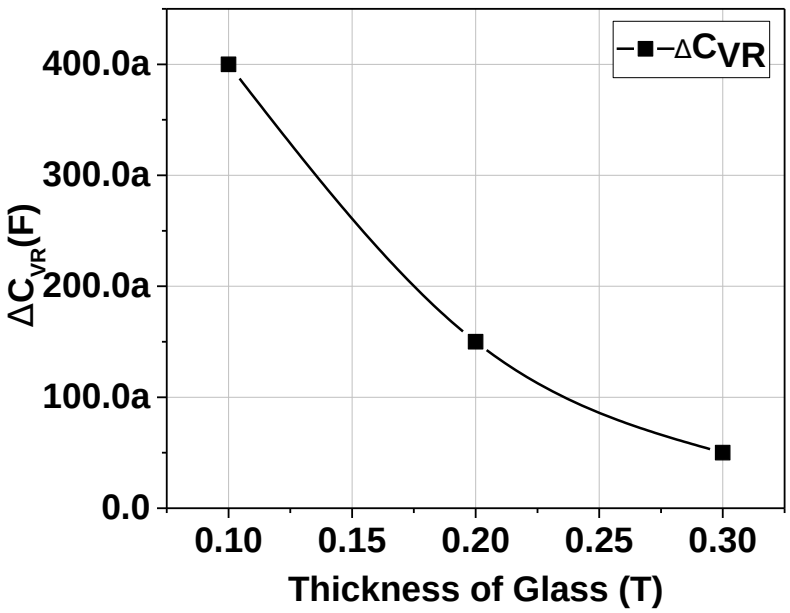

Fig.4. 2 Capacitance difference between ridges and valley according to the thickness of glass

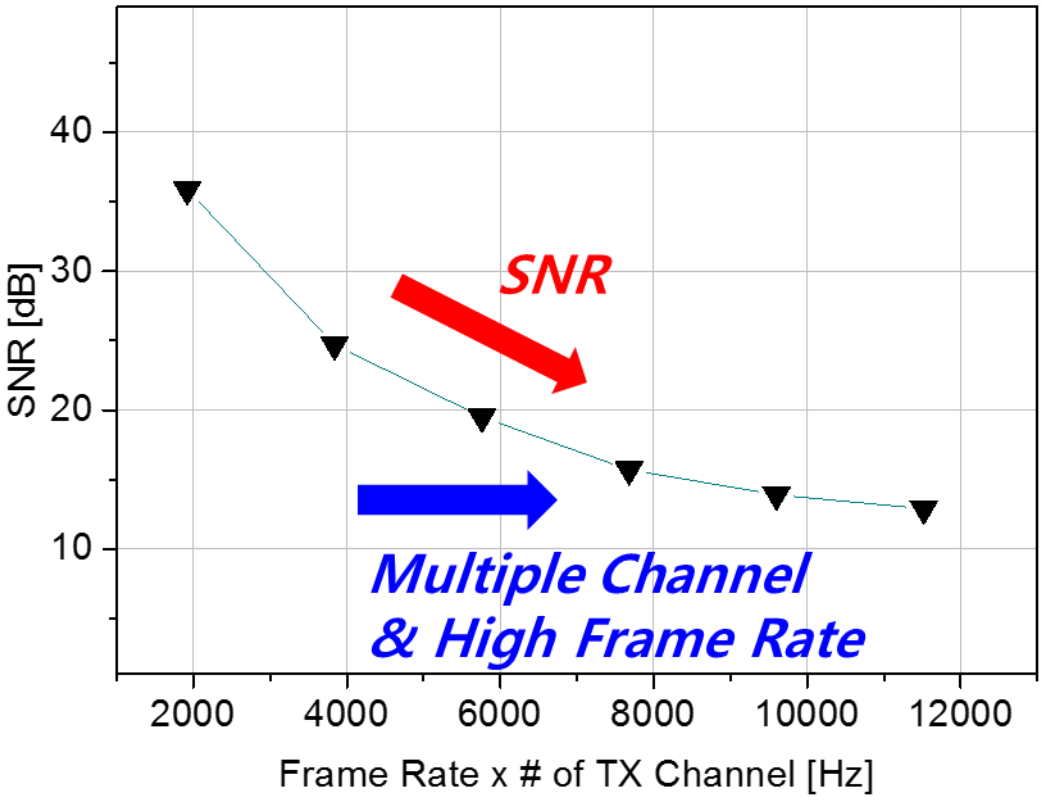

Fig.4. 3 Signal-to-Noise reduction by the multiple channel and high frame rate

The readout IC for mutual capacitive type fingerprint TSP has difficulties in fingerprint recognition, unlike the conventional touch screen drive circuit [4.1], [4.2], [4.3]. Three major reasons are as follows.

Firstly, the mutual capacitance difference by the valley and the ridge (CVR) in the fingerprint TSP is very small as shown in Fig.4.1 and 4.2. CVR is reduced to a few atto-farads by the cover glass, which is placed over the display to protect the touch screen panel. To obtain the fingerprint, the fingerprint recognition readout IC can detect the atto-farads capacitance, which corresponds to one thousandth of the capacitance difference in TSP. In addition, a cover glass is placed on the fingerprint TSP, which increases a distance between finger and fingerprint TSP. As shown in graph, as a result, CVR, is reduced by the thickness of cover glass.

Secondly, the number of electrodes of fingerprint recognition TSP is much larger than the number of TSP electrodes, as shown in Fig. 4.3. Fingerprint recognition also requires a fast response time with accurate recognition rate. As the number of electrodes increases, the number of nodes to be read increases. As a result, the number of samples collected by the ROIC decreases for the limited time. The multiple sampling improves SNR by dispersing noise. However, small number of sampling by multiple electrodes for the limited time result in low SNR.

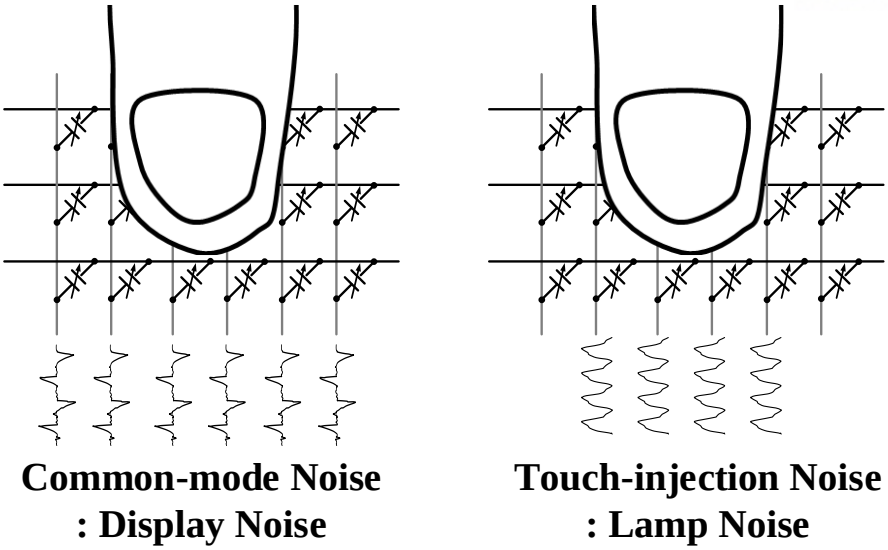

Fig.4. 4 Common-mode noise and Touch-Injection Noise in fingerprint touch screen panel

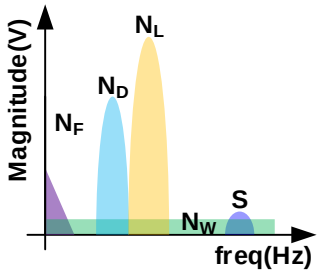

Fig.4. 5 Frequency spectrum of the touch screen environment noise, Display Noise (N_D), Lamp Noise (N_L), Flicker Noise (N_F), White Noise (N_W)

Thirdly, in the touch screen environment, there are common-mode noise such as Display Noise and Touch-injection Noise such as Lamp Noise [4.4]. Display noise is converted into current through the coupling capacitor between the TSP and the display panel. Since the common-mode noise is commonly coupled into all the electrodes of TSP, it can be removed by a differential structure. Lamp Noise, a Touch Injection Noise, is injected to the electrode of TSP which a finger touches. As shown in fig. 4.4, in the case of the fingerprint recognition touch screen, since the fingerprint of the finger must touch all the touch screen areas, the Touch Injection Noise also exists as a common-mode noise [4.5]. Touch injection noise is not perfectly equal because of the size of coupling capacitance in not same due to the ridge and valley of the fingerprint. Thus, analog-front-end (AFE) should have a higher external noise immunity. Fig.4.5 shows a frequency spectrum of the noise in TSP. An internal noise is also decreases SNR due to the low signal intensity, as shown in fig 4.5. Though a noise reduction circuit like a lock-in sensing architecture, differential architecture attenuates a noise signal of which frequency is far from the driving frequency, in-band noise source decreases a SNR of a fingerprint recognition readout IC.

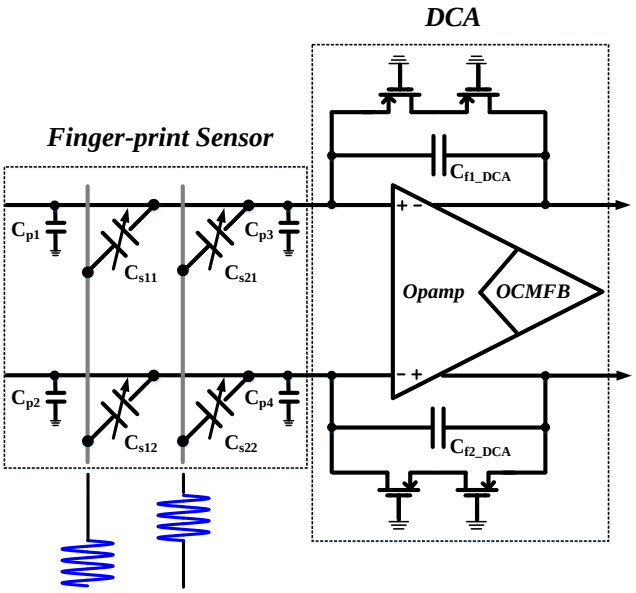

Fig.4. 6 Differential Charge Amplifier with Time-Interleaved Method

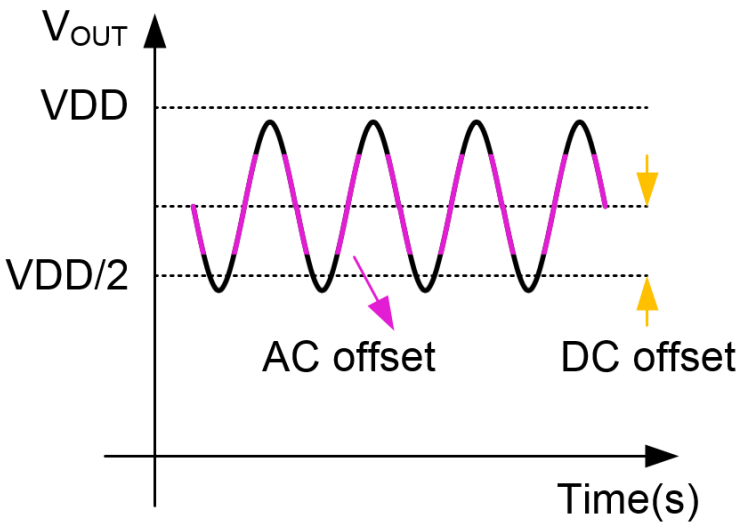

Fig.4. 7 AC offset and DC offset by the mismatch in TSP and internal circuits

As mentioned earlier, a differential circuit is required to remove touch screen external noise. However, when a differential circuit is used, AC offset component of which frequency is same with frequency of the signal is occurred due to mismatch of as Mosfet, passive component, and mutual capacitance in TSP [4.6], [4.7], [4.8]. The capacitance to be sensed is sub 1 femto-farad. Even with a 0.1% mismatch, the 1 pF capacitance produces an error of 1 fF. Fig. 4.7 shows a AC offset and DC offset by the mismatch in TSP and internal circuits. When AC offset is amplified, the dynamic range of the output is reduced, when it gets worse, the receiver output is saturated, and the function is disabled.

4.2 Proposed Approach for fingerprint TSP

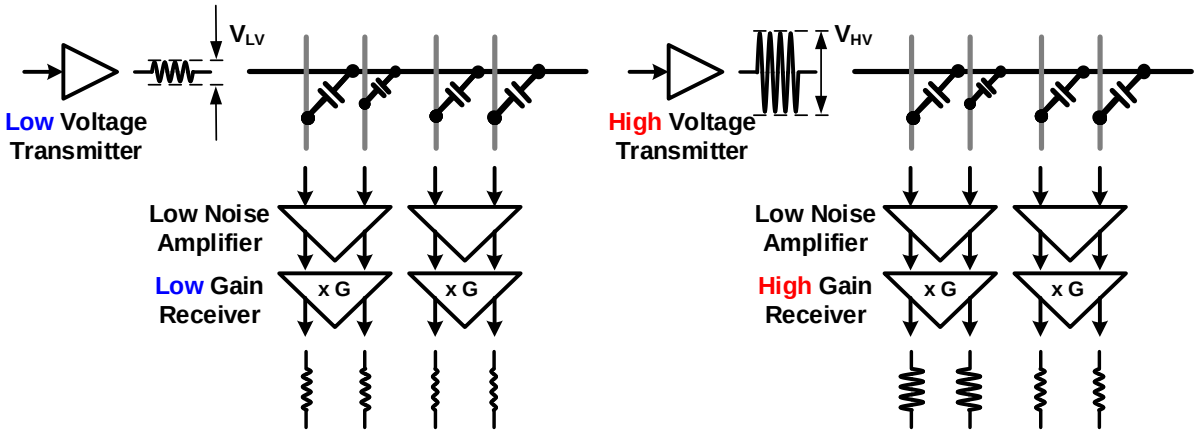

Fig.4. 8 Capacitance difference between ridges and valley according to the thickness of glass

An output of the single-ended capacitor sensing circuit has a larger portion of the static value due the static mutual capacitance which reduces a dynamic range of the single-ended output. In contrast with single-ended output circuit, there is no static component in the differential circuit and only output component of differential circuit is proportional to capacitance difference. In addition, the differential architecture removes a common-mode noise like a display noise. Thus, the differential sensing is essential to distinguish the low capacitance difference in fingerprint TSP environment.

In mutual capacitive fingerprint TSP, the CVR value of the TSP is only several atto-farads. In the case of the conventional touch screen driving IC, since it senses the size of several hundred femto farad capacitance, not only the driving voltage is small but also the gain of the receiver is small. Using the low voltage transmitter and low gain receiver in Figure 4.8 will prevent the output from exceeding the output range at the final output stage, but it will be difficult to get enough dynamic range because the CVR in fingerprint TSP is very small. The small dynamic range of output means that the boundaries between ridges and valleys are very ambiguous. As a result, as the thickness of the glass continues to grow, the boundaries will continue to shrink, and no matter how high the resolution ADC is used, it will not be able to distinguish between ridge and valley. By increasing the signal strength through the high voltage signal and increasing the output by CVR through the receiver circuit with high gain, the dynamic range of the output is improved, as shown in Fig. 4.8. When multiple sampling is superimposed to improve the dynamic range, it is possible to effectively make a difference in output by CVR even if the signal intensity by the glass thickness is reduced. The scan time required for the channel, TCH, is much needed for accumulation as the signal strength is low. When high voltage driving signal and high gain receiver are used, the T_{CH} is effectively reduced because of the large dynamic range. As a result, the total scan time can be reduced.

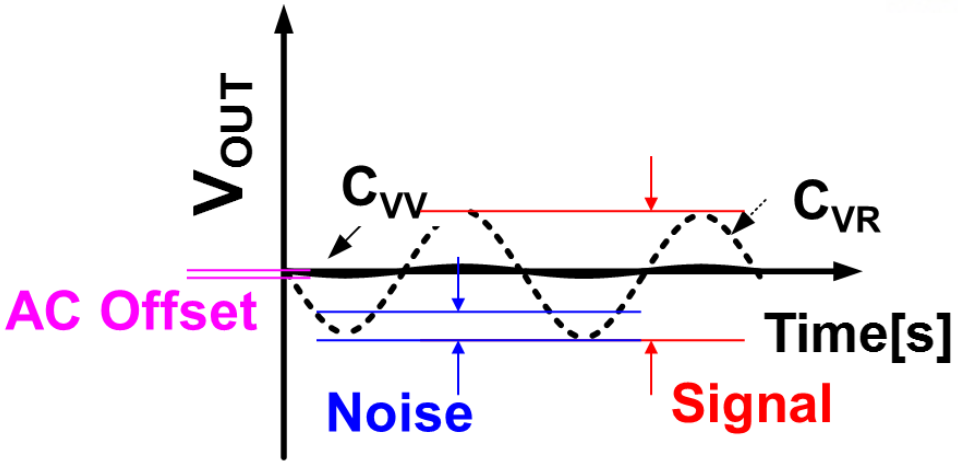

Fig.4. 9 System Architecture for fingerprint recognition

A differential architecture removes a static component and a common-mode noise component and high voltage transmitter and high gain receiver enhances a dynamic range of output by CVR. However, when using differential architecture, an additional AC offset is occurred due to the mismatch from the passive component, a Mosfet sizing in differential circuit. The magnitude of AC offset is proportional to the driving voltage and gain of receiver. In addition, since frequency of AC offset is same with that of a dominant signal. Thus, it is hard to detach AC offset from signal component.

A large AC offset component reduce a dynamic range and makes output saturated in the worst case. Previously, DCA with input-common-mode feedback circuits (ICMFB) reduces an AC offset due to the parasitic mismatch [4.8], [4.9]. However, ICMFB cannot remove internal mismatch. Also additional noise from ICMFB is caused. A first stage of the receiver for fingerprint TSP should be designed a low noise amplifier since the noise of the first stage amplifier is maximized by the high gain of the receiver, which has the greatest effect on the system SNR. Thus, it is required to remove the AC offset without generating additional noise when using differential architecture.

To detect fingerprints effectively in this chapter, we use a high-voltage driven transmitter and a receiver with high gain and high noise immunity. As a result, the dynamic range of the output signal is greatly increased as shown in Fig 4.9, and the noise signal is minimized. In addition, we propose a signal processing method that can remove AC offset only by signaling method without additional active circuit, and can to improve high speed and signal intensity by using parallel operation simultaneously.

4.3 A Proposed System Architecture

4.3.1 System Architecture

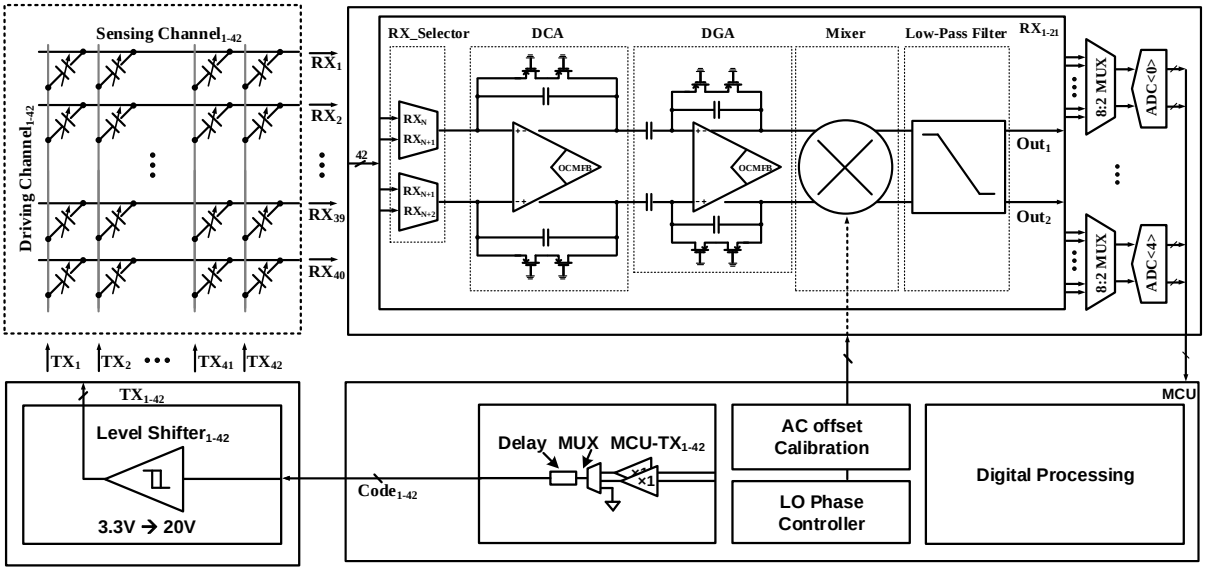

Fig.4. 10 System Architecture for fingerprint recognition

Fig. 4.10 shows a system architecture for mutual capacitive fingerprint TSP. A proposed system architecture is composed of a high - voltage transmitter, a fully differential receiver and a micro control unit (MCU) which includes an analog - to - digital converter. The transmitter is composed of a MCU part which includes signal selector for selecting an in-phase or out-phase signal and a delay cell for synchronization in multi-driving and high voltage IC for level shifting from 3.3V to 20V. Each transmitter channel is connected to each TX electrodes of TSP.

The receiver consists of a multiplexer, a differential charge amplifier (DCA), a differential gain amplifier (DGA), a multiplier, a low-pass filter, an ADC, and an MCU. The multiplexer selects one of two neighboring channels in the differential receiver, and the differential receiver circuit can alternately compare two neighboring channels using a multiplexer. DCA is a charge amplifier consisting of differential structure of op-amp, feedback resistor and capacitor. Since it is the first active amplifier in the analog-front-end stage, it directly affects noise, offset and signal magnitude. Therefore, it is necessary to make effort to minimize noise and offset in design. The input of the DGA is connected to the output of the DCA. The DGA was supposed to amplify the DCA signal. The circuit was composed of a capacitive charge amplifier and the gain was set to 20. The input of the multiplier is connected to the output of DGA. The mixer consists of a charge amplifier with a chopper switch, and its gain is set to 1-20. The output of the multiplier is connected to a low-pass filter to accomplish the lock-in sensing

structure. The gain of the receiver is designed to be controlled from 1-400. The output of the low-pass-filter is connected to the ADC in the MCU and converted to digital, which is demodulated by the MCU to recognize the fingerprint. The analog outputs of a fully differential receiver are converted to the digital signal using ADC inside the MCU, and the specification of the ADC is 40-channel, 48-mbps of 12-bit.

4.3.2 A Proposed Differential Signaling Method with High Voltage Transmitter

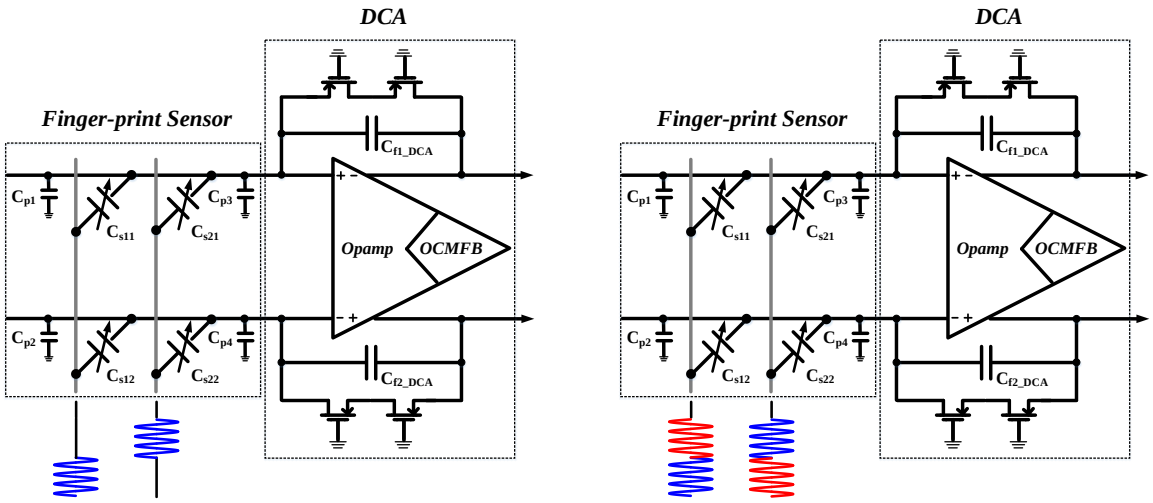

Fig.4. 11 Differential Charge Amplifier with Time-Interleaved Method and Differential-Time Interleaved Method

Fig.4.11 shows a differential charge amplifier with time-interleaved method and differential-Time interleaved method in mutual capacitive in fingerprint TSP. $C_{s11,12,21,22}$ is a mutual capacitor of fingerprint TSP and $C_{p1\text{-}4}$ is a parasitic capacitor of each electrodes. Differential charge amplifier is composed of a feedback capacitor, $C_{f1\text{-}2\_DCA}$, feedback resistor, operational amplifier and mutual capacitive fingerprint TSP. The mutual capacitive TSP has driving electrodes and sensing electrodes. Driving channel are connected to the driving signal and sensing channel are connected to the input of DCA.

$$V_{DCA\_STX} = V_{out+} - V_{out-} = -V_{s+}\frac{\Delta C_S}{C_F} + V_{AC\_offset}$$
$$= -V_{s+}\frac{\Delta C_{S11} - \Delta C_{S12}}{C_F} - V_{s+}\frac{\alpha\Delta C_F + \beta\Delta C_P}{C_F} + V_{s+}\frac{C_{S11\_pr} - C_{S12-pr}}{C_F} \quad (4.4.1)$$

Equation 4.4.1 shows a differential output with a Time-Interleaved Method (STX), which means that one driving signal is connected to the driving electrodes. In Equation 4.4.1, $\Delta C_{s,i}$ is a capacitance difference of between adjacent driving electrodes, C_F is a feedback capacitor of DCA, ΔC_F is a mismatch of feedback capacitors, $C_{f1,2\_dca}$, ΔC_p is a parasitic capacitance mismatch in fingerprint TSP, α and β are

coefficients of AC offset occurred by mismatch of feedback capacitors and parasitic capacitors, Acm_err is a common-mode rejection error and $\Delta C_{s\_process}$ is a process mismatch of mutual capacitor in fingerprint TSP. In the output of differential circuit with STX, AC offset is occurred by above mismatch and process variation, which reduces a dynamic range of the output.

$$\begin{aligned} V_{DCA\_DTX} &= V_{out+} - V_{out-} = -V_{s+}\frac{C_{S11}-C_{S12}}{C_F} + V_{s-}\frac{C_{S21}-C_{S22}}{C_F} + V_{AC\_offset} \\ &= -V_{s+}\frac{\Delta C_{S11}-\Delta C_{S12}-\Delta C_{S21}-\Delta C_{S22}}{C_F} \\ &\quad -V_{s+}\frac{\alpha\Delta C_F+\beta\Delta C_P}{C_F} + V_{s-}\frac{\alpha\Delta C_F+\beta\Delta C_P}{C_F} \\ &\quad -V_{s+}\frac{C_{S11\_pr}-C_{S12\_pr}}{C_F} + V_{s-}\frac{C_{S21\_pr}-C_{S22\_pr}}{C_F} \end{aligned} \tag{4.4.2}$$

Proposed Differential TX driving (DTX) is a method of simultaneously driving opposite phase signals, Vs+ and Vs-, to neighboring driving electrodes. The amplitude of AC offset is proportional to driving signal and frequency of AC offset is same with the driving signal. Thus, when driving DTX in Fig.4, a phase of AC offset by V_{s+} and V_{s-} is opposite. As a result, AC offset occurring from mismatch from the internal component is canceled each other like equation 4.4.2.

The influence of in-band noise at the receiver is largest at the first stage. The advantage of the DTX is that it does not require an additional ac offset cancelation circuit, so that it is possible to minimize an input-referred noise of DCA.

However, it is hard to remove AC offset error completely since there are process capacitance error, ΔCs_process and differential signal is not perfectly synchronized. To solve this problem, a digital AC offset calibration method is presented. The digital offset calibration is a method of pre-storing the residual AC offset in each channel, and eliminating digitally the offset by subtracting the residual offset at the final output.

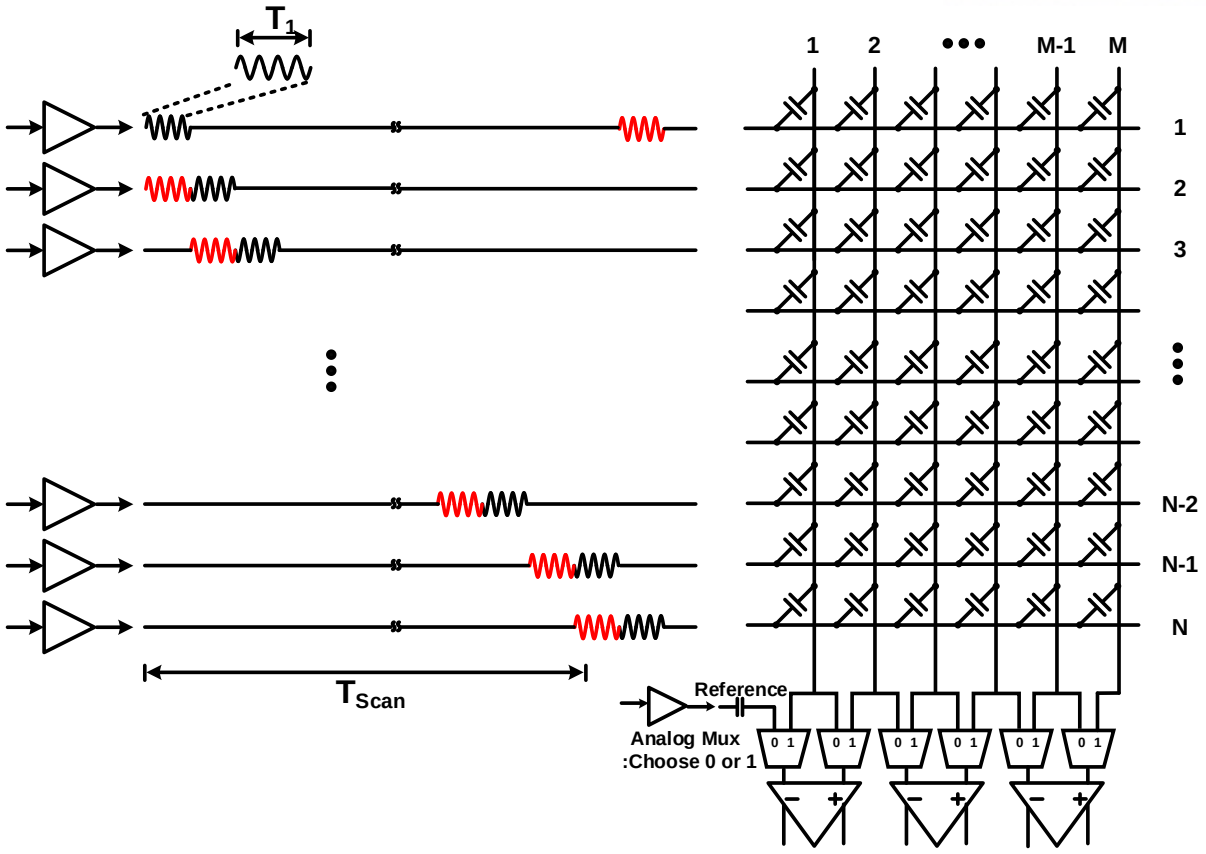

Fig.4. 12 Differential Charge Amplifier and Differential-Time Interleaved Method

Fig.4.12 shows a differential charge amplifier with differential-time interleaved method and Fig. 4.13 shows a process of AC offset cancelation. $T_{1\text{-}15}$ is assigned time when a driving signal is connected to the $TX_{1\text{-}15}$ electrode. In fig.6, the wave in a divided time is 1-channel output of differential receiver (DRX).

STX- DRX wave shows the output of the DCA when STX is applied to the fingerprint recognition touch screen. The large mismatch makes output out of the operating range, which is not recovered. As shown is DTX-DRX wave, by applying DTX to the fingerprint recognition TSP, the output of the DCA is not saturated in the mismatch environment. Finally, by applying digital calibration which removes the residual AC offset of each channel, the receiver can obtain the final output for fingerprint recognition.

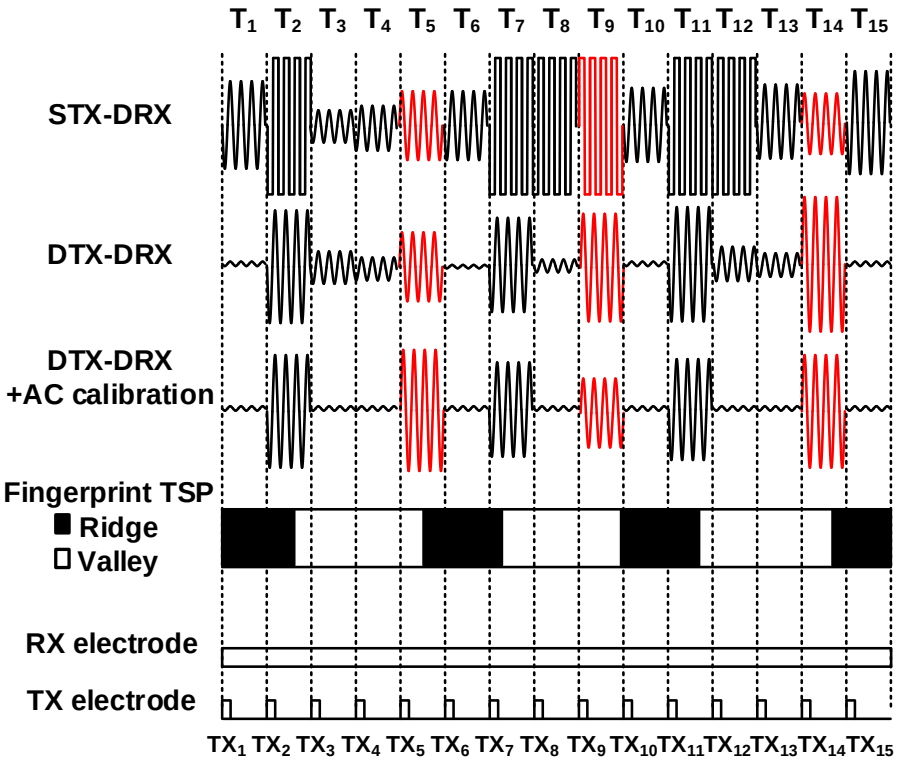

Fig.4. 13 Comparison of relative SNR verse Frame Rate

An output of the single-ended charge amplifier is directly proportional to the mutual capacitance in fingerprint TSP. In the case of the differential output, since the differential output is proportional to the neighboring capacitor difference value, a demodulation process for converting the differential signal to the single-ended output is required.

$$b_k = a_k - a_{k-1} + O_k + N_k \tag{4.4.3}$$

$$a_k = a_{REF} + \sum_{k=1}^{n-1} b_k - \sum_{k=1}^{n-1} O_k - \sum_{k=1}^{n-1} N_k \tag{4.4.4}$$

As shown in equation 4.4.3, the differential output, b_k, is expressed the difference of the single-ended output, a_k and a_{k-1}, the sampled offset, O_k, and sampled noise, N_k, in the differential output circuit. A differential receiver demodulation means that the differential output, b_k, is converted to the single ended output, a_k, as shown in equation 4.4.4. As shown in Fig. 4.12, the time-division differential signal method is driving the signals of opposite phases to the neighboring channels on the touch screen in a divided time. When the differential driving method and the fully differential receiver are applied

together, the demodulation of a differential receiver with DTX is expressed as the following Equation 4.4.5. c_k denotes an output of the differential receiver by DTX signal processing. As shown in equation 4.4.6, b_k is the output of the differential receiver that can be obtained by processing a STX signal. Equation 4.4.7 show that the differential-signal-ended output of the differential receiver is converted into a single-ended output value, a_k. O_k is the AC offset value obtained from the differential receiver, and N_k is the noise signal sampled by the differential receiver.

$$c_k = b_k - b_{k-1} + O_k + N_k \tag{4.4.5}$$

$$\begin{aligned} b_{k\_DTX} &= b_{REF} + \sum_{k=1}^{n-1} c_k \\ &= b_{REF} + b_k - \sum_{k=1}^{n-1} O_k - \sum_{k=1}^{n-1} N_k \end{aligned} \tag{4.4.6}$$

$$a_k = a_{REF} + b_{REF} + \sum_{k=1}^{n-1} b_k - \sum_{k=1}^{n-1}\sum_{k=1}^{n-1} O_k - \sum_{k=1}^{n-1}\sum_{k=1}^{n-1} N_k \tag{4.4.7}$$

Equation 4.4.7 shows that a sampled AC offset and noise is accumulated after the demodulation of a differential receiver with DTX. In the case of accumulated noise, it is possible to disperse through multiple samples. On the other hand, if the AC offset is accumulated, it is increased without being scattered, which causes a considerable error. In that reason, a differential driving method and digital AC offset calibration method is required in the differential receiver with DTX to remove AC offset component. By applying a differential driving signaling method, AC offset occurring in each channel should be controlled within the range that the output is not saturated. The residual AC offset is stored in advance in digital form and to remove it in the process of demodulation.

$$SNR_{DTX} = \frac{2\alpha \sum_k a_k}{\alpha \sum_k O_k + \sum_k \beta_k N_k} \tag{4.4.8}$$

Equation 4.4.8 shows a SNR of the differential receiver with DTX. Since a differential charge amplifier has a bandpass characteristic, each signal of which frequency is different has different gain. α is a gain of main output signal by CVR and β is a gain of each noise signal. By acquiring a multiple sampling from each output of channel, an added noise is dispersed. SNR with DTX is two times larger than that with STX. By removing AC offset effectively while increasing a dynamic range, SNR in differential receiver with DTX is maximized.

$$\begin{bmatrix} A & 0 & 0 & 0 & 0 & 0 & 0 & 0 \\ \overline{A} & A & 0 & 0 & 0 & 0 & 0 & 0 \\ 0 & \overline{A} & A & 0 & 0 & 0 & 0 & 0 \\ 0 & 0 & \overline{A} & A & 0 & 0 & 0 & 0 \\ 0 & 0 & 0 & \overline{A} & A & 0 & 0 & 0 \\ 0 & 0 & 0 & 0 & \overline{A} & A & 0 & 0 \\ 0 & 0 & 0 & 0 & 0 & \overline{A} & A & 0 \\ 0 & 0 & 0 & 0 & 0 & 0 & \overline{A} & A \end{bmatrix} \quad \begin{bmatrix} A & \overline{D} & D & \overline{C} & C & \overline{B} & B & \overline{A} \\ \overline{A} & A & \overline{D} & D & \overline{C} & C & \overline{B} & B \\ B & \overline{A} & A & \overline{D} & D & \overline{C} & C & \overline{B} \\ \overline{B} & B & \overline{A} & A & \overline{D} & D & \overline{C} & C \\ C & \overline{B} & B & \overline{A} & A & \overline{D} & D & \overline{C} \\ \overline{C} & C & \overline{B} & B & \overline{A} & A & \overline{D} & D \\ D & \overline{C} & C & \overline{B} & B & \overline{A} & A & \overline{D} \\ \overline{D} & D & \overline{C} & C & \overline{B} & B & \overline{A} & A \end{bmatrix}$$

$T_1\ T_2\ T_3\ T_4\ T_5\ T_6\ T_7\ T_8$ $\qquad$ $T_1\ T_2\ T_3\ T_4\ T_5\ T_6\ T_7\ T_8$

Fig.4. 14 Differential Driving Code, 8x32bit Differential Coded Multiple Signaling

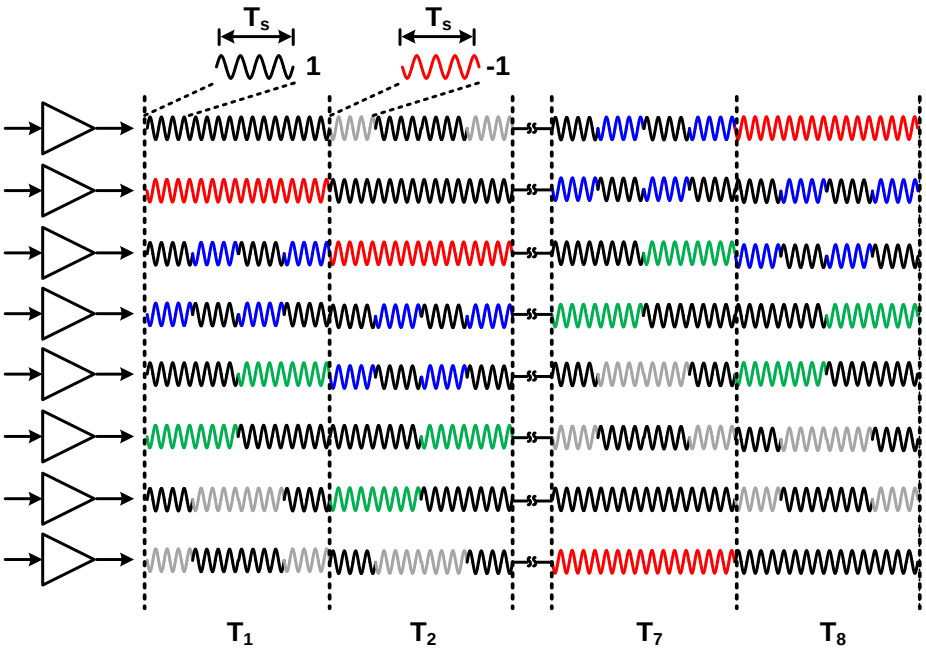

Fig.4. 15 8x32-bit Differential Coded Multiple Signaling

Since fingerprint recognition TSP consists of multiple channels of electrodes, multiple driving is required to achieve high product of SNR and frame rate. However, in the case of the conventional multi-drive method, code offset occurs in the process of transmitting signals simultaneously in multiple [4.10], [4.11], [4.12], [4.13]. In the case of the N-bit Walsh-Code, there are N orthogonal codes composed of N bits. The N offset of the code is generated during the transmission of the first bit. Various codes have been developed to remove these Walsh code offsets, but failed to make zero offset. Since the very small capacitance must be distinguished in the case of the fingerprint recognition circuit, a high gain of the receiver is required to increase a dynamin range. However, if the code offset of the output is much larger than the signal level, a high gain receiver makes an output saturated.

A differential coded multiple signaling method (DCMS) is presented to overcome the code offset problem in fingerprint sensing. As shown in Fig. 4.14, the code was generated by applying the Walsh code to the differential driving code simultaneously.

$$\begin{array}{ccccc} H \times X = K & & c_k = b_k - b_{k-1} & & b_k = a_k - a_{k-1} \\ X = H^{-1} \times K & \rightarrow & b_k = b_{REF} + \sum_{k=1}^{n-1} c_k & \rightarrow & a_k = a_{REF} + \sum_{k=1}^{n-1} b_k \\ \text{(a)} & & \text{(b)} & & \text{(c)} \end{array}$$

Fig.4. 16 A demodulation process of Differential Coded Multiple Sensing Method

In Fig.4.15, 8-bit-DCMS consists of positive and negative orthogonal code sequences, such as a, b, c, d and -a, -b, -c, -d. The offset does not occur because the sum of the multi-differential-driving codes is always zero. In Equation 6, H denotes a multi-differential-driving code sequence, and X denotes a capacitor of each node of the fingerprint TSP. Fig.4.16 shows a method to demodulate the multi-differential-driving code. Firstly, the sum of outputs K is multiplied by the inverse matrix of the orthogonal code sequence using equation (a) in Fig.4.16. It means the DCMS sequence is converted to the differential driving method. These code sequences are demodulated using equation (b) in Fig.4.17, differential driving demodulation method, which means the differential TDMA converted to TDMA. Lastly, a differential output of the receiver is also demodulated by using differential receiver demodulation method in an equation (c) in Fig. 4.18. By using the multi-differential-driving method, a low-offset, high product of SNR and frame rate with large TX channel is accomplished.

$$SNR_{DCMS} = \frac{2 \times N \times \alpha \sum_k a_k}{\alpha \sum_k O_k + \sum_k \beta_k N_k + \sum_k I_k} \tag{4.4.9}$$

A SNR of DCMS is shown in equation 4.4.9. A signal intensity is N times larger than that of DTX and the number of sample in DCMS is also N times larger than that of DTX. As the number of samples increases, the added noise decreases. The interference of DCMS, I_k, is added in the demodulation of DCMS. By adjusting the synchronization of neighboring signals, the interference generated in the DCMS is minimized and consequently the SNR of the DCMS is greatly improved.

4.4 A Proposed High Voltage Transmitter and Fully Differential Receiver with Lock-in Sensing Architecture

4.4.1 High Voltage Transmitter

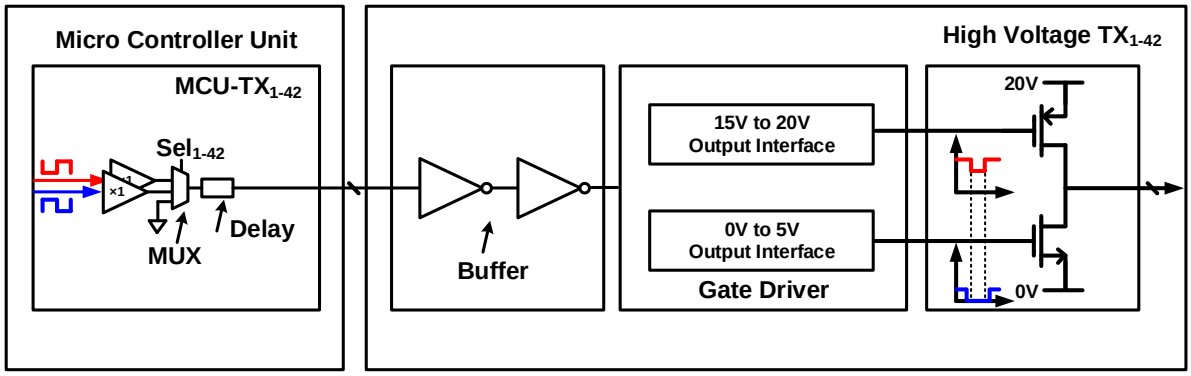

Fig.4. 17 High Voltage Transmitter with non-overlapping gate driver

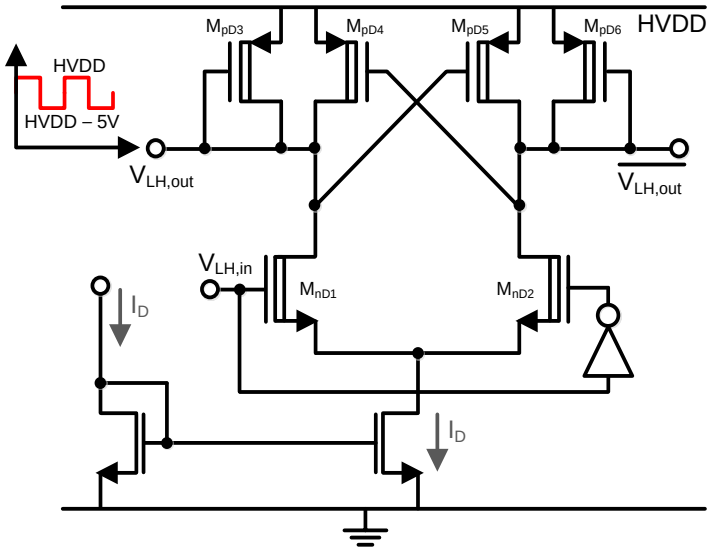

Fig.4. 18 (a) 0V to 5V voltage output interface circuit(level shifter) for LS MOSFET on/off,

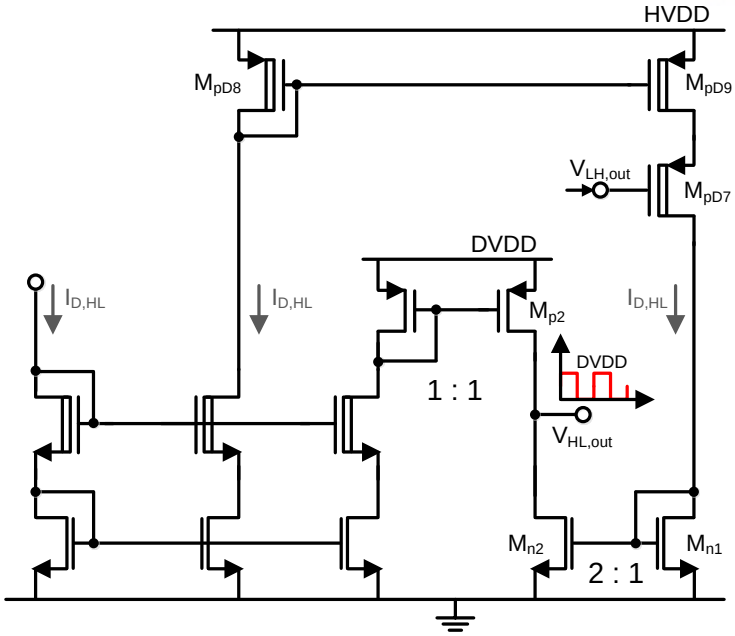

Fig.4. 19 (b) 15V to 20V voltage output interface circuitry (level shifter) for HS MOSFET on/off,

The transmitter consists of a 42-ch Code Generator for generating code signlas and a 42-ch High Voltage Level Shifter for increasing the voltage from 3.3V to 20V. Figure 4.17 shows a 42-channel High Voltage Transmitter that generates a high-voltage code signal [4.14], [4.15].

The code signal is generated by using the reference signal inside the MCU. The frequency of reference signal is 1 MHz and it has two phases, in-phase and out-phase. The multiplexer (MUX) selects one of the in-phase signal, the out-phase signal and the DC voltage through the selection code signal. In addition, Delay of output is controlled to synchronize the multiple driving signals.

These outputs of 42-ch code generator part in MCU is connected to the input of high voltage transmitter.

The first stage of the high voltage transmitter is buffer. The output of buffer is connected to the gate voltage driver. Since the high-voltage transmitter is manufactured by the BCD process, the voltage difference between gate and source of the MOSFET must be controlled below 5V. Figure 4.18 (a) shows the 0V to 5V voltage output interface circuit (level shifter) for LS MOSFET on / off. Figure 4.18 (b) 15V to 20V voltage output interface circuitry (level shifter) for HS MOSFET on / off. By using proposed gate drivers, the gate of the PMOS of the output stage is controlled at 15 ~ 20V, and the NMOS of the output stage is controlled at 0 ~ 5V. Finally, the outputs of high voltage transmitter is induced to the transmitter electrodes.

4.4.2 Fully Differential Receiver with Lock-in Sensing Architecture

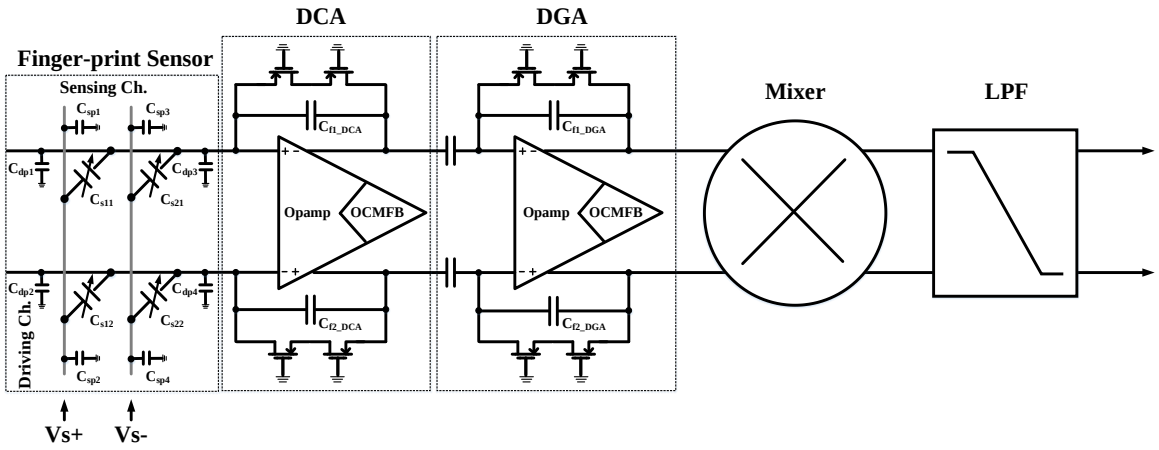

Fig.4. 20 Fully differential Receiver for fingerprint recognition

The receiver has four stages, DCA, DGA, multiplier, and LPF to realize the lock-in-sensing structure [4.16], [4.17], [4.18], [4.19]. As shown in Fig. 4.19, a frequency of driving signal is 1MHz. 1.1MHz signal is used as a chopping frequency in the mixer. There are external noise sources such as display noise and lamp noise in the touch screen environment. Display noise is a common-noise coupled between the display common plate and the electrode of touch screen. Lamp noise is a type of self-noise that is coupled to TSP via the human body when touched from a lamp. These noise signal of which frequency is far from the 1MHz, which is removed by the lock-in sensing architecture. However, an in-band noise in DCA, DGA of which frequency is near 1 MHz is amplified along with the signal by CVR.

The gain of the DGA is 20 and the gain of the mixer is also 20, so that the in-band noise of DCA and DGA is the main noise of the output. For the same reason, AC offset from DCA and DGA is major offset in output of the receiver.

$$RX_{out} = G_{DGA}G_{Mixer}\left(V_{drv}\frac{\Delta C_S}{C_F} + AC_{offset,DCA} + N_{in,DCA}\right) + G_{Mixer}\left(AC_{offset,DGA} + N_{in,DGA}\right) \quad (4.4.2.1)$$

Equation 4.4.2.1 shows a system noise and offset of the fully-differential receiver. AC offset and noise of DCA are amplified by the gain of DGA and mixer. AC offset and noise of DGA are amplified by the gain of the mixer. Thus, it is important to minimize the noise and ac offset of DCA and DGA. Thus, in-band noise and AC offset of which frequency is near the driving signals, should be lower

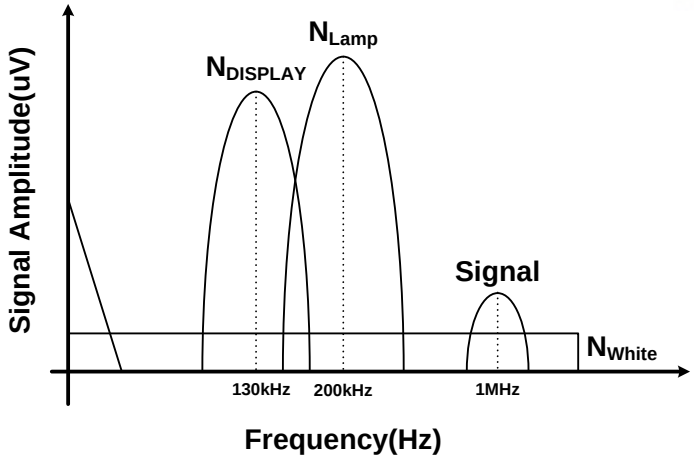

(a) Output of differential charge amplifier

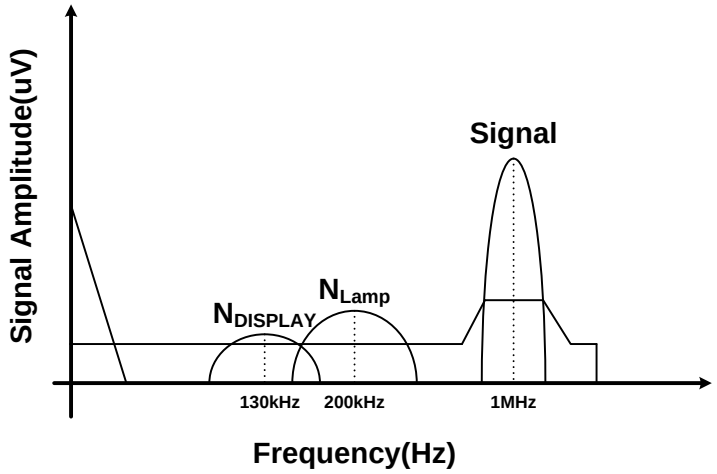

(b) output of differential gain amplifier

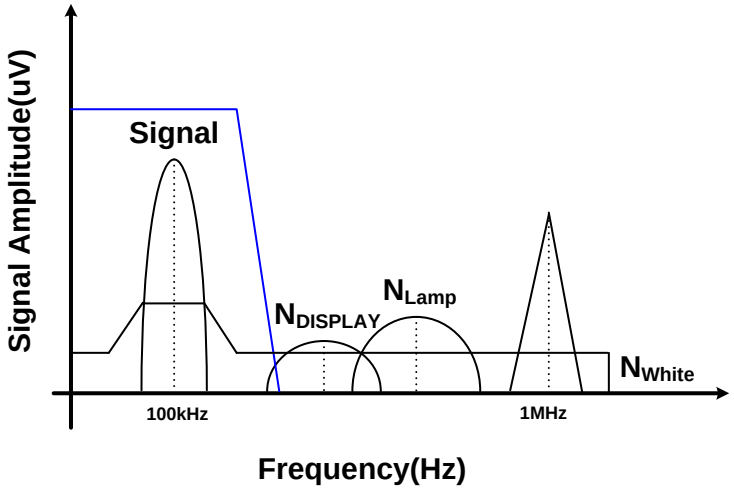

(c) output of low pass filter

Fig.4. 21 Fully differential Receiver for fingerprint recognition

Circuit Implementation

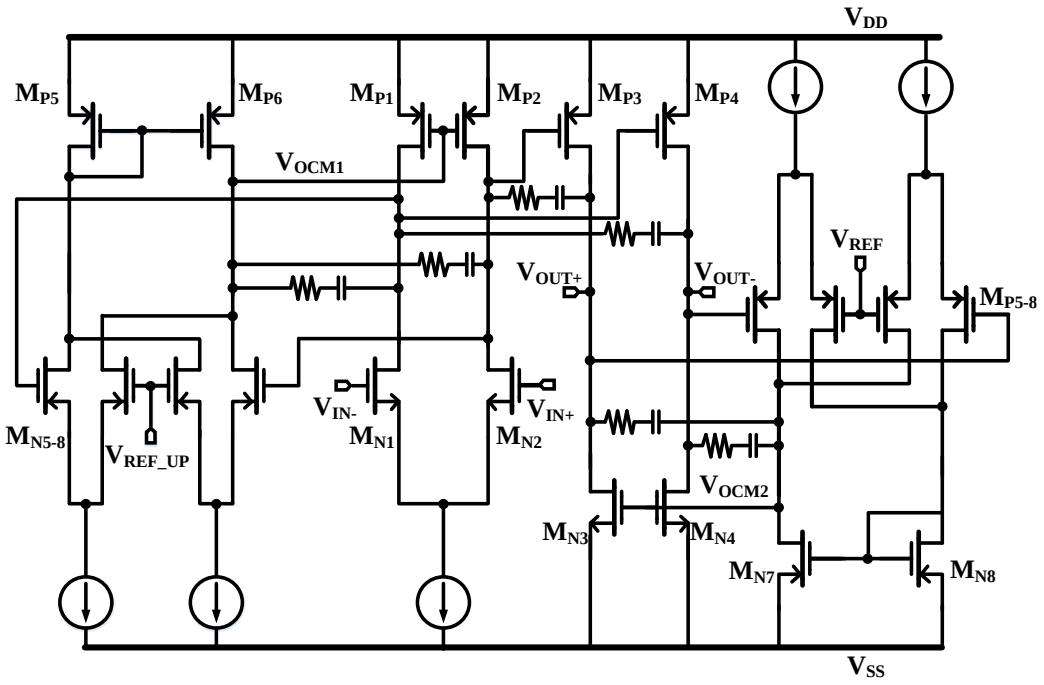

Fig.4. 22 Fully differential 2-st operational amplifier

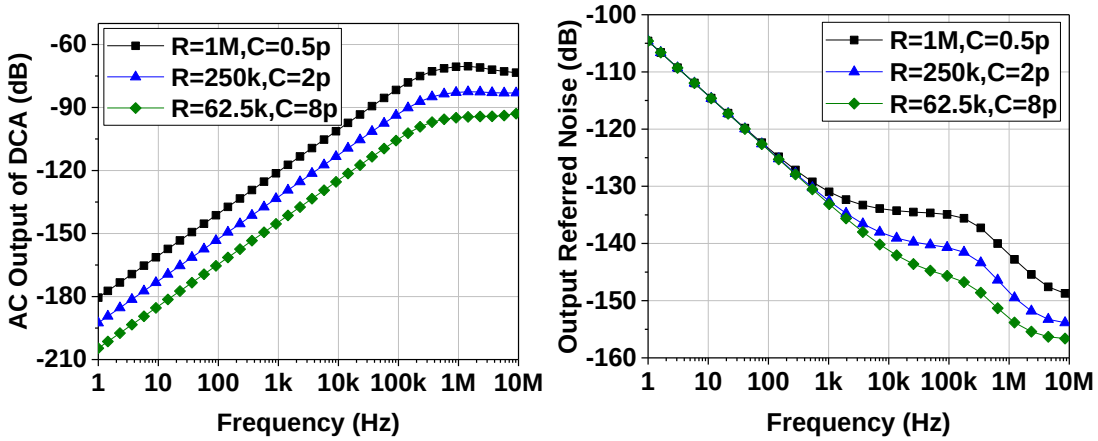

Fig.4. 23 AC output and output referred noise of differential charge amplifier according to feedback capacitor and resistor size

In this section, a noise and offset of charge amplifier is analyzed. As mentioned, the internal noise of DCA and DGA is main noise component to decide SNR of the receiver. Also, AC offset of DCA should be controlled under mV for the receiver to operate within the operating range.

$$\overline{v_{n,DCA}^2} = \frac{1}{k_{CMRR}}\left(\left(1+\frac{C_S+C_P}{C_F}\right)^2\left(\overline{v_{n,ota1}^2}\right)+2\left(\frac{1}{2\pi fR_FC_F}\right)^2\overline{v_{n,\mathrm{R}}^2}+\sum_i\frac{C_{ext,i}}{C_F}\overline{v_{n,ext,i}^2}\right) \tag{4.5.1}$$

$$\overline{V_{n,ota1}^2} = \frac{16kT}{3}\frac{1}{g_{m1}^2}\left[g_{m1}+g_{m3}+\frac{g_{m5}+g_{m7}}{g_{m5}^2(r_{o1}\,\|\,r_{o2})^2}\right]+\overline{v_{n,cmfb}^2} \tag{4.5.2}$$

The product of feedback resistance and feedback capacitor determines the center frequency of DCA which has a bandpass filter characteristic. Fig. 4.22 shows frequency spectrum of output and output referred noise of DCA according to feedback capacitor and resistor size. The product of the feedback resistor and the feedback capacitor is constant to design the same center frequency of DCA. The smaller the feedback capacitor value, the larger the gain of DCA. Also, the smaller the feedback resistance value, the less the feedback resistor noise. Considering the noise due to the resistance and the magnitude of the signal output due to the feedback capacitor size, the feedback capacitor of the first stage was determined to be 2 pF and the feedback resistance was determined to be 250k ohm.

Equation 4.5.1 shows an input referred noise of DCA. Equation 4.5.25 shows a input referred noise of 2nd stage op-amp in DCA. As shown in Fig.4.23, where C_s is the sensing capacitance, C_p is the parasitic capacitance of the sensing electrode, $\overline{v_{n,DCA}^2}$ is the output referred noise of DCA, $\overline{v_{n,OTA}^2}$ is the input referred noise of OTA, $\overline{v_{n,R_F}^2}$ is the thermal noise of a feedback resistance and $\overline{v_{n,ext,\iota}^2}$ is the external noise source coupling from external capacitance, $C_{ext,i}$. k_{CMRR} is the coefficient of common-mode rejection ratio in the differential structure.

The output of the DCA is affected by the external noise, the feedback resistance noise, and the internal noise of op-amp. External noise, such as display noise and lamp noise, is removed by the DCA's bandpass filter characteristics. The noise generated by the feedback resistor and the op-amp are white noise components, so even if filtered, an in-band noise of which frequency is near the driving signal remains. The in-band noise component substantially determines the SNR of the output since it cannot be removed. To minimize the op-amp noise component, the op-amp was designed with a 2-stage structure. The main noise occurs in the input $M_{N1,2}$ of the first stage and in the $M_{P1,2}$ in second stage. To minimize noise, we designed $gm_{N1,2}$ to be maximized and $gm_{P1,2}$ to be minimized.

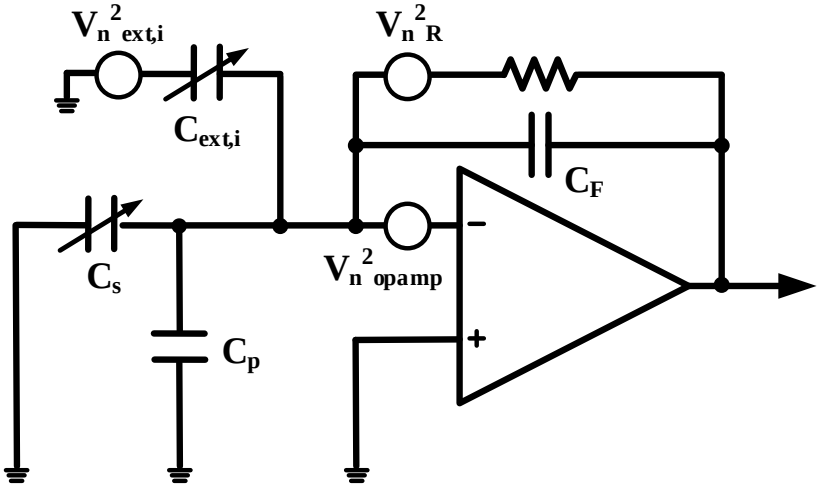

Fig.4. 24 Noise sources in the differential charge amplifier

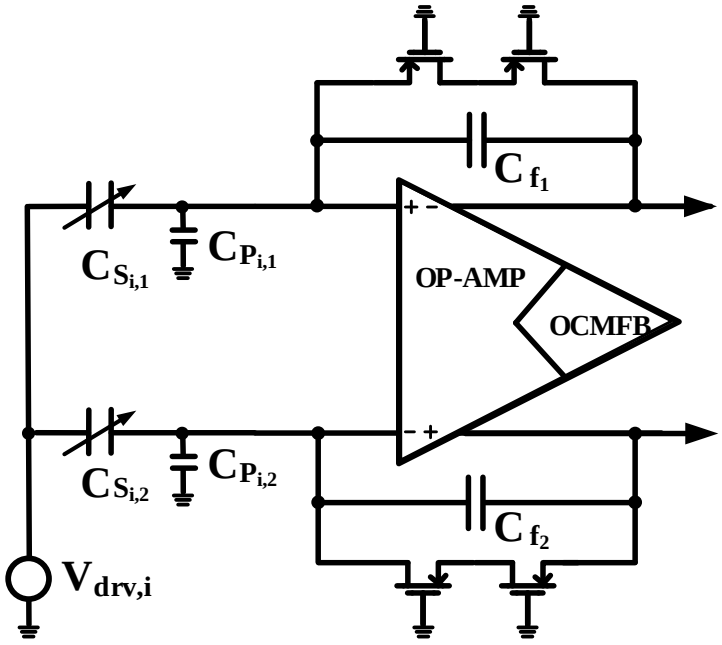

Fig.4. 25 Offset analysis of a differential charge amplifier

$$
\begin{aligned}
V_{DCA\_DTX} &= V_{out+} - V_{out-} = -V_{drv}\frac{\Delta C_S}{C_F} + V_{AC\_offset} \\
V_{AC\_offset} &= V_{drv}\frac{\Delta C_{f_1} - \Delta C_{f_2}}{C_F} + \left(V_{drv} - V_{OS,in}\right)\frac{C_S}{C_F} \\
&\quad + \sum_{i=1}^{N}\left(A_{cm\_err}V_{in}\frac{C_{S_{i,1}} - C_{S_{i,2}}}{C_F} + V_{drv}\frac{C_{P_{i,1}} - C_{P_{i,2}}}{C_F} + V_{drv}\frac{C_{S_{i,1}} - C_{S_{i,2}}}{C_F} \right)
\end{aligned}
\tag{4.5.3}
$$

As shown in Fig 4.24, AC offsets occurred in DCA are caused by OP-amp offset, passive component mismatch, parasitic capacitor mismatch, and process error of TSP capacitor. Since the output signal in DCA is less than 1mV and the gain of the receiver is about 400, the first AC offset should be less than 1mV. Although DTX can cancel the AC offset caused by mismatch, it is necessary to minimize it because the differential TX signal is not completely synchronized. To minimize the offset occurring in the differential structure, the common centroid layout technique is used for the receiver layout. In addition, Monte-Carlo simulation was performed to minimize AC offset caused by component mismatch. In addition, the delay cell in TX minimizes synchronization of the differential signals.

When the TX signal is applied to the touch screen, the current proportional to the size of the mutual capacitors of fingerprint TSP enters the input of DCA. Fig. 4.21 shows a 2-stage operational amplifier with two output-common-mode feedback circuit (OCMFB) for DCA. The two OCMFB are placed in the first stage and the second stage. In the second stage, OCMFB removes a common-mode current and differential current is integrated in feedback capacitor of DCA.

The OCMFB circuit is an error amplifier based on a differential difference amplifier (DDA) structure. The OCMFB circuit compares the output voltage with the reference voltage and fixes the output voltage to the reference voltage using negative feedback. By controlling the gate voltage of the output $M_{N3,4}$ in DCA, a common-mode current is absorbed or sourced by the output $M_{P3\text{-}4}$. In case of STX, the currents with the same phase, different amplitude flow to the feedback capacitor. In case of DTX, in-phase current and out-phase current are mixed in the feedback capacitor and differential current is only integrated. Since OCMFB in DTX don't need to absorb or source a common current, error from OCMFB is minimized compared to that of STX, which makes Common-Mode Rejection Ratio (CMRR) of DCA improves. To accomplish the common-mode current rejection by OCMFB in real time, the frequency characteristic of the close loop of the OCMFB is sufficiently faster than the frequency of the in-phase signal.

4.5 Measurement Result

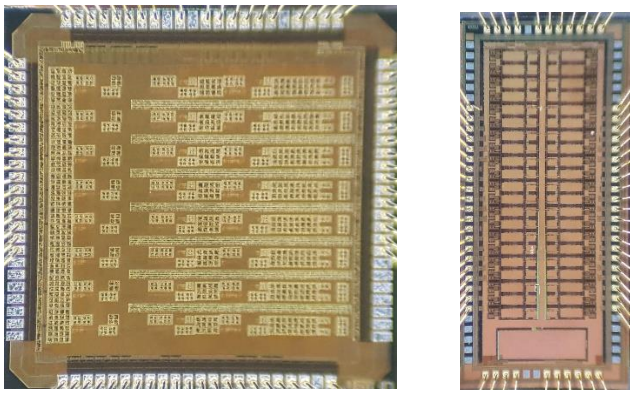

Fig.4. 26 Fully differential Receiver for fingerprint recognition (a) 16-ch Low Voltage Receiver (b) 42-ch High Voltage Transmitter

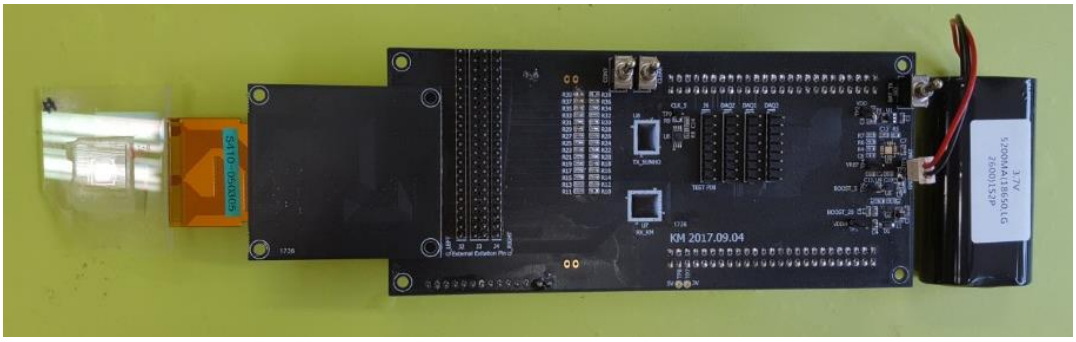

Fig.4. 27 Platform for the fingerprint TSP recognition with 42-ch High Voltage Transmitter, 16-ch Low voltage Receiver, Micro Controller Unit and 42 by 42 fingerprint TSP.

Figure 4.25 (a) shows a 16-channel receiver IC fabricated with 3.3V 0.18um process. Figure 4.26 shows a 42-channel transmitter IC fabricated with a high-voltage BCD process. Transmitter IC can transmit signal up to 20V. Figure 4.25 shows the PCB board including the transmitter and receiver IC and fingerprint TSP. In 42 x 42 mutual capacitive fingerprint TSP which is made of metal mesh electrodes, the mutual capacitance value of each node is 25 fF, CVR is 400 aF when it is below 0.1 T glass and 150 aF when it is below 0.2T glass, and if it is below 0.3T glass, it has 50 aF. The frequency of driving signal by transmitter is 1 MHz, and the voltage of driving signal can be adjusted from 3.3V to 20V. MCU determines the in-phase and out-phase code signal and can adjust the delay of each channel. The MCU can also determine the frequency and the phase of the LO signal. Using the three Prototype 16 channel receivers, it is possible to detect fingerprint TSP with 42-driving electrodes and 42-sensing electrodes. The output of the receiver is connected to the external ADC of the MCU. The 32-channel ADC in the MCU operates at 12-bit, 4M sample/s. The digitized output through the ADC is subjected to an offset calibration process in the MCU, followed by a demodulation process according to the code sent from the transmitting circuit, and finally the fingerprint image is generated.

Fig.4. 28 The outputs of High Voltage Transmitter with Differential Time-interleaved method: Amplitude of output = 20 V, frequency of output = 1 MHz

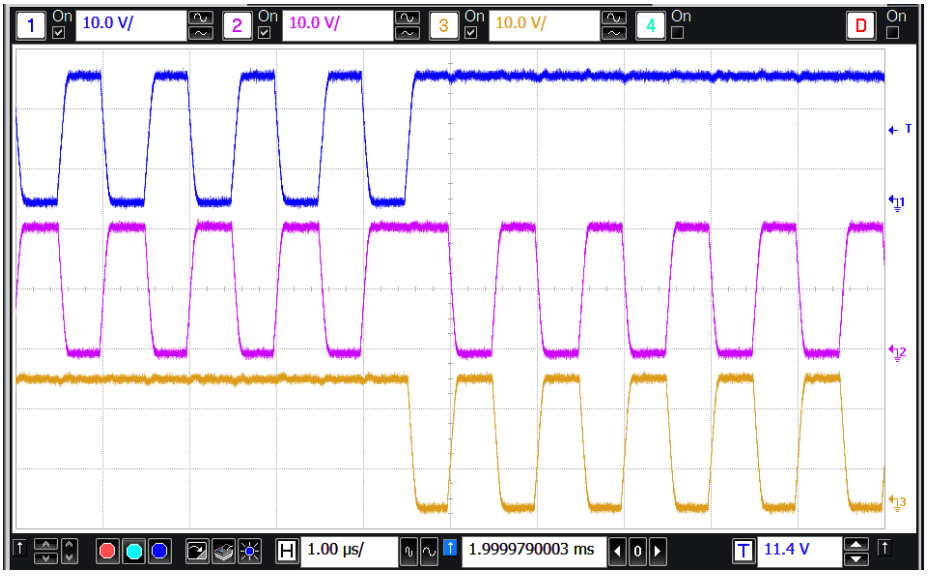

Fig.4. 29 a detailed output waveform of the high voltage transmitter with differential Time-interleaved method.

Fig 4.27 shows an output of the 20V high voltage transmitter. Transmitter sends a differential time-interleaved output of which amplitude is 20V. The frequency of the transmitter output signal is 1MHz. Scan time per channel is 1 ms. Fig. 4.28 shows a detailed output waveform of high voltage transmitter. The transmitter transmits the signal using Time-interleaving method. The time is divided to send both the in-phase signal and the out-phase signal at the same time. As a result, the signal strength can be improved while effectively eliminating the AC offset of the differential structure circuit.

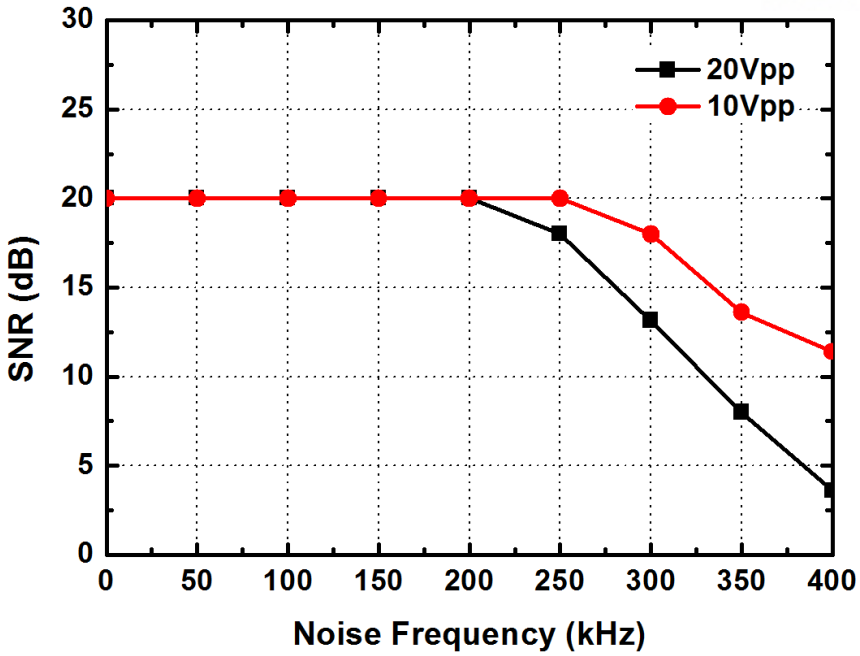

Fig.4. 30 Signal to noise ratio according to the external noise source.

Figure 4.29 shows external noise immunity of a receiving circuit when an external signal is applied to a metal pillar that a metal pillar of 0.3 mm in diameter is in contact with a fingerprint TSP. The external sinusoidal signal with amplitude of 10V and 20V was applied to the fingerprint TSP through the metal pillar while varying frequency from 1Hz to 600kHz. The proposed receiver circuit is design with a lock-in sensing structure, and external noise signal far from 1MHz is filtered, so external signals below about 200kHz are completely removed. As the frequency of the external signal approaches 1 MHz, the SNR decreases.

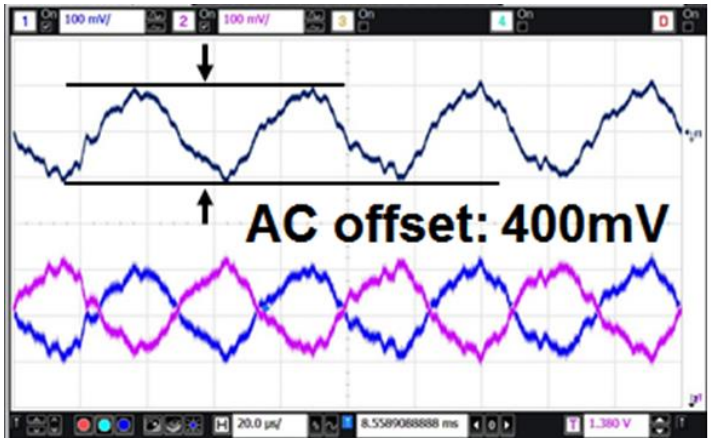

Fig.4. 31 AC offset of the receiver when using Time-Interleaved Method

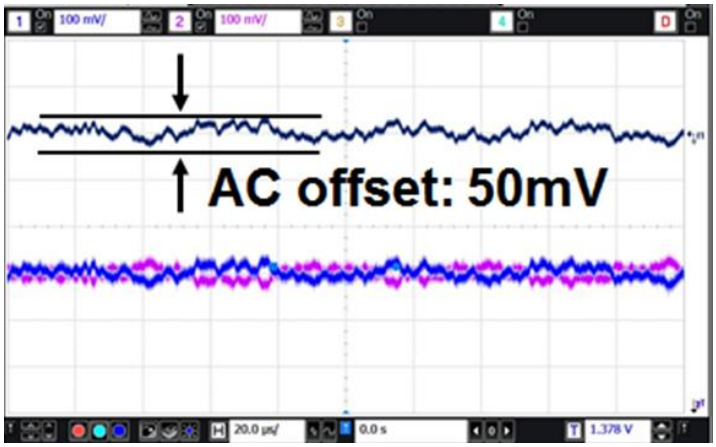

Fig.4. 32 AC offset of the receiver when using Differential Time-Interleaved Method

Fig.4.30 and Fig.4.31 show the AC offset of the receiver output when STX and DTX are applied to the transmitter electrodes. When STX is applied, the AC offset of the receiver output occurs due to the mismatch generated in the touch screen, the MOSFET, the passive component in the receiver IC. The magnitude of the AC offset is proportional to the amplitude of the transmitted signal, and the frequency of AC offset is the same with the transmitted signal. Also, the phase of the AC offset follows the phase of the transmitted signal. When DTX is applied, AC offset resulting from mismatch in receiver IC is canceled by the differential signaling. Figure 18 shows the AC offset of the output when DTX is applied. The AC offset is reduced from about 400mV to 50mV and the output dynamic range of the receiving circuit is greatly improved.

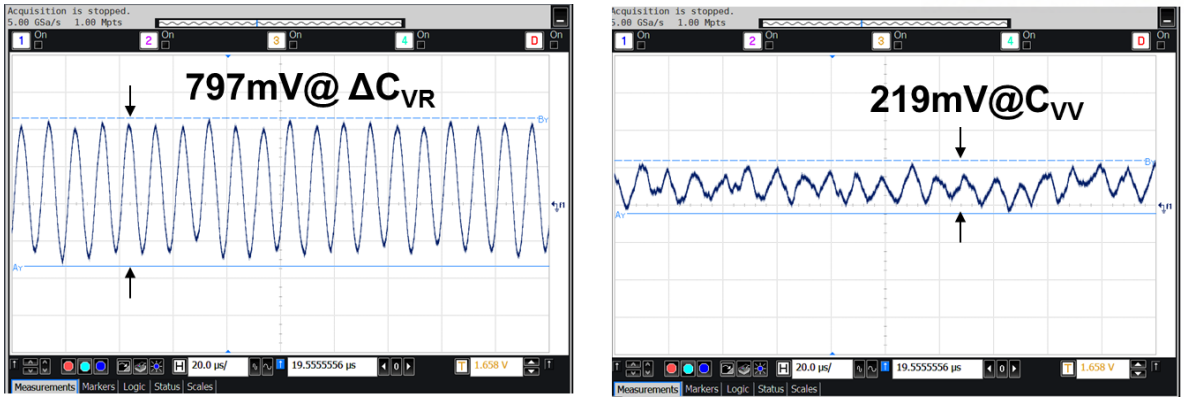

Fig.4. 33 Receiver output in the fingerprint TSP under the 0.2T glass.
(left) Maximum output value by the capacitance difference between the valley and the ridges
(right) minimum output value by the same capacitance

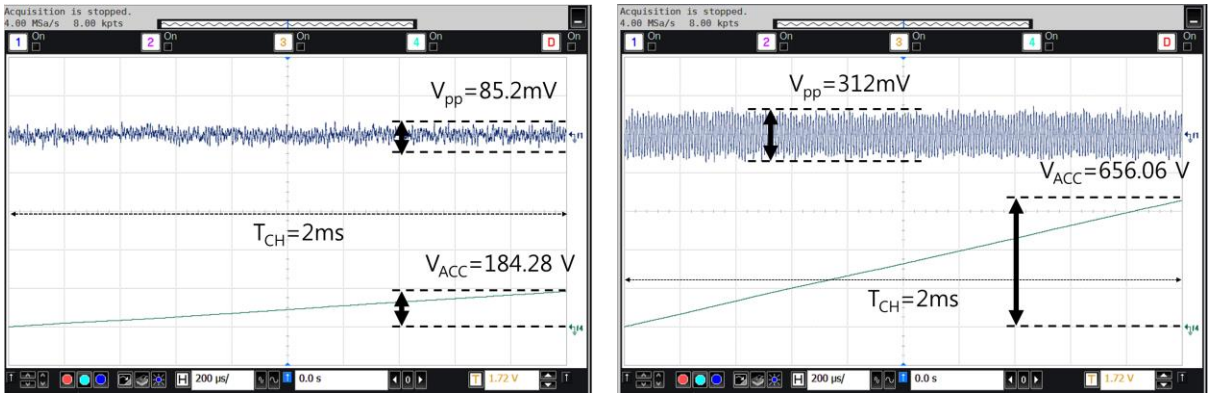

Fig.4. 34 Cumulative output of the receiver in the fingerprint TSP under the 0.3T glass.
(left) Maximum output value by the capacitance difference between the valley and the ridges
(right) minimum output value by the same capacitance

Fig. 4.32 shows the peak-to-peak output signals of the receiving circuit caused by the valley and ridge when the DTX signals are applied to the fingerprint TSP under 0.3T Glass. The frequency of the input signal is 1MHz, the amplitude is 20V. The LO frequency is 900 kHz and the frequency of the receiver output signal is 100 kHz. The maximum output power of the DTX and the proposed receiver circuit was 797 mV and the minimum power output was 281 mV. Fig. 4.33 show the output graph obtained by using the proposed transceiver circuit in the fingerprint TSP under 0.3T Glass according to the scan time. The frequency of the transmitted signal is 1MHz, the voltage amplitude is 20V, and the DTX code is used. The maximum output by the melting and bore is 797mV and the minimum output is 212mV. The integrated output waveforms below the output signals in Fig. 4.33 are obtained digitally. The MCU samples the output signal of the receiving circuit with an ADC of 4 M samples / s. MCU accumulates it digitally, the amplitude of signal continues to increase, and noise signal of which frequencies below 4 M are dispersed by moving average effect.

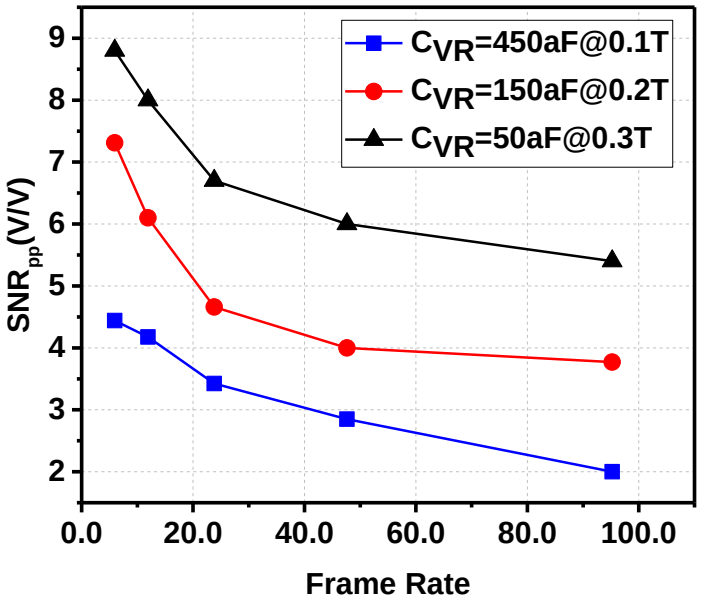

Fig.4. 35 Signal to Noise Ratio according to the frame rate for 42-channel TX

The SNR of the fingerprint recognition circuit using the accumulated signal is as follows.

$$SNR = \frac{\sum_{k=1}^{N}\left(Signal_{CVR}[k] - Signal_{CVV}[k]\right)}{Noise_{RMS}}$$

$$Noise_{RMS} = \sqrt{\frac{\sum_{k=1}^{N}\left\{\left(\sum_{1}^{N} Signal_{CVR}[k]\right) - Signal_{CVR\_AVG}\right\}^{2}}{N^{2}}}$$

In the SNR definition, the magnitude of the signal is proportional to the cumulative value of the difference between the output produced by the ridge and valley and the output generated by the ridge and ridge, and the magnitude of the noise is the RMS value of the accumulated output noise.

Figure 4.34 shows SNR by adjusting frame rate for 42-channel TX. As the frame rate increases, the SNR value is reduced. To get higher SNR, a low frame rate is required. However, low frame rate reduces a response time for fingerprint recognition.

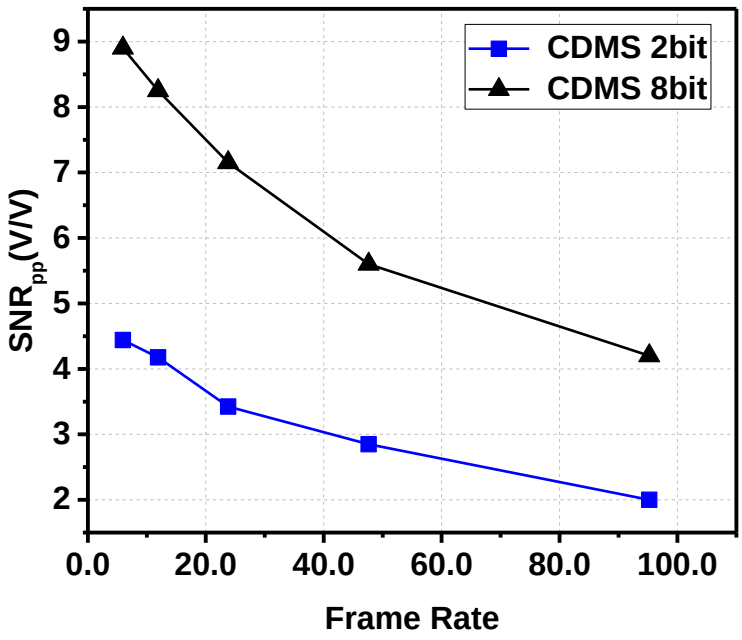

Fig.4. 36 Signal to Noise Ratio according to the number of code in DCMS

Figure 4.35 shows the SNR by the signaling method. When 2-bit DCMS, 8bit-DCMS is applied to the TSP, the number of signals applied to the touch screen at one time is improved to 2, 8. That is, the number of signals allocated to each channel increases within a limited total scan time. Of course, as the code signal increases, the interference per channel increases, but the interference can be minimized through the delay cell of transmitter. The SNR is improved by increasing code bits. By applying DCMS, it is possible to increases a SNR for the limited time in the large number of channels environment. This measurement uses a 42 x 42 fingerprint recognition touch screen under 0.3T glass with 95Hz, and the voltage used is 20V.

Table 2 Comparison Table regarding to readout IC for fingerprint sensor

	This Work		JSSC 2017		JSSC 2008
Method	Mutual Capacitive		Mutual Capacitive		Capacitive
Resolution [dpi]	254		500		462
Channels	42 x 42		70 x 50		200 x 160
Sensor Pitch [μm]	100		50		58
Sensor-IC Connection	FPCB		FPCB		On Chip
Sensing Capacitor [fF]	0.3 T	0.05	0.15 T	0.1	75
SNR_{pp}	4.2 dB		-		-
Frame rate	120		19		100
# of TX and frame rate	95 Hz x 42 =3990		19 Hz x 70 =1330		20000
Power [mW]	21		7.1		25

Fig.4. 37 Measurement result of fingerprint under 0.3T Glass (a) frame rate=200 Hz (b) frame rate= 50 Hz. Figure 4.36 shows the fingerprint image obtained from the manufactured board. A fingerprint TSP has 42-TX channel, 42-RX channel. A 0.3 T Glass is placed on the fingerprint TSP and CVR is equal to the 50 atto farad. A proposed IC achieves 6dB SNR with 120Hz Frame rate. Table 1 is a comparison table comparing the results of the research with existing fingerprint recognition sensors and ICs. The mutual capacitance type transparent fingerprint TSP used in this paper has the lowest sensitivity of 50aF compared with the conventional sensor under the environment of 0.3T Glass. A proposed IC achieves 6dB peak-to-peak SNR with a frame rate of 120Hz for TX of 42 channels. Product of number of TX channel and Frame Rate is highest among transparent mutual capacitive fingerprint TSP.

Chapter V

V. Summary

In this thesis, touch screen controller IC with high SNR and high frame rate for fingerprint mutual capacitive TSP under thick glass is presented. Prior to the research of the multi-channel fingerprint recognition capacitive touchscreen drive circuit, a large-sized touch screen research was conducted in advance.

In a large-sized TSP, the parasitic resistor and capacitance reduce input frequency along with an increased number of channels. Thus, a readout IC for large-sized is required to have a high SNR and frame-rate product for large number of TX channel. DCPA is proposed to achieve high noise immunity and fast frame rate suitable for a large-sized TSP by using a differential-parallel operation in a continuous-mode. Common noise, like display noise, is rejected by a differential structure. Self-noise, like lamp noise, is attenuated by a CA circuit which acts like a band-pass filter. In addition, the signal power spectrum density is enhanced, and the external noise signal is distributed by the parallel driving operation. The proposed DCPA effectively take advantages of both the differential-continuous driving method and the parallel signaling method by canceling timing-skew and gain error. The proposed work has the highest SNR performance compared to other state-of-the-art ROIC at 72 dB with a 240 HZ frame rate, 32 channel TX and 8 channel RX. Moreover, the proposed ROIC achieved a 36.1 dB SNR with the additional injection of 6 V_{pp} lamp noise and 20 V_{pp} display noise all applied at the same time. The proposed work demonstrated superior performance under such conditions and it is expected that the ROIC can perform with high SNR in a practical noisy for larger-sized TSP environment

An environment of fingerprint mutual capacitive under thicker glass is a much more challenging than a large-sized touchscreen. The first reason is that CVR is only several tens of atto-farad. Furthermore, the CVR is reduced by the cover glass. Secondly, fingerprint TSP requires more channels than large touchscreens to achieve high resolution and high recognition rates. Thirdly, external noise and internal noise components also seriously reduce the SNR. Finally, the error caused by the mismatch generated inside the circuit makes an AC offset which reduces a dynamic range, when it gets worse, output is saturated. In this thesis, to solve this problem, a transmitter capable of transmitting a high voltage signal and a high gain receiver having a high noise immunity with a lock-in-sensing structure is proposed to achieve both a higher a signal intensity than noise signal and a sufficient dynamic range. In addition, the AC offset problem, which get worse when using a high-voltage transmission signal and a high gain, is effectively eliminated by using a differential sensing method. In multichannel TSP such as fingerprint

recognition, multiple signaling with orthogonal code signals is effective to increases frame rate. Since the code offset of existing orthogonal code is large, dynamic range is greatly reduced. In this thesis, we propose a DCMS applying the differential sensing method with zero code offset. Through the DCMS and proposed transmitter and receiver circuit, 84 TRX TSP under 0.3T glass was sensed with 4.2dB SNR_{pp} and 120Hz frame rate.

REFERENCES

[1.1]Tang, Hao-Yen, et al. "3-D Ultrasonic Fingerprint Sensor-on-a-Chip." *IEEE Journal of Solid-State Circuits* 51.11 (2016): 2522-2533.

[1.2] Kim, Seong-Jin, et al. "A CMOS fingerprint system-on-a-chip with adaptable pixel networks and column-parallel processors for image enhancement and recognition." IEEE Journal of Solid-State Circuits 43.11 (2008): 2558-2567.

[2.1] T.-H. Hwang, et al, "A highly area efficient controller for capacitive touch screen panel systems," IEEE Trans. Consum. Electron., vol. 56, no. 2, pp. 1115–1122, May 2010.

[2.2] H. Shin, et al, "A 55 dB SNR with 240Hz frame scan rate mutual capacitor 30x24 touch-screen panel read-out IC using code-division multiple sensing technique," in IEEE ISSCC Dig. Tech. Papers, Feb. 2013, pp. 388–389.

[2.3] Yang, Jun-Hyeok, et al. "A highly noise-immune touch controller using filtered-delta-integration and a charge-interpolation technique for 10.1-inch capacitive touch-screen panels." Solid-State Circuits Conference Digest of Technical Papers (ISSCC), 2013 IEEE International. IEEE, 2013.

[2.4] Heo, Sanghyun, et al. "72 dB SNR, 240 Hz Frame Rate Readout IC With Differential Continuous-Mode Parallel Architecture for Larger Touch-Screen Panel Applications." IEEE Transactions on Circuits and Systems I: Regular Papers 63.7 (2016): 960-971.

[2.5] Park, Jun-Eun. Design of Analog Front-End of Touch-Screen Controller with Enhanced Noise Immunity and Configurable SNR and Frame Rate. Diss. Seoul National University, 2017.

[2.6] Galy, Nicolas, Benoît Charlot, and Bernard Courtois. "A full fingerprint verification system for a single-line sweep sensor." IEEE Sensors Journal 7.7 (2007): 1054-1065.

[2.7] K. Lim, et al, "A fast and energy efficient single-chip touch controller for tablet touch applications," IEEE/OSA J. Display Technol., vol. 9, no. 7, pp. 520–526, Jul.2013.

[3.1] T.-H. Hwang, et al, "A highly area efficient controller for capacitive touch screen panel systems," IEEE Trans. Consum. Electron., vol. 56, no. 2, pp. 1115–1122, May 2010.

[3.2] I.-S. Yang and O.-K. Kwon, "A touch controller using differential sensing method for on-cell capacitive touch screen panel systems," IEEE Trans. Consum. Electron., vol. 57, no. 3, pp. 1027–1032, Aug.2011.

[3.3] K.-D. Kim, et al, "A capacitive touch controller robust to display noise for ultrathin touch screen displays," in IEEE ISSCC Dig. Tech. Papers, Feb. 2012, pp. 116–117.

[3.4] J.-H. Yang, et al, "A Noise-Immune High-Speed Readout Circuit for In-Cell Touch Screen Panels," IEEE Trans. Circuits Syst. I, vol.60, no.7, pp.1800,1809, July 2013.

[3.5] J.-H. Yang, et al., "A highly noise-immune touch controller using Filtered-Delta-Integration and a charge-interpolation technique for 10.1-inch capacitive touch-screen panels," in IEEE ISSCC Dig. Tech. Papers, Feb. 2013, pp. 390-391.

[3.6] Park, Jun-Eun, et al. "11.6 A 100-TRX-channel configurable 85-to-385Hz-frame-rate analog front-end for touch controller with highly enhanced noise immunity of 20Vpp." Solid-State Circuits Conference (ISSCC), 2016 IEEE International. IEEE, 2016.

[3.7] J.-E. Park, et al, "A Reconfigurable 40-to-67 dB SNR, 50-to-6400 Hz Frame-Rate, Column-Parallel Readout IC for Capacitive Touch-Screen Panels," IEEE J. Solid-State Circuits, vol.49, no.10, pp.2305-2318, Oct. 2014

[3.8] K. Lim, et al, "A fast and energy efficient single-chip touch controller for tablet touch applications," IEEE/OSA J. Display Technol., vol. 9, no. 7, pp. 520–526, Jul.2013.

[3.9] K.-D. Kim, et al., "A fully-differential capacitive touch controller with input common-mode feedback for symmetric display noise cancellation," in VLSI Circuits Digest of Technical Papers, 2014 Symposium on, 2014, pp. 1-2.

[3.10] H. Shin, et al, "A 55 dB SNR with 240Hz frame scan rate mutual capacitor 30x24 touch-screen panel read-out IC using code-division multiple sensing technique," in IEEE ISSCC Dig. Tech. Papers, Feb. 2013, pp. 388–389.

[3.11] H. Jang, et al, "12.5 2D Coded-aperture-based ultra-compact capacitive touch-screen controller with 40 reconfigurable channels," in IEEE ISSCC Dig. Tech. Papers, Feb. 2014, pp. 218-219.

[3.12] S. Heo, et al, "Highly improved SNR differential sensing method using parallel operation signaling for touch screen application," in Proc. IEEE ASSCC, Nov. 2014, pp. 157-160.

[3.13] L. Lah, J. Choma Jr, and J. Draper, "A continuous-time common-mode feedback circuit (CMFB) for high-impedance current-mode applications," IEEE Trans. Circuits Syst. II, vol. 47, pp. 363-369, 2000.

[3.14] Z. Czarnul, S. Takagi, and N. Fujii, "Common-mode feedback circuit with differential-difference amplifier," IEEE Trans. Circuits Syst. I, vol. 41, pp. 243-246, 1994.

[3.15] M. Lemkin and et al, "A three-axis micromachined accelerometer with a CMOS position-sense interface and digital offset-trim electronics," Solid-State Circuits, IEEE J. Solid-State Circuits, vol. 34, pp. 456-468, 1999.

[3.16] J. Wu, et al, "A low-noise low-offset capacitive sensing amplifier for a 50-μg/√ Hz monolithic CMOS MEMS accelerometer," IEEE J. Solid-State Circuits, vol. 39, pp. 722-730, 2004.

[3.17] M. Maymandi-Nejad, et al, "Continuous time common mode feedback technique for sub 1 V analogue circuits," Electronics Letters, vol. 38, pp. 1408-1409, 2002.

[3.18] T. Kwan, et al, "An adaptive analog continuous-time CMOS biquadratic filter," IEEE J. Solid-State Circuits, vol. 26, pp. 859-867, 1991.

[3.19] S. Yan, et al, "A continuous-time sigma-delta modulator with 88-dB dynamic range and 1.1-MHz signal bandwidth," Solid-State Circuits, IEEE J. Solid-State Circuits, vol. 39, pp. 75-86, 2004.

[3.20] A. Gupta, et al, "Multipath common-mode feedback scheme suitable for high-frequency two-stage amplifiers," Electronics Letters, vol. 42, pp. 499-500, 2006.

[3.21] H. Ma, S. Heo, J. J. Kim, and F. Bien, "Algorithm for improving SNR using high voltage and differential Manchester code for capacitive touch screen panel," Electronics Letters, vol. 50, pp. 1813-1815, 2014.

[3.22] S. Heo, et al, "Dynamic range enhanced readout circuit for a capacitive touch screen panel with current subtraction technique," in 40th Eur. Solid- State Circuits Conf, Sep. 2014, pp. 327-330.

[3.23] W. R. Krenik, A. Dabak, “Touch-sensitive interface and method using orthogonal signaling” U.S. Patent, 2012/0056841, Mar. 8, 2012

[4.1] Hwang, Hyunseok, et al. "A 1.8-V 6.9-mW 120-fps 50-Channel Capacitive Touch Readout With Current Conveyor AFE and Current-Driven ΔΣ ADC." IEEE Journal of Solid-State Circuits(2017).

[4.2] Galy, Nicolas, Benoît Charlot, and Bernard Courtois. "A full fingerprint verification system for a single-line sweep sensor." IEEE Sensors Journal 7.7 (2007): 1054-1065.

[4.3] Kim, Seong-Jin, et al. "A CMOS fingerprint system-on-a-chip with adaptable pixel networks and column-parallel processors for image enhancement and recognition." IEEE Journal of Solid-State Circuits 43.11 (2008): 2558-2567.

[4.4] H. Shin, et al, “A 55 dB SNR with 240Hz frame scan rate mutual capacitor 30x24 touch-screen panel read-out IC using code-division multiple sensing technique,” in IEEE ISSCC Dig. Tech. Papers, Feb. 2013, pp. 388–389.

[4.5] Park, Jun-Eun. Design of Analog Front-End of Touch-Screen Controller with Enhanced Noise Immunity and Configurable SNR and Frame Rate. Diss. Seoul National University, 2017.

[4.6] Ma, Wei-Jhe, Ching-Hsing Luo, and Hong-Yi Huang. "A low power analog front-end (AFE) circuit dedicated for driving bio-electrochemical sensors and peripheral devices." Biomedical Circuits and Systems Conference (BioCAS), 2012 IEEE. IEEE, 2012.

[4.7] Menolfi, Christian, and Qiuting Huang. "A low-noise CMOS instrumentation amplifier for thermoelectric infrared detectors." IEEE Journal of Solid-State Circuits 32.7 (1997): 968-976.

[4.8] Lemkin, Mark, and Bernhard E. Boser. "A three-axis micromachined accelerometer with a CMOS position-sense interface and digital offset-trim electronics." IEEE Journal of solid-state circuits 34.4 (1999): 456-468.

[4.9] Heo, Sanghyun, et al. "72 dB SNR, 240 Hz Frame Rate Readout IC With Differential Continuous-Mode Parallel Architecture for Larger Touch-Screen Panel Applications." IEEE Transactions on Circuits and Systems I: Regular Papers 63.7 (2016): 960-971.

[4.10] Park, Jun-Eun, et al. "11.6 A 100-TRX-channel configurable 85-to-385Hz-frame-rate analog front-end for touch controller with highly enhanced noise immunity of 20Vpp." Solid-State Circuits Conference (ISSCC), 2016 IEEE International. IEEE, 2016.

[4.11] Heo, Sanghyun, et al. "72 dB SNR, 240 Hz Frame Rate Readout IC With Differential Continuous-Mode Parallel Architecture for Larger Touch-Screen Panel Applications." IEEE Transactions on Circuits and Systems I: Regular Papers 63.7 (2016): 960-971.

[4.12] Shin, Hyungcheol, et al. "A 55dB SNR with 240Hz frame scan rate mutual capacitor 30× 24 touch-screen panel read-out IC using code-division multiple sensing technique." Solid-State Circuits Conference Digest of Technical Papers (ISSCC), 2013 IEEE International. IEEE, 2013.

[4.13] Park, Changbyung, et al. "A pen-pressure-sensitive capacitive touch system using electrically coupled resonance pen." IEEE Journal of Solid-State Circuits 51.1 (2016): 168-176.

[4.14] Park, Sang-Hui, et al. "A 0.26-nJ/node, 400-kHz Tx Driving, Filtered Fully Differential Readout IC With Parasitic RC Time Delay Reduction Technique for 65-in 169 x 97 Capacitive-Type Touch Screen Panel." IEEE Journal of Solid-State Circuits 52.2 (2017): 528-542.

[4.15] Heo, Sanghyun, et al. "Dynamic range enhanced readout circuit for a capacitive touch screen panel with current subtraction technique." European Solid State Circuits Conference (ESSCIRC), ESSCIRC 2014-40th. IEEE, 2014.

[4.16] Xu, Jiawei, et al. "A $160um -Channel Active Electrode System for EEG Monitoring." IEEE Transactions on Biomedical circuits and systems 5.6 (2011): 555-567.

[4.17] Ng, Kian Ann, and Yong Ping Xu. "A low-power, high CMRR neural amplifier system employing CMOS inverter-based OTAs with CMFB through supply rails." IEEE Journal of Solid-State Circuits 51.3 (2016): 724-737.

[4.18] Pertijs, Michiel AP, and Wilko J. Kindt. "A 140 dB-CMRR current-feedback instrumentation amplifier employing ping-pong auto-zeroing and chopping." IEEE Journal of Solid-State Circuits45.10 (2010): 2044-2056.

[4.19] Bagheri, Arezu, et al. "56-channel direct-coupled chopper-stabilized EEG monitoring ASIC with digitally-assisted offset correction at the folding nodes." Biomedical Circuits and Systems Conference (BioCAS), 2014 IEEE. IEEE, 2014.

PUBLICATIONS

[1] **Sanghyun Heo**, et al. "72 dB SNR, 240 Hz Frame Rate Readout IC With Differential Continuous-Mode Parallel Architecture for Larger Touch-Screen Panel Applications." IEEE Transactions on Circuits and Systems I: Regular Papers 63.7 (2016): 960-971.

[2] **Sanghyun Heo**, Hyunggun Ma, and Franklin Bien. "An Excessive Current Subtraction Technique to Improve Dynamic Range for Touch Screen Panel Applications." JOURNAL OF SEMICONDUCTOR TECHNOLOGY AND SCIENCE 16.3 (2016): 375-379.

[3] Ma Hyunggun, **Sanghyun Heo**, et al. "On-Display Transparent Half-Diamond Pattern Capacitive Fingerprint Sensor Compatible With AMOLED Display." IEEE Sensors Journal 16.22 (2016): 8124-8131.

[4] Ma Hyunggun, **Sanghyun Heo**, et al. "Algorithm for improving SNR using high voltage and differential Manchester code for capacitive touch screen panel." Electronics Letters 50.24 (2014): 1813-1815.

[5] **Sanghyun Heo**, et al. "A 200 atto farad capacitance sensing with a differential signaling method for a mutual capacitive finger-print sensors." Consumer Electronics-Asia (ICCE-Asia), IEEE International Conference on. IEEE, 2016.

[6] **Sanghyun Heo**, et al. "Highly improved SNR differential sensing method using parallel operation signaling for touch screen application." Solid-State Circuits Conference (A-SSCC), 2014 IEEE Asian. IEEE, 2014.

[7] **Sanghyun Heo**, et al. "Dynamic range enhanced readout circuit for a capacitive touch screen panel with current subtraction technique." European Solid State Circuits Conference (ESSCIRC), ESSCIRC 2014-40th. IEEE, 2014.

[8] **Sanghyun Heo**, Hyunggun Ma, Franklin Bien, Jae-Joon Kim,″Touch screen panel and method of driving the same”, UTP15371KR-00

[9] **Sanghyun Heo**, Hyunggun Ma, Kyungmin Na, Franklin Bien, Jae-Joon Kim, “Touch panel and display device having the same″, UTP15350KR-00

[10] **Sanghyun Heo**, Hyunggun Ma, Franklin Bien, Jae-Joon Kim, “Touch sensor and display device including the same″, UTP15013KR-00

[11] **Sanghyun Heo**, Kyung-Hwan Park Ma, Franklin Bien, Jae-Joon Kim, “Touch detection device and touch detection method using the same″, UTP13067KR-00

[12] **Sanghyun Heo**, Kyung-Hwan Park Ma, Franklin Bien, Jae-Joon Kim, “Touch-screen lead-out circuit using switch type Cartesian coordinates″ UTP13066KR-00

CURRICULUM VITAE

Sanghyun Heo (S'14) Sang Hyun Heo received the B.S. degree in electrical and electronic engineering from Pusan National University, Pusan, Korea, in 2012. He is currently working on the Combined Master-Doctoral program in Electrical Engineering at the Ulsan National Institute of Science and Technology (UNIST), Ulsan, Republic of Korea. His current research interests are readout ICs for flexible touch screen panels, fingerprint touch screen panels, especially focused on sensors and sensor interfaces.